Journal of Manufacturing Processes 36 (2018) 571–600

Contents lists available at ScienceDirect

Journal of Manufacturing Processes

journal homepage: www.elsevier.com/locate/manpro

Review

Prospects of laser beam welding and friction stir welding processes for aluminum airframe structural applications

Nikolai Kashaev[a,*], Volker Ventzke[a], Gürel Çam[b,*]

[a] Helmholtz-Zentrum Geesthacht, Zentrum für Material und Küstenforschung, Institute of Materials Research, Materials Mechanics, Department of Joining and Assessment, Max-Planck-Str. 1, 21502 Geesthacht, Germany

[b] Iskenderun Technical University, Faculty of Engineering and Natural Sciences, Department of Mechanical Engineering, 31200 Iskenderun-Hatay, Turkey

ARTICLE INFO

Keywords:
Laser beam welding
Friction stir welding
Aluminum alloys
Aerospace
Structural performance
T-joints

ABSTRACT

The present study deals with laser beam welding (LBW) and friction stir welding (FSW) applied to high-strength aluminum alloys used in aircraft industry and displays their advantages compared with the riveting technique regarding structural integrity, weight and material savings. First of all, it is shown with respect to different applications and strength levels which high-strength aluminum alloys represent the state-of-the-art and which aluminum alloys are proposed as substitutes in the future. Furthermore, the respective joining process principles are described and demonstrated on different joint configurations, whereby mechanical and microstructural properties of laser beam- and friction-stir-welded joints are discussed and compared. The current study clearly demonstrates that these two joining techniques are not competing but complementary joining techniques in the aircraft industry.

FSW, as a solid-state joining process, has the advantage that the joining is conducted at temperatures below the melting point of the materials to be joined. Therefore, improved mechanical performance of joints is expected compared to that of fusion joining processes such as LBW. Furthermore, better mechanical properties can be obtained when heat input during joining is reduced by employing stationary shoulder FSW and/or external cooling. On the other hand, LBW offers several advantages such as low distortion, high strength of the joint, and high welding speeds due to its low localized-energy input. Thus, LBW - as a high-speed and easily controllable process - allows the welding of optimized complex geometrical forms in terms of mechanical stiffness, strength, production velocity, and visual quality. Both joining processes have advantages and disadvantages, depending on joint geometries and materials. They both have the potential to reduce the total weight of the structure. The FSW process (particularly lower heat input stationary shoulder FSW process) is more advantageous in producing long-distance straight-line butt joints or overlapped joints of aircraft structures, whereas the high-speed and easily controllable LBW process allows the joining of complex geometrical forms due to its high flexibility, particularly in the new generation high strength Al-alloys (such as AA2198), the strengthening phases of which are more heat resistant.

1. Introduction

In the transportation industry, the recognized solution to achieve both weight reduction and increase passenger safety is the development of lightweight load-bearing structures with improved structural performance. Despite their good mechanical properties, the composite materials show a number of disadvantages in comparison to metallic materials due to (1) their susceptibility for delamination, since composites are constructed of different ply layers into a laminate structure, (2) their high-cost since fabrication concept is usually labor-intensive and complex, (3) difficulties in damage inspection because cracks in composites are mostly internal and hence require complicated inspection techniques for detection, and (4) their low recyclability. In the beginning of the 21st century, the two leading aircraft manufacturers—Boeing and Airbus—pushed the usage of composite materials in aircraft fuselage. The advances made in composite manufacture have allowed the aeronautical industry to significantly increase the use of composite materials. Boeing jumped from 12% usage of composite materials on the 777 to 50% on the 787 while Airbus moved from 10% on the A340 to 25% on the A380 and finally to 53% on the A350XWB [1]. Composite and metallic structures are competing for the next generation of single-aisle aircraft. Considering metallic materials

* Corresponding author.
E-mail addresses: nikolai.kashaev@hzg.de (N. Kashaev), gurel.cam@iste.edu.tr (G. Çam).

https://doi.org/10.1016/j.jmapro.2018.10.005
Received 18 July 2018; Received in revised form 17 September 2018; Accepted 4 October 2018
Available online 20 November 2018

in fuselage, environmental issues regarding recyclability can be better fulfilled, while recyclability is still problematic in the case of composite materials. In this domain, both composite and metallic structures have the potential of weight-savings of approximately 20%, leading to improvement in the fuel consumption efficiency and reduction of the CO_2 emission by the same amount [1,2]. Depending on aircraft design, acceptable manufacturing cost, environmental issues etc., a reasonable decision can be made to use more composite or metallic materials in the fuselage.

High-strength aluminum alloys are key materials in structural aircraft applications, where riveting - as a state-of-the-art joining technology used since the 1920s - is mostly applied [3–6]. This joining technology demands a large material amount, which restricts the weight-saving requirements currently applied. The riveting process is characterized by long manufacturing time because of high manual workload required to drill the holes and set the rivets. It is difficult to make any further improvements, e.g. in process automatization, since the joining technology is already highly mature. Riveting can be applied where materials to be joined are overlapped, which results in additional weight of the structure. Since the assembly of structural components by riveting is a significant cost element, cost-efficient joining techniques with a high degree of automatization are of high interest in the transportation industry. From the technological point of view, welding is the most important example of integrated material technology solution developed for a fuselage primary structure application [7]. Using welding instead of riveting results in a reduced final weight of the fabricated structure due to the removal of non-required material overlapping, rivets, and sealant between the joined parts (Fig. 1).

There are currently two competing joining technologies of high interest for the transportation industry – namely laser beam welding (LBW) and friction stir welding (FSW). FSW, as a solid-state joining process, has the advantage that the joining is conducted at temperatures below the melting point of the materials to be joined. Therefore, improved mechanical performance of joints is expected compared to that of fusion joining processes such as LBW. On the other hand, LBW - as a high-speed and easily controllable process - allows the welding of optimized complex geometrical forms in terms of mechanical stiffness, strength, production velocity, and visual quality. Both joining processes have advantages and disadvantages, depending on joint geometries and materials.

Other joining methods also exist in the transportation industry, e.g. riveting, adhesive bonding, rotary friction welding, gas tungsten arc welding (GTAW) etc, which will not be discussed in details within this study. Thus, this study focuses only on the comparison of the two joining technologies: LBW and FSW.

Recent reviews regarding LBW, FSW and joining of aluminum alloys in general were mostly dealing with metallurgical aspect of the joining technologies, where mechanical properties obtained in static tests (e.g. microhardness and tensile) were only briefly discussed [8–16]. For the potential aircraft applications, the more detailed information about the applicability of these two joining technologies to the potential high strength aluminum alloys, possible geometries to be joined by these techniques and structural integrity of the welded structures is required. To make it possible for the aircraft designers find the best choice between these two processes a comparison between them regarding the obtained microstructural and mechanical properties as well as structural integrity is required. Thus, this study aims to evaluate the current achievements in these two joining technologies for the welding of high-strength aluminum alloys for airframe applications. It is also intended in this study to summarize the current achievements in LBW and FSW that can be helpful to make a decision about the most appropriate welding process for the given aircraft structural application.

2. High-strength aluminum alloys used in airframe structures

Aluminum alloys are classified into two groups depending on their strengthening mechanism - heat-treatable and non-heat-treatable alloys. For airframe structural applications, heat-treatable alloys of 2xxx (principal alloying element Cu), 6xxx (principal alloying elements Mg and Si), and 7xxx (principal alloying element Zn) series are mostly used (Table 1). Most of the conventional aluminum alloys were developed in the beginning or middle of the 20th century and optimized through several decades. The typical state-of-the-art alloys are AA2024 and AA7075 alloys, which are still commonly used in aircraft fuselage structures (AA2024 in T351 heat-treatment condition as skin material where higher ductility is required and AA7075 in T6511 heat-treatment condition as stringer material where higher strength is demanded). In order to compete with high-strength composite materials, aluminum producers were forced to developed new higher-strength and lower-density aluminum alloys to replace conventional state-of-the-art aluminum alloys. The development of innovative joining techniques like LBW has driven aluminum producers to develop 6xxx series alloys with improved weldability. Examples of this development include the alloy combination AA6013 as skin material and AA6110 as stringer material, which are used for lower fuselage panels manufactured by LBW process in the Premium Aerotec Company [17]. Another example is the 2xxx series Al-Cu-Ag alloy AA2139, which was developed for LBW applications [18]. New trends are moving in the direction of weldable Al-Li alloys of the third generation (Al-Cu-Li alloys of 2xxx series like AA2198, AA2196, and AA2050) or Al-Mg-Sc alloys (which are classified as 5xxx series alloys since the principal alloying element is Mg) [19,20]. The high-strength and low-density aluminum alloys have the potential to replace conventional state-of-the-art alloys. The new aluminum alloys, in combination with innovative joining technologies like LBW or FSW, can offer the breakthrough response for the aircraft industry in achieving weight reduction of metallic fuselages of future aircrafts.

3. LBW process

3.1. Process, joint design, and challenges in welding high-strength aluminum alloys

LBW is an appropriate joining technology for high-strength aluminum alloys because of its low localized-energy input, which leads to

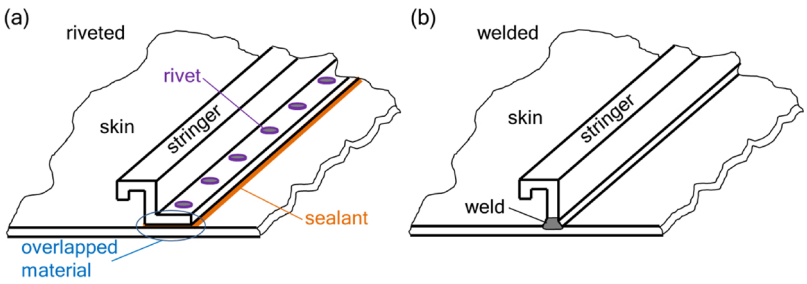

Fig. 1. (a) Conventionally riveted and (b) welded T-joint representing the skin-stringer connection of an aircraft fuselage structure.

Table 1
Actual and proposed uses of conventional aerospace aluminum alloys in airframe structures. Additional alloys included in the table according to Prasad et al. [19,20].

Product	Strength levels	State-of-the-art alloy/ temper	Proposed substitute alloy/ temper	Applications
Sheet	Damage-tolerant/medium-strength	AA2024-T3, AA2524-T3/351, AA6013-T6	AA2198-T8, AA2199-T8E74, AA5028-H116	Fuselage/pressure cabin skins
Plate	Damage-tolerant	AA2024-T351, AA2324-T39, AA2624-T351, AA2624-T39	AA2199-T86, AA2060-T8E86	Lower wing covers
	High-strength	AA7150-T7751, AA7055-T7751, AA7055-T7951, AA7255-T7951	AA2055-T8X, AA2195-T82	Upper wing covers
	Medium-/high-strength	AA7050-T7451	AA2050-T84, AA2060-T8E33	Spars, ribs, other internal structures made from thick plate
	High-strength	AA2219-T87	AA2195-T82	Launch vehicle cryogenic tanks
Forgings	High-strength	AA7175-T7351, AA7050-T7452	AA2050-T852, AA2060-T8E50	Wing-to-fuselage attachments
Extrusions	Damage-tolerant	AA2024-T3511, AA2026-T3511, AA2024-T4312, AA6110-T6511	AA2099-T81, AA2076-T8511	Lower wing stringers, fuselage/pressure cabin stringers, and frames
	Medium-/high-strength	AA7075-T79511, AA7150-T6511, AA7175-T79511, AA7055-T77511	AA2099-T83, AA2196-T8511, AA2055-T8E83	Fuselage/pressure cabin stringers and frames, floor beams, upper wing stringers

low distortion, high strength of the joint, and high welding speeds [21]. The principle of the LBW process is schematically shown in Fig. 2. The laser beam generated from a solid-state laser (typically Nd:YAG, pumped diode, disk laser, or fiber laser) or a gas laser (typically CO_2 laser) is focused on the workpiece. In the case of a solid-state laser with a wave length of approx. 1 μm, the laser beam is delivered to the focusing optic using a fiber (Fig. 2(a)). CO_2 lasers have output wavelengths of 10.6 μm. Therefore, laser beam can only be delivered and focused on the workpiece by a system of moveable copper mirrors and ZnSe lenses (Fig. 2(b)) [22]. This offers some challenges for the CO_2-laser optic system in order to adjust laser-beam focus position by the welding of complex geometries.

LBW of aluminum alloys can be accomplished in both heat conduction mode (Fig. 2(c)) and keyhole mode (Fig. 2(d)). In the case of the heat conduction mode, the laser power density is high enough to cause the metal to melt. Weld penetration is achieved by the heat of the laser conducting down into the metal from the surface. Above a certain intensity, the aluminum material starts to evaporate. A keyhole is generated, leading to a strong increase in laser-beam absorption [23]. Due to the formation of keyhole through concentrated heat input, a deep penetration effect of the LBW can be achieved, leading to small but deep weld seams [21]. The start of the laser welding process of aluminum is difficult in itself because of the high reflection coefficient of laser radiation. When the liquid metal appears, the radiation absorption increases, although it remains at a relatively low level. The keyhole technique is more widely used on aluminum because of the higher welding speed in comparison to the relatively lower welding speeds in the case of the heat conduction mode. Welding at higher speed is more efficient from the industrial point of view [24].

At the beginning of the last decade of the last century, two main types of industrial lasers were of interest for industrial applications – CO_2 and Nd:YAG lasers [25]. CO_2 lasers were then available with power of up to 6 kW (although there are currently CO_2 laser welding machines, with a power of up to 30 kW available in the market), while Nd:YAG lasers were available with power of up to 4 kW. The Nd:YAG lasers were gaining interest for the assembly of complex geometries because of their flexible fiber-optic beam delivery [25]. The Nd:YAG laser, with a low wavelength of 1.06 μm, shows a good coupling to aluminum alloys [26]. As the result, aluminum alloys absorb the laser energy more efficiently [27].

The CO_2 laser-beam with a wavelength of 10.6 μm, however, is absorbed in any sort of acrylic or glass, which are the materials for windows used to safely view lasers and operating laser systems. Acrylic-laser safety windows are usually less expensive than glass laser windows, which are required for solid-state lasers operating at shorter wavelengths. Due to its higher wavelength, the CO_2 laser exhibits high surface reflectivity when its beam impinges on the surface of aluminum alloys. Therefore, a higher amount of laser-energy is reflected from the specimen surface during welding in the case of CO_2 lasers. This could be why only a few researchers have recently investigated CO_2 LBW of aluminum alloys [12]. CO_2 lasers are also more efficient and generate higher power in comparison to the Nd:YAG lasers [12].

At the beginning of the last decade of the last century, it was probably much easier to implement CO_2 LBW in industrial environment. In this case, the cost for the implementation of the laser safety requirements is much lower than that of LBW with Nd:YAG lasers, because the large productions hall can be equipped with relatively cheap acrylic windows. The laser-protective windows required for solid-state lasers are even now very expensive. High availability of laser power and relatively lower costs for safety issues were probably the reasons for the development of CO_2 LBW for aluminum airframe fuselage components at Airbus [28].

Diode laser obtains its laser beam from a high-brightness semiconductor or diode. This category of lasers uses a wavelength in the near infrared region of spectrum, usually in nanometers, like 808 nm [29]. As the beam quality of diode lasers is relatively low, the type of

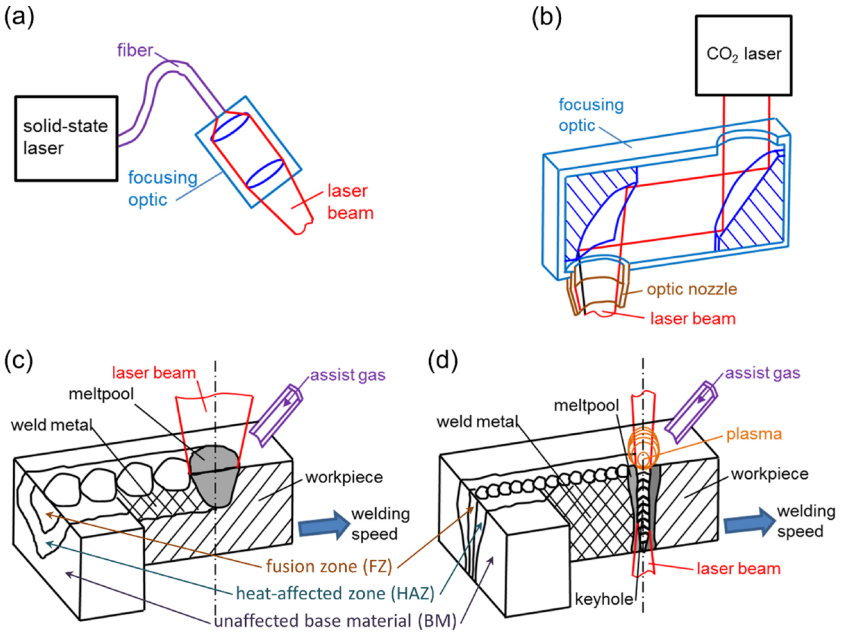

Fig. 2. Principle of LBW with: (a) solid-state laser, (b) CO_2 laser, (c) heat-conduction welding, (d) keyhole welding. Depicted and adopted from Schubert et al. [21] and Behler et al. [23].

lasers is more suitable for welding in heat conduction mode. New developments in laser sources have made two laser sources available at high power with very good laser-beam quality - disk laser and fiber laser. Disk laser is a type of a diode-pumped solid-state laser that is characterized by a heat sink and laser output, which are realized on opposite sides of a thin layer of active gain medium [30]. Disk lasers can generate laser beams of higher quality at higher powers in comparison to Nd:YAG lasers [31]. This makes the industrial application of disk lasers for welding of structural materials more favorable.

In the case of a fiber laser, the active gain medium is an optical fiber doped with rare-earth elements such as erbium or ytterbium. Currently available on the market, high-power fiber lasers with very good beam quality are favorable laser sources for industrial welding applications. Fiber lasers are compact compared to other laser sources of comparable power, because the fiber can be bent and coiled to save space. The compact size and lower cost of ownership make fiber lasers very attractive for industrial welding applications.

In laser science, beam parameter product (BPP) is defined as the product of beam waist radius ω_0 and the divergence angle Θ (Fig. 3(a)) [31,32]. The BPP is often used to describe the beam quality of a laser beam – the higher the BPP, the lower the beam quality. Fig. 3(b) shows that three laser types – CO_2, disk laser, and fiber laser – show lower BPP values at higher powers. New developments in disk lasers and fiber lasers bring to the market laser sources at attractive prices, with lower BPP values operating at higher powers. Therefore, two competing laser types with comparable beam quality are available – fiber lasers and disk lasers. The advantage of using disk lasers is that the producer company of the disk lasers (Trumpf) offers not only the lasers but the complete system with welding cell, where the laser is integrated with the robot station [33]. In the case of fiber laser, the IPG Photonics company offers only laser sources; the customer has to take care of the integration of the fiber laser with the welding cell with robot and other required equipment [34]. This could be why disk lasers are better represented in larger industries now. In the scientific community, however, fiber lasers are of high interest because of their highest beam quality and higher availability of operating powers.

Using LBW, it is possible to realize different joint geometries like butt joints, overlap joints, and T-joints. In the case of airframe structural applications, the most relevant geometries are butt joints (Fig. 4(a)) and T-joints (Fig. 4(b–c)). T-joints can be welded from either one side (single-sided LBW, Fig. 4(b)) or both sides (Fig. 4(c))—using two laser beams simultaneously in order to have one keyhole or successively from one side and then from another. In the aeronautical industry, the T-joint configuration is commonly used to join stringers to the skin (Fig. 1(b)).

LBW can be performed autogenously or with an additional filler-wire material added as wire, powder, foil, or extruded profile [10,12,35–39]. The use of additional filler material offers an opportunity to control the metallurgical processes during LBW. The filler material is used for the reduction of porosity and solidification-cracking of welds. The additional filler material can also positively influence the weld morphology by achieving regular weld shape without any discontinuities. With the help of filler material, it is possible to fill or bridge the gap and avoid underfills or undercuts.

The success of the LBW of a high-strength aluminum alloy or alloy combinations in butt joint or T-joint strongly depends on the composition of the alloys, process gases, filler materials, material preparation technique, and process parameters [10]. In particular, LBW process parameters have a great influence on the quality and the microstructural and mechanical performance of the resulting joints. The main challenges in LBW of high-strength aluminum alloys lie in the formation of porosity and cracks. Generally, aluminum alloys of 2xxx and 7xxx series show greater challenges in overcoming the problems of porosity and cracks during the LBW. The alloys of 7xxx series have an additional problem - the vapor pressure for alloying elements such as Zn, which are required for achieving the highest strength, is significantly higher than for Al. At the same time, the evaporating temperature of Zn is lower than that of Al. Therefore, in the case of keyhole welding, loss of the easily vaporized alloying elements occurs. This results in a significant porosity formation in the weld. New trends have therefore been toward the development of high-strength Al-Li or Al-Mg-Sc alloys with improved weldability [20,37]. On the other hand, new developments in laser sources and process strategies enable the LBW of 2xxx and 7xxx alloys [38–43]. The following sections provide a summary of the achievements pertaining to the most relevant alloys for airframe applications.

3.1.1. *Al-Cu-Mg alloys*

Al-Cu alloys belonging to the 2xxx-family are the primary alloys

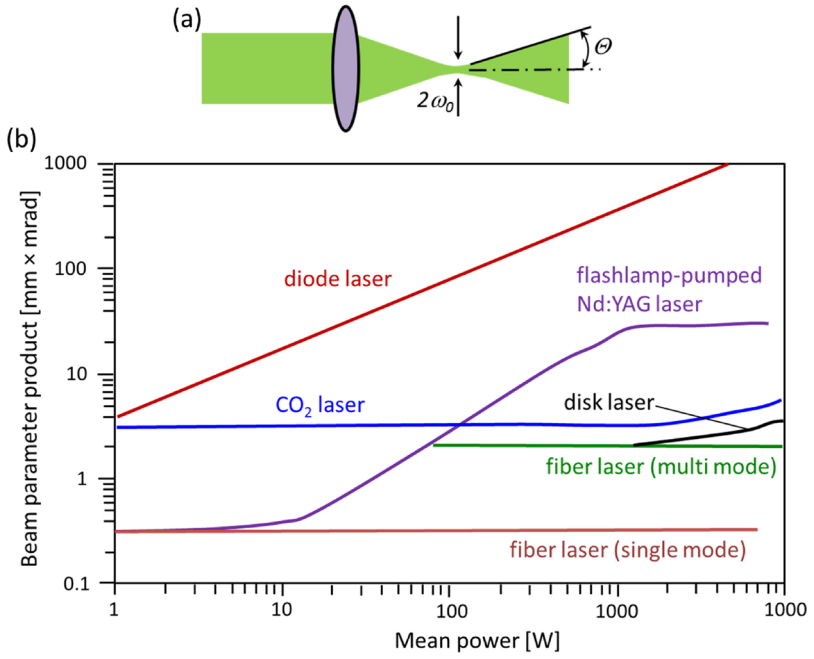

Fig. 3. (a) Sketch of the laser beam and (b) beam parameter product in dependence on the mean laser power for different laser types. Depicted and adopted according to Brockmann and Havrilla [31], and Poprawe [32].

used in airframe structural applications, where damage tolerance is the main criterion. Higher strength of the 2xxx alloys containing Mg is achieved through the precipitation of Al_2Cu and Al_2CuMg phases. The Al-Cu-Mg alloys show superior damage tolerance and good resistance to fatigue-crack growth. Well-known Al-Cu-Mg alloys include AA2024 and AA2014.

Typically, aluminum alloys of 2xxx series show high cracking susceptibility. However, the use of filler wire can improve their weldability [10].

Numerous studies have been conducted on LBW of Al-Cu-Mg alloys up to date [42–51]. Even earlier studies report good results. For instance, Kutsuna et al. reported defect-free welds in the case of autogenous CO_2 LBW of AA2219 alloy [49]. Recent studies also reported successful LBW of AA2024 alloy using disk and fiber lasers with high beam quality, where joint efficiencies of up to 80% were achieved (Table 2) [42–44]. On the other hand, cracks were observed by Weston et al. in the case of CO_2 LBW and Nd:YAG LBW of AA2219 alloy [50]. However, using AA2319 and AA2014 filler wires, crack-free welds were achieved in the case of LBW of AA2024 alloy [51]. Ahn et al. also demonstrated that the addition of AA4043 filler wire reduces the risk of welding defects and improves ductility [42,43]. Moreover, Enz at el. also reported that the AA2024 can be successfully laser-beam-welded in combination with the AA7050 alloy (typical combination of the alloys AA2024 as skin and AA7050 as stringer, joined by means of riveting used in aircraft airframe) using a fiber laser [38]. A very recent study of Wang et al. also reported good results for autogenous LBW of 2A14 alloy using a disk laser [45].

3.1.2. Al-Cu-Mg-Ag alloys

Al-Cu-Mg-Ag alloys can offer improved mechanical performance and thermal stability relative to other alloys in the 2xxx series [52,53]. However, silver-containing alloys are more expensive and their density is higher than that of the recently available high-strength Al-Li alloys. The Al-Cu-Mg-Ag alloy AA2139 shows excellent thermal stability in T8 condition; therefore, it is a promising candidate for high-temperature aeronautical applications such as the high-speed civil transport [53]. In addition, AA2139 shows improved weldability [18]. Successfully laser-beam-welded AA2139 butt joints were presented by Kermanidis et al. and Zervaki et al. [54,55]. Viscusi et al. described the high-quality laser-beam-welded T-joint where AA2139 as stringer was welded to the AA6156 skin [56].

3.1.3. Al-Cu-Li alloys

Newly developed lithium-bearing alloys of 2xxx series offer great potential for aerospace applications due to their high specific strength and high stiffness. It is known that every 1 wt.-% of Li blended into Al increases the elastic modulus by about 6% while reducing the density of the alloy by about 3% [57]. Recent developments in the metallurgical

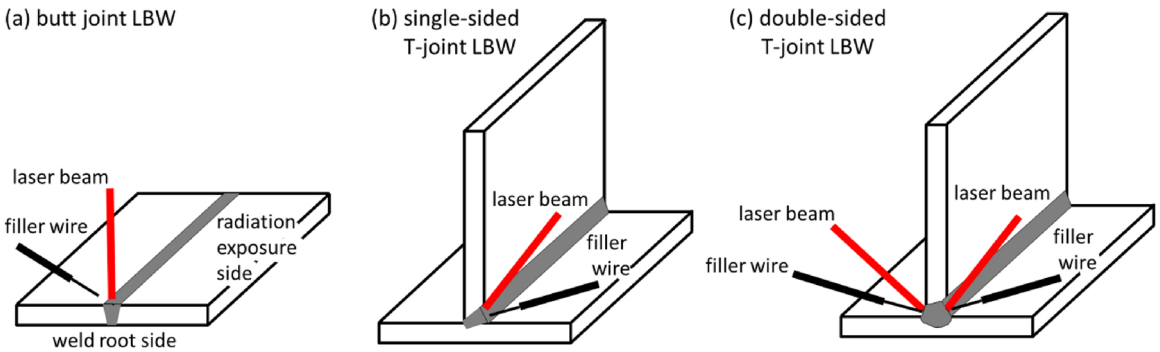

Fig. 4. Typical joint configurations for the LBW of aircraft structures.

Table 2
Joint efficiency values of laser-beam-welded joints of high-strength aerospace Al alloys.

Base Material / Filler Material	Thickness, mm	R_m of BM, MPa	R_m of LBW, MPa	Joint Efficiency, %	Reference
Al-Cu-Mg Alloys					
AA2024-T3/ autogenously	1.25	480	384	80	Alfieri et al. [44]
AA2024-T3/ autogenously	3.0	463	364	79	Ahn et al. [42]
AA2024-T3/ AA4043	3.0	463	370	80	Ahn et al. [42]
AA2024-T3/ autogenously	3.2	480	317	66	Alfieri et al. [44]
AA2024-T3 (skin)-AA7050-T76 (stringer)/ AA4047 (T-joint, hoop-stress)	2.0 (skin), 2.0 (stringer)	490	445	91	Enz et al. [38]
2A14-T6	2.0	428	262	61	Wang et al. [45]
Al-Cu-Mg-Ag Alloys					
AA2139-T8/ AA4047	3.2	460	350	76	Daneshpour et al. [46]
AA2139-T3/ autogenously	3.2	465	320	69	Carrarin [47]
AA2139-T3/ AA4047	3.2	465	294	63	Carrarin [47]
AA6156-T4 (skin)-AA2139-T3 (stringer)/ AA4047 (T-joint, hoop-stress, PWHT: skin T6, stringer T8)	3.0 (skin), 2.7 (stringer)	378 (AA6156-T6)	378	100	Viscusi et al. [56]
Al-Cu-Li Alloys					
AA2198-T3/ AA4047	3.2	461	300	65	Kashaev et al. [62]
AA2198-T3/ AA4047 (PWHT T8)	3.2	495	341	69	Kashaev et al. [63]
AA2198-T8/ AA4047	3.2	495	318	64	Kashaev et al. [63]
AA2198-T3 (skin)-AA2198-T8 (stringer)/ AA4047 (T-joint, hoop-stress)	5.0 (skin), 1.9 (stringer)	430 (AA2198-T3)	335	78	Enz et al. [58,59]
AA2198-T8 (skin)-AA2196-T8 (stringer)/ AA4047 (T-joint, hoop-stress)	3.2 (skin), 1.6 (stringer)	481 (AA2198-T8)	435	90	Kashaev et al. [101]
AA2060-T8/ AA4047	2.0	500	416	83	Zhang et al. [64]
AA2060-T8/ AA5087	2.0	498	317	64	Zhang et al. [65]
AA2060-T8 (skin)-AA2099-T83 (stringer)/ AA4047 (T-joint, hoop-stress)	2.0 (skin), 2.0 (stringer)	501 (AA2060-T8)	391	78	Han et al. [67]
AA2060-T8 (skin)-AA2099-T83 (stringer)/ Al-6.2%Cu-5.4%Si (T-joint, hoop-stress)	2.0 (skin), 2.0 (stringer)	501 (AA2060-T8)	411	82	Han et al. [67]
2A97-T3/ autogenously	1.5	390	235	60	Ning et al. [69]
2A97-T3/ AA2319	1.5	390	191	49	Ning et al. [69]
2A97-T4/ autogenously	2.0	446	370	83	Fu et al. [70]
Al-Mg-Li Alloys					
AA1420/ AA2319 (laser-MIG hybrid welding)	5.0	391	223	57	Yan et al. [80]
AA1420/ AA2319 (laser-MIG hybrid welding, PWHT)	5.0	391	267	68	Yan et al. [80]
Al-Mg-Sc Alloys					
5xxx + Sc/ 015XX	–	–	–	71	Lenczowski [83]
5xxx + Sc/ 015XX	–	–	–	90 (PWHT)	Lenczowski [83]
Al-Mg-Si Alloys					
AA6013-T4/ AlMg5	1.6	345	282	82	Braun [35]
AA6013-T6/ AlMg5 (PWHT)	1.6	397	310	78	Braun [35]
AA6013-T6/ AlMg5	1.6	397	276	70	Braun [35]
AA6013-T4/ AA4046	1.6	345	301	87	Braun [35]
AA6013-T6/ AA4046 (PWHT)	1.6	397	361	91	Braun [35]
AA6013-T6/ AA4046	1.6	397	288	73	Braun [35]
AA6013-T4/ AA4047	1.6	345	316	92	Braun [35]
AA6013-T6/ AA4047 (PWHT)	1.6	397	362	91	Braun [35]
AA6013-T6/ AA4047	1.6	397	300	76	Braun [35]
AA6013-T4 (skin)-AA6013-T4 (stringer)/ autogenously	1.6 (skin), 1.6 (stringer)	323	278	86	Oliveira et al. [92]
AA6056-T4/ AA4047	1.6 (2.5)	–	–	77	Fabrègue et al. [88]
AA6056-T6/ AA4047	6.0	371	275	74	Pakdil et al. [89]
Al-Zn-Mg-Cu Alloys					
7xxx-T6/ autogenously	2.0	676	471	70	Zhang et al. [118]
AA7075-T6/ (V foil + AA5087)	2.0	592	151 (118, milled surfaces)	26, 20 (milled surfaces)	Enz et al. [41]
AA7075-T6/ autogenously	2.0	592	358 (408, milled surfaces	60, 68 (milled surfaces)	Enz et al. [41]

field offer laser-weldable Al-Cu-Li alloys of the 2xxx series, such as AA2196 and AA2198, with high structural efficiency index due to their high strength and low density [37,58,59]. The main challenge of LBW of Al-Li alloys lies in porosity formation and high hot-cracking susceptibility (HCS) [59,60]. The influence of the chemical composition of the filler wire material on the solidification-cracking susceptibility in CO_2 LBW of the AA2195 Al-Cu-Li alloy butt joint was studied by Jan et al. [61]. The authors investigated different filler wires such as Al-Si, Al-Mg, and Al-Cu alloy wires. They report that the Al-Si wire is most effective in reducing the susceptibility to solidification-cracking.

Kashaev et al. investigated Nd:YAG LBW of AA2198 butt joints using AA4047 filler wire, where joints of low porosity and without any noticeable welding defects were produced [62,63]. The specimen welded in T3 heat treatment condition and heat treated into T8 condition after welding showed a slightly higher microhardness in the FZ compared with specimens welded in T3 and T8 conditions. However, the level of the AA2198-T8 base material (BM) was not reached because the chemical composition in the fusion zone (FZ) was influenced by the used AA4047 filler wire material. Joints efficiency of 69% was achieved for the post-weld heat-treated specimens (Table 2). Zhang et al. reported very promising results in case of fiber LBW of AA2060 butt joints, where joint efficiency of 83% was achieved [64]. Fiber LBW was also successfully applied to this alloy using Al-Mg-alloy AA5087 as filler wire material [65]. However, in the last case, the joint efficiency of 64% was reported (Table 2).

The HCS of welded Al-Cu-Li alloys was modelled by Tian et al. [66].

The results obtained by the authors indicated relatively higher HCS in the case of double-sided CO_2 LBW of AA2198-AA2196 T-joint at a higher laser power (more than 1.7 kW). Nevertheless, by the use of a Si-rich AA4047 filler wire, good results were achieved in the case of double-sided LBW of AA2198-AA2196 T-joints by Tian et al. and AA2060-AA2099 T-joints by Han et al. [66,67].

Three different approaches were investigated by Enz et al. with the objective of reducing hot-cracking: pre-heating of the weld samples to elevated temperatures, pre-loading of the weld samples perpendicular to the welding direction, and optimization of the LBW parameters [68]. All approaches suggested by the authors led to an improvement in the HCS. The best results in terms of low total crack lengths were achieved for higher heat inputs with low laser power and welding velocity levels.

Autogenous and non-autogenous (AA2319 filler wire) fiber LBW of 2A97-T3 butt joints was investigated in a very recent study by Ning et al. [69]. The authors showed that the FZ in both types of joints were relatively soft. They reported that the width of the softened zone and the degree of softening with autogenous laser welding was approximately 1/3 and 3/4 those with non-autogenous laser welding, respectively. Autogenously laser-beam-welded butt joints showed higher joint efficiency of 60% in comparison to the joints welded with AA2319 filler wire. However, Fu et al. reported joint efficiency of 83% for autogenous fiber LBW of 2A97 which is sufficiently high (Table 2) [70].

Due to their lower density and higher strength, the Al-Cu-Li alloys are potential candidates for airframe structural applications. Therefore, structural integrity issues were also addressed by the development of laser welding processes. Kashaev et al. demonstrated that the identified LBW process parameters for Al-Cu-Li alloys at laboratory scale can be successfully transferred to the welding of four-stringer panels using a large-scale LBW facility [62,63,71]. Thus, the industrial maturity of the developed LBW process was proved, whereby sound long-distance fillet T-joints (without lack of penetration) were produced.

3.1.4. Al-Mg-Li alloys

Al-Mg-Li alloys are characterized by their extremely low density. For instance, the material AA1420 has a density of 2.47 g/cm^3, while the reference material AA2024 has a density of 2.78 g/cm^3. The former is achieved by the substitution of copper with lithium and magnesium in the chemical composition. The addition of magnesium to the Al-Li system results in higher strength of the alloy and does not lead to the formation of precipitates, except Al_2MgLi in the overaged condition [57]. This allows further reduction in the weight of welded structures for aircrafts with improved specific mechanical properties. Current trends are leading toward novel Al-Mg-Li alloys with improved fatigue behavior and better weldability, resulting in further weight reductions of 5% and 10% compared to Al-Cu-Mg alloys [72].

The first Al-Mg-Li alloys were developed and produced in Russia in the 1960s. Since the 1970s, they have been produced and used on an industrial scale. One of the first applications of these alloys was their use in the welded fuel-tank structures of the supersonic fighter aircrafts MIG-29 and YAK-38 (first and only operational vertical take-off and landing strike fighter). Later, these alloys also found applications in the structures of passenger aircrafts such as TU-155, TU-156, TU-204, and TU-334 [73]. However, the main disadvantage of Al-Mg-Li alloys is their low ductility, especially by impact-loading with high strain rates and low values of fracture strain. Recently published results on laser-welded structures of AA1420 show non-permissible critical properties like insufficient thermal stability > 3000 h at 85 °C (especially a drop in fracture toughness) and accelerated fatigue-crack propagation in NaCl (especially at low frequencies) [72]. Therefore, further developments in metallurgy have followed [57,74–76]. The key research has been accomplished by the All-Russian Scientific Research Institute of Aviation Materials [77].

Similar to the Al-Cu-Li alloys, a similar challenge posed by the LBW of Al-Mg-Li alloys is their susceptibility to weld-cracking. It is assumed that the high magnesium content in the alloy reduces the cracking susceptibility, but this effect has not been studied in detail up to now [74–76]. The difficulties are also subjected to the absence of all-purpose and commercially available filler wire material. However, based on the conducted research on filler material development for the welding of Al-Mg-Li alloys, it can be stated that filler wires with high magnesium content and scandium and zirconium additions are effective for improving the weldability [57,74].

Appropriate welds were reported in the case of autogenous butt-joint welding of the alloy AA1420 using a 4.5 kW Nd:YAG laser [78]. The authors have investigated the effect of LBW on tear toughness and report that the tear toughness of the weld can be increased through a post-weld heat treatment (PWHT). In the case of the post-weld heat-treated specimens, the tear toughness of the weld was comparable to the value obtained in the heat-affected zone (HAZ). Zhuang et al. also reported reduced mechanical properties of AA1420 welds due to the presence of porosity [79]. Joint efficiency of 57% was reported by Yan et al. in case of laser-MIG hybrid welding of AA1420 alloy (Table 2) [80]. The low availability of studies regarding the LBW of Al-Mg-Li alloys can be explained by the difficulties faced by research institutes in accessing commercially available alloys.

3.1.5. Al-Mg-Sc alloys

The application of Al-Mg-Sc alloys in the aeronautics industry is increasing due to their higher toughness, mechanical and fatigue resistance, and light weight compared to other structural materials such as AA7075-T6 alloy. Scandium is added as a grain-refining element; thus, the alloy has a very fine grain structure with improved resistance. Another alloying element is Mg. Hence, Al-Mg-Sc is comparable with the 5xxx series according to the Aluminum Association classification, in the group of work-hardenable non-heat-treatable alloys [81]. Al-Mg-Sc alloys are now being considered for upper fuselage panels, where higher strength is required [82].

The traditional manufacturing route for many structural aerospace applications involves the procurement of large aluminum plates and forgings, which are subsequently machined into the final structure. Due to the significant amount of machining required to produce the final shape, the associated manufacturing costs are considerable. To overcome these issues, the aerospace industry has focused on replacing the machining of thick plates with near-net-shaped manufacturing solutions, such as the welding of stiffeners to thin sheets, followed by forming operations to produce the desired final shape. The proposed manufacturing route can be realized using the advanced Al-Mg-Sc alloys, as they show very good weldability and ease creeping of formed sheets to a final shape without significant loss of properties [83].

The advantageous combination of formability and excellent weldability of Al-Mg-Sc alloys offers the possibility of a low-cost manufacturing solution for many structural launchers applications. Currently, four Al-Mg-Sc alloys are available for aircraft applications: AA5082 or KO8242 from Aleris, C557 from Alcoa, RUS1570 from Russia and Scalmalloy® developed by EADS/Airbus [20,84,85]. Although the Scalmalloy® has not been commercially produced, its applications have been tailored toward the aerospace industry, in particular for the production of stiffened fuselage skins for the lower rear part of the fuselage. Therefore, the main focus of the research activity in the alloy development has been to adapt the alloy and subsequent processing (welding and forming) for aerospace-related applications. Lenczowski reports very promising results regarding the mechanical properties and corrosion behavior of laser-beam-welded 5xxx + Sc alloys. As filler metal for the LBW of Al-Mg-Sc alloys, the author used an alloy similar to the material itself (015xx with scandium). The highest joint efficiency of 71% was achieved with the use of a CO_2 laser. Heat treatment of the welded joints increased the joint efficiency to 90% [83].

3.1.6. Al-Mg-Si alloys

6xxx series alloys (Al-Mg-Si) are of primary interest for LBW

applications because of their better weldability in comparison to the 2xxx and 7xxx alloys. In particular, the alloy AA6013 was developed for aircraft applications with the potential to replace the widely used alloy AA2024. The alloy AA6013, compared to the widely used alloy AA2024 (Al-Cu-Mg), shows about 10% less strength at the same density and comparable corrosion resistance at the same production cost [86]. Al-Mg-Si-Cu alloys AA6013 and AA6056 are already used for lower fuselage applications in Airbus aircrafts, where the skin-stringer panels of lower shells are joined by LBW [28]. The welding process is industrially realized at a large-scale LBW facility equipped with two CO_2 lasers for simultaneous double-sided welding of long-distance T-joints. The simultaneous LBW from both sides with one keyhole enables the maintenance of porosity of welds at a lower level. Another challenge of LBW of 6xxx alloys is to overcome the susceptibility to hot-cracking through the use of AA4047 filler wire with a high Si content. Solidification-cracking in high-strength aluminum alloys can usually be avoided by modifying the weld-pool chemistry with appropriate filler wires and dilution ratios. Aluminum filler wire alloys containing excess Si and Mg are recommended for Al alloys of 6xxx-family [87]. The best results were also achieved for Nd:YAG LBW of AA6013 butt-joints using the AA4047 filler wire [35]. However, the porosity in the FZ was still present. Similar results were reported by Fabrègue et al. for Nd:YAG LBW of AA6056 butt joints using AA4047 filler wire [88].

The formation of porosity in the FZ is also the main problem of single-sided LBW of T-joints. Some porosity was also reported for CO_2-laser-beam-welded AA6056 alloy [89]. Ventzke et al. demonstrated that the formation of pores is determined by not only the types of the aluminum alloys, the variations in the welding directions, and the preparation of the joining faces, but also an excessive angle of incidence between the laser beam and the skin field [90]. Significant improvement can be achieved using high-power lasers with top-hat profile, like fiber laser. Although solidification-cracking is still unavoidable in the case of autogenous LBW, the porosity level can be decreased significantly [91,92].

3.1.7. Al-Zn-Mg-Cu alloys

Welding defects such as pores and cracks resulting from volatile elements are a major challenge in the case of LBW of 7xxx series alloys [93]. Vaporization of zinc reduces the threshold power required to hold the keyhole. Due to the loss of zinc, the hardness in the welded condition and the hardness that can be achieved through the post-weld heat treatment (PWHT) are reduced [10]. Keyhole instabilities bring additional challenges to LBW of high-strength 7xxx series aluminum alloys [10].

Zhang et al. investigated autogenous LBW of Al-Zn-Mg-Cu alloy sheets in T6 temper condition [93]. By optimizing the welding process parameters, the authors obtained appropriate welds with a low porosity level. The main attention of the work was on investigating the microstructure and mechanical properties of the butt joints. The FZ was the weakest region of the joint, where plenty of alloying elements existed in T phases along grain boundaries and some of them dissolved in matrix. The primary phases at grain boundaries in FZ were T phase of $Al_2Mg_3Zn_3$ dissolved in a few Cu, which consume significant amount of alloying elements.

Enz et al. showed that with an increase in total amount of Zn, Cu, and Mg, the laser weldability of high-alloyed Al-Zn alloys deteriorates (Fig. 5(a)) [39]. The authors explained this fact by the thermophysical properties of the alloys, which were considerably influenced by the main alloying elements and their proportion in the investigated alloys. The authors used an approach for improving the weldability of Al-Zn alloys that includes the use of vanadium foil as additional filler wire material. The resulting weld seams showed a significantly improved outer appearance and a reduced amount of porosity (Fig. 5(b)). Another approach reported in the second paper was to apply a fiber laser with a large beam diameter that considerably improved the degassing of the weld pool. Weld discontinuities were minimized and the outer appearance of the welds was significantly improved (Fig. 5(c)) [40]. In a more recent study of the authors the formability of similar and dissimilar joints welded using the two approaches was also investigated [41].

3.2. Geometry and microstructure of welded joints

The typical weld shapes of laser-beam-welded butt joints and T-joints are shown in Fig. 6 [38,42,58,66,92,94]. In the case of Nd:YAG butt-joint welding with filler wire, laser-beam-welded joints display a “V” shape (Fig. 6(a) and (c)). Apart from avoiding hot cracks, another advantage of using filler material is to eliminate geometrical imperfections like underfills and undercuts. Through the use of fiber laser, it is possible to achieve deep and narrow welds with an “I” shape (Fig. 6(b)). The formation of underfills due to the expulsion/evaporation of material in the case of high-speed LBW is often unavoidable (Fig. 6(b)). In the case of the fiber LBW of butt joints with filler wire, the joints can also exhibit an “X” shape (Fig. 6(e)). In comparison to the “V” shape (Fig. 6(a) and(c)), the butt joint with an “X” shape can have advantages in mechanical properties because of more symmetrical weld to the centerline of the sheet.

In the case of simultaneous double-sided LBW, T-joints with symmetrical weld shape can be achieved (Fig. 6(d) and (f)). If LBW is performed by feeding a higher amount of additional filler wire material (Fig. 6(f)) that can be required to avoid hot cracks in the case of difficult-to-weld alloys like AA2196 for example, the T-joint has a seam with pronounced rippled vaulting. In the case of autogenous fiber laser T-joint welding (single-sided), more narrow joints can be achieved (Fig. 6(g)). The use of filler wire results in increasing of weld seam area (Fig. 6(h)). The double-sided welding (successive) has an advantage that the penetration depth into the skin material can be reduced (Fig. 6(i)). It can be advantageous because the weakening of the skin material due to the heat input is reduced, due to which the mechanical properties of the skin are less influenced. However, the main challenges of successive double-sided welding in comparison to the simultaneous double-sided LBW with one keyhole is in the formation of porosity in the seam root because of the higher cooling gradients. In this regard, simultaneous LBW with only one keyhole results in better degassing conditions in the weld root, thus reducing the porosity level. Moreover, simultaneous double-sided welding results in symmetrical shapes that can be advantageous in terms of mechanical properties. However, the use of single-sided LBW is unavoidable in the cases where access from both sides cannot be achieved - e.g. in the case of welding of clips between the stringers [95].

A typical microstructure of the Nd:YAG laser-beam-welded AA6013 alloy is shown in Fig. 7 [35]. Laser-beam-welded joint shows a dendritic structure in the FZ (Fig. 7(a)). In the case of the AA6013 butt joint, the FZ exhibits a fine cellular dendritic solidification structure with the formation of many equiaxed grains. Fine equiaxed grains reduce solidification-cracking susceptibility and improve the mechanical performance of joints [96]. Adjacent to the FZ boundaries, a partially melted zone (PMZ) can be observed (Fig. 7(b)). The typical width of the PMZ is two to three grains. The PMZ is formed due to the heating of the area surrounding the FZ to a temperature between the eutectic temperature and the liquidus temperature of the alloy [96]. Therefore, the grain boundaries that contain eutectic phases locally melt in the area adjacent to the fusion boundaries. The HAZ displays the transition region between the FZ and unaffected base material (BM) (Fig. 7(b)). In the HAZ, rapid heating occurs up to the temperatures less than the alloy melting point, with subsequent cooling. However, the heating temperature in the HAZ is high enough to cause microstructural changes, such as changes in the precipitation state of the base material. At the HAZ/BM boundary, the temperature reaches a critical value; there are no detectable microstructural changes in the BM below this value.

In contrast to the Al-Mg-Si alloys, laser-beam-welded Li-bearing alloys show a small area of fine equiaxed grains adjacent to the fusion

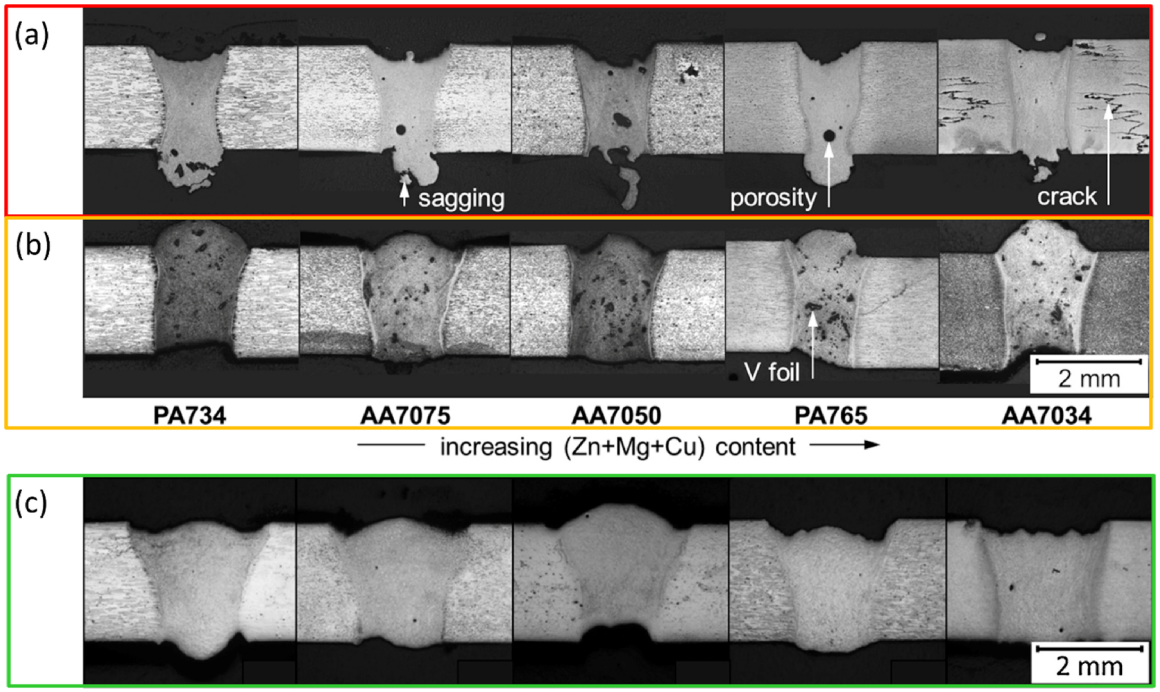

Fig. 5. Micrographs of laser-beam-welded Al-Zn alloys with a different (Zn + Mg + Cu) content. (a) Worst case is the typical process parameters, (b) optimized LBW parameters by using a V foil and 5xxx wire as filler material and (c) optimized autogenous LBW parameters using an Yb fiber laser with a large beam diameter [39,40]. Reprinted with permissions from Springer Nature and Elsevier.

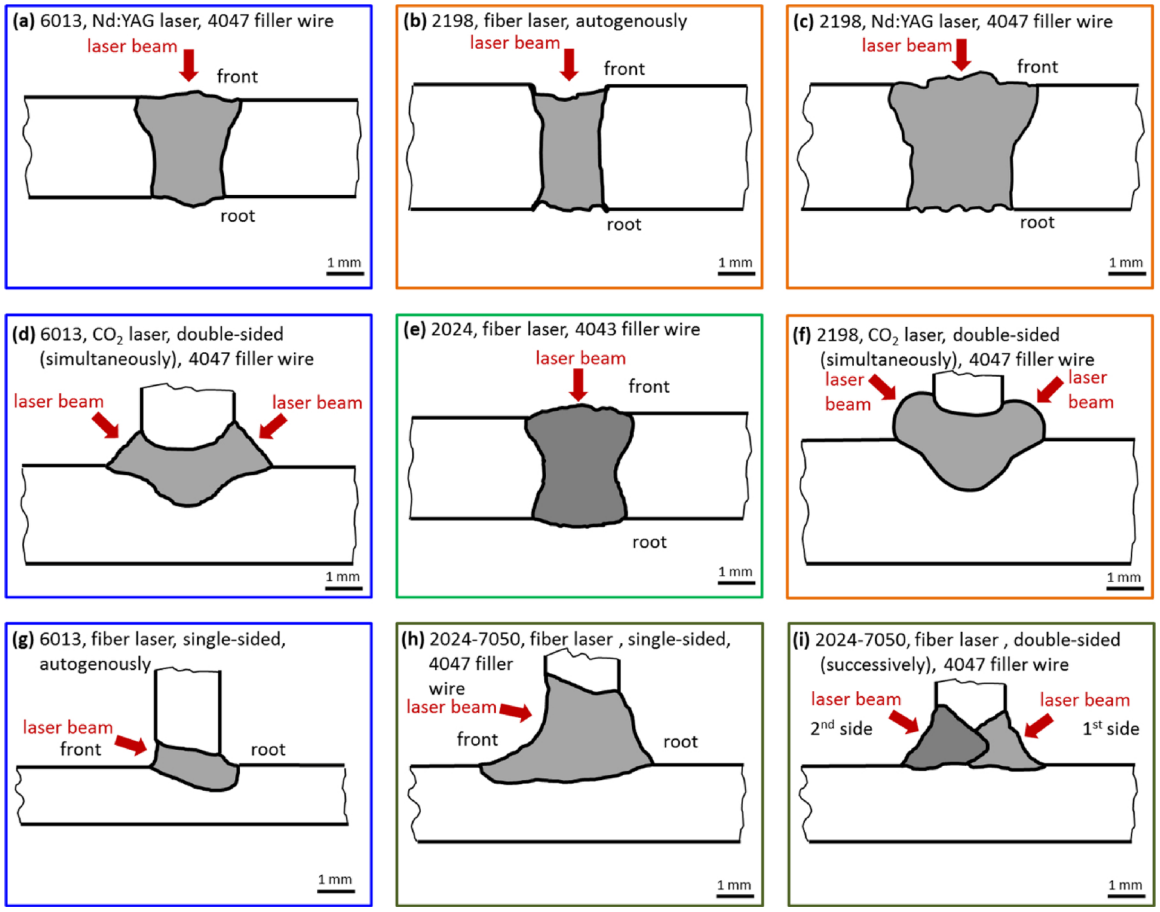

Fig. 6. Typical weld shapes of laser-beam-welded butt joints and T-joints of aluminum alloys AA6013, AA2198, AA2024 and AA7050. Depicted and adopted from Seib [94], Tian et al. [66], Ahn et al. [42], Enz et al. [58], Oliveira et al. [92], and Enz et al. [38].

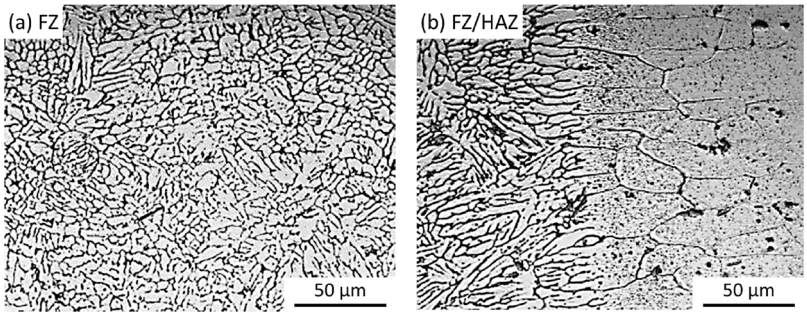

Fig. 7. Optical micrographs of Nd:YAG laser-beam-welded butt joint of AA6013 alloy using aluminum alloy powder AlSi12Mg5, showing (a) the dendritic structure of the FZ and (b) the PMZ at the FZ/HAZ boundary [35]. Reprinted with permission from Elsevier.

boundary within the FZ (Fig. 8(a)). Zhang et al. report that the so-called equiaxed grain zone (EQZ) is characterized by non–dendritic equiaxed grains with a size of 5–10 µm, separated from the adjacent grains in the PMZ [64]. The EQZ only occurs in Li-bearing aluminum alloys. Gutierrez and Lippold proposed that the EQZ is formed in consequence to the heterogeneous nucleation of new grains at the fusion boundary [97]. Next to the EQZ, the grains grow toward the center of the weld, following the gradient of the heat flow [66]. The microstructure variation of a laser-beam-welded AA2060 Al-Cu-Li alloy is schematically shown in Fig. 8(b). In the middle of the FZ, equiaxed dendrites are present. The columnar dendrites are formed in the outer FZ areas. The transition from columnar to equiaxed dendrites typically occurs in the transition zone at the fusion boundary between the FZ and the PMZ [64].

The hardness values in the FZ and hardness profiles of Nd:YAG laser-beam-welded AA6013 butt joints in two different heat treatment conditions, T4 and T6 (as-welded condition), as well as the hardness values and the hardness profile of the laser-beam-welded AA6013 butt joint in T4 heat-treatment condition and post-weld heat-treated in T6 condition are represented in Fig. 9.

Braun investigated Nd:YAG LBW of aluminum alloy AA6013 with different aluminum powder materials - AlMg5, AlSi12 (AA4047), AlSi12Mg5, and AlSi10Mg (AA4046) [35]. For butt joints in as-welded condition fairly similar hardness values in the FZ were measured (Fig. 9(a)). In most cases, the hardness of the FZ was lower than that of the corresponding base materials. Higher hardness values were observed in the FZ in comparison to that of the base material in the as-welded T4 heat-treatment condition only when the AlSi12Mg5 filler powder was used. This fact can be explained by the increasing amount of brittle eutectic phases and constituent particles when using this highly alloyed filler material. However, the use of high-alloyed filler material resulted in considerable porosity in the butt joints, as can be seen in the cross-section represented in Fig. 9(b).

The drop in hardness in the FZ in relation to that of the base material is even higher when the welding is performed in T6 heat-treatment condition. The reduction in hardness can be slightly recovered if LBW is performed in T4 heat treatment condition and butt joint is post-weld heat-treated in T6 condition after the LBW. However, it is still not possible to achieve base-material hardness level in the FZ and HAZ (Fig. 9). The hardness in the HAZ is less influenced through the heat input if the LBW is performed in T4 heat-treatment condition. In the case of as-welded butt-joint in T6 heat-treatment condition, there is considerable decrease in hardness in the annealed zone between the FZ and the overaged zone. The locations of the overaged zone and the annealed zone are schematically shown in Fig. 9(b). The difference between the annealed zone and the overaged zone is in the heat input, which is much higher in the annealed zone. From the annealed zone, the hardness in the overaged zone continuously approaches that of the base material. The two zones - the annealed zone and the overaged zone - form the so-called HAZ that is introduced in the case of steels. In the case of the aluminum alloys, the correct identification is the annealed and the overaged zone.

The increase in hardness in the FZ after the PWHT is caused by precipitation strengthening, as confirmed in the work of Braun through transmission electron microscopy (TEM) [35]. The TEM micrographs in Fig. 10(a) reveal needle-shaped precipitates. According to Edwards et al., these precipitates correspond to the β´´ phase, which mainly contributes to the strength in 6xxx series aluminum alloys [98]. An additional strength in Cu-containing Al-Mg-Si alloys like the alloy AA6013 is also provided by the Q´ phase [99]. Both β´´ and Q´ phases are coherent with the matrix and aligned along the ⟨1 0 0⟩ crystal direction in aluminum [35].

Braun also investigated the effect of LBW on microstructure in HAZ using TEM [35]. The author observed grain boundary precipitation in the HAZ in the as-welded T4 condition (Fig. 10(b)). The precipitates were enriched with silicon and magnesium. The grain boundary particles were not observed in naturally aged base material.

The presence of alloying elements such as copper, magnesium, and silicon in the AA2024 alloy makes the alloy crack-susceptible. The addition of silicon to the weld lowers the solidification temperature and decreases the total shrinkage during freezing to prevent cracking. Ahn et al. investigated the effect of adding AA4043 filler wire during fiber LBW of aluminum alloy AA2024-T3 [42]. Analogous to the 6xxx series alloys, in the case of the aluminum alloy AA2024, the dilution of the

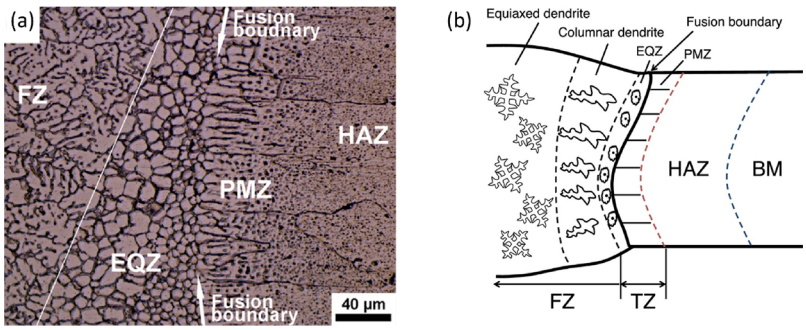

Fig. 8. (a) OM microstructure of the weld cross–section, showing the transition zone (TZ) of a fiber-laser-beam-welded AA2060-T8 butt joint. PMZ and EQZ in the TZ around the fusion boundary. (b) Schematic of microstructure variation in the laser-beam-welded butt joint. According to Zhang et al. [64]. Reprinted with permission from Elsevier.

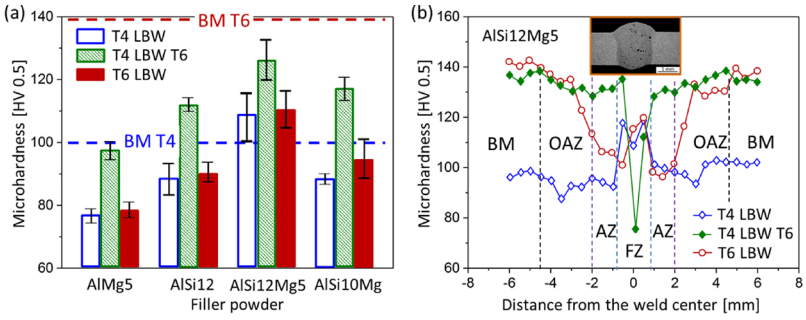

Fig. 9. (a) Microhardness values in the FZ and (b) microhardness profiles of laser-beam-welded aluminum alloy AA6013 in the as-welded T4 and T6 heat-treatment conditions and welded in T4 heat-treatment condition and post-weld heat-treated into T6 condition. LBW was performed with different Al-Si powder as filler material. FZ – fusion zone, AZ – annealing zone, OAZ – overaged zone, BM – base material. Depicted and adopted according to Braun [35].

weld pool with excess silicon by welding with the AA4043 filler metal effectively reduced the percentage of Mg_2Si in the weld. The microstructure in the HAZ of the AA2024 alloy was extensively studied by Yang et al. [100]. The authors explained the reduction of strength in the weld HAZ by the coarsening of the S´ phase and the transformation of the S´ phase to the S phase. The weakest HAZ region with the lowest strength was observed at a peak temperature of 414 °C. PWHT to the T81 had no effect on improving the HAZ strength and ductility [100].

It can be concluded, that the high-strength aluminum alloys for aircraft applications are laser weldable if the process parameters and the material to be welded are perfectly matched to one another. This has been proven in many cases, such as in the case of successful LBW of high-strength Al-Zn-Mg-Cu alloys (Fig. 5). At the same time, LBW allows the joining of geometrically complex structures. Thus, T-joints can be welded by using either single-sided or double-sided joining technique, whereby defect-free welds can be realized. Depending on the alloy composition in the case of precipitation-hardened aluminum alloys, the LBW process affects the hardening condition in the FZ as well as in the HAZ. The following section describes how these microstructural changes correlate with the strength loss in the weld region.

3.3. Mechanical properties of welded joints

The mechanical properties of laser-beam-welded aluminum alloy butt joints and T-joints depend on geometrical characteristics like joint shape, presence of geometrical defects like underfills or undercuts, as well as on joint microstructure and microstructural defects like porosity or solidification-cracking. Eliminating the geometrical and microstructural defects allows the achievement of joints of high efficiencies. The mechanical properties of the joints with appropriate geometrical characteristics and lower microstructural defects are mostly determined by the strength in the FZ. The FZ of the melted and subsequently cooled aluminum alloy joints at higher cooling rates after LBW shows lower strength in comparison to that of heat-treated and rolled sheet material. The strength of the FZ can be increased by applying PWHT after welding. The decrease in hardness and tensile strength of the joint is more pronounced in the aluminum alloys with the highest strength (such as Al-Zn alloys of 7xxx series). Table 2 shows an overview of the tensile properties achieved in laser-beam-welded aluminum alloys.

Due to the heat input into the skin during LBW of T-joints, the tensile strength of the skin in the so-called hoop-stress test is reduced. The hardness decreases in the skin in the FZ and HAZ; therefore, the strength decrease of the skin in the case of laser-beam-welded T-joints can be compensated by introducing a geometrical reinforcement - namely the so-called socket. Fig. 11(a) depicts the hardness map of a laser-beam-welded AA2198-AA2196 T-joint using two CO_2 lasers (simultaneous double-sided LBW). It can be seen that the fusion boundary has the lowest hardness, which corresponds to the EQZ in the case of the Al-Cu-Li alloys. The hardness in the fusion boundary drops to about 60% of BM and recovers to about 75% of BM in the weld center. The partial recovery of hardness in the center of the weld is due to the solidified structure, which results in the loss of the precipitation-hardening effects.

To determine the thickness of the geometrical reinforcement to compensate the decrease in strength of the skin, the size of HAZ in skin material has to be calculated based on the hardness change. In order to compensate the weakening of the skin due to the LBW, the welding of the stringer is considered on a socket with the total thickness that is the sum of the thickness of the skin and the width of the HAZ (Fig. 11(b)) [101].

Fig. 12(a) shows the hoop-stress test results with the tensile test results of BMs. Due to softening resulting from the welding, in the case of the tensile specimen with T-joint, the strain is localized in the softer regions, leading to a limited strain to fracture. As reported in the study by Kashaev et al., the maximal loss of strength determined in the tested laser-beam-welded specimens was 24%, which will lead in direct comparison to a necessary socket under the weld of 0.8 mm (Fig. 12(b)) [101]. Moreover, it has to be mentioned that the laser-beam-welded T-joint of high-strength Al-Cu-Li alloys shows higher tensile strength in comparison to the state-of-the-art riveted joint of the widely used AA2024-AA7075 material combination Fig. 12(a).

For laser-beam-welded structures, it is recommended that the weld zone shall be reinforced by a socket. This socket will protect the weld area; therefore, the fracture should occur in the BM. According to Kashaev et al., the laser-beam-welded AA2198-AA2196 T-joint led to a difference in thickness of 0.8 mm [101]. The authors investigated the deformation behavior of T-joint in hoop-stress test at different positions: the global strain of skin with the T-joint and local strains in the

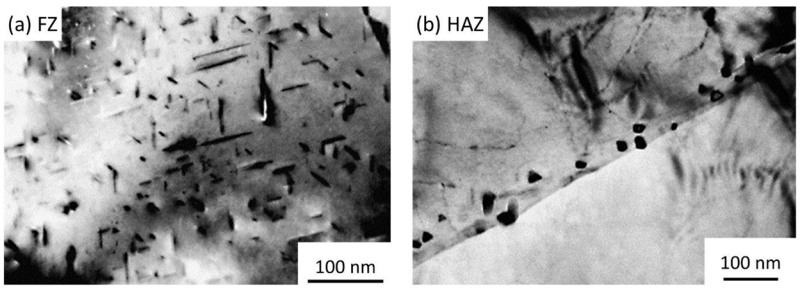

Fig. 10. (a) TEM micrograph showing strengthening precipitates in the FZ (LBW using AA4046 filler wire, butt joint was post-weld heat-treated into T6 temper). (b) TEM micrograph of the AA6013 HAZ in the as-welded T4 condition, showing grain boundary precipitates. Reprinted from Braun with permission from Elsevier [35].

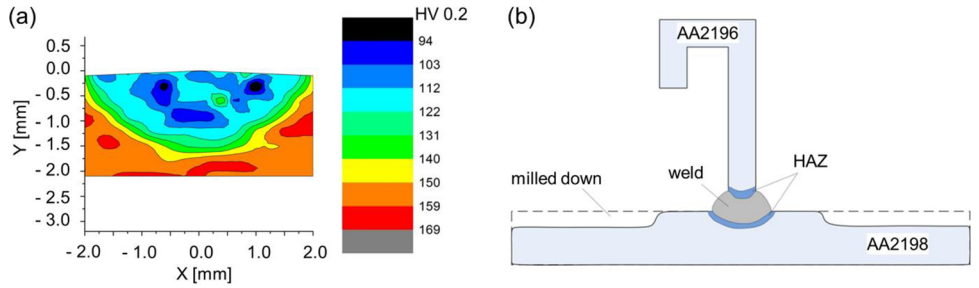

Fig. 11. (a) Microhardness map of a simultaneously double-sided CO_2-laser-beam-welded AA2198-AA2196 T-joint (skin under the stringer) and (b) schematic configuration of welded coupon with material to be removed from skin fusion boundary on stringer (socketing) [101].

weld. The data evaluation was limited to the inner region (socket area) and the global strain for the whole specimen. Two of these curves are displayed in Fig. 12(b). The stresses were calculated according to the thickness of the section. The shielding effect of the socket is clearly visible. All of the specimens with T-joints tested broke in the thin region of the BM; therefore, the joint was protected against mechanical damage in the hoop-stress test.

Despite the hardness decrease in the HAZ and the FZ due to the thermally induced changes in the precipitation-hardening state the laser-beam-welded joints show a sufficient joint efficiency regarding strength. The strength losses can be compensated through the local increase of wall thickness in critical structure areas where LBW is applied. The literature suggests that the overall mechanical properties of laser-beam-welded high-strength aluminum alloys are promising.

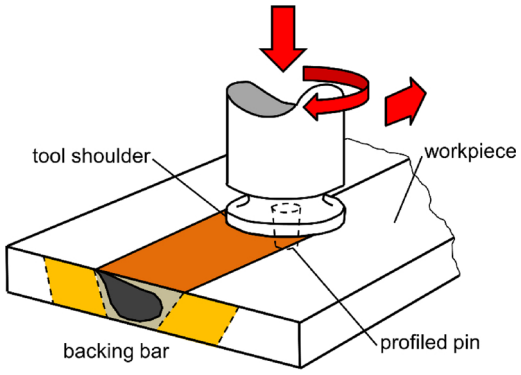

Fig. 13. Schematic illustration of FSW process. Depicted and adopted according to Toumpis et al. [105].

4. FSW process

The FSW process is widely considered to be the most promising joining technique to emerge in welding technology over the last three decades, as pointed out in three recent overview papers discussing the state-of-the-art of this welding method [15,16,102]. The technique was originally developed for joining low-melting temperature materials, such as difficult-to-fusion-weld Al alloys in the early 1990s by the Welding Institute and patented by Thomas et al. [103]. Although there are numerous studies aiming at employing this joining technique to higher-melting materials such as steels, its industrial use lies mostly in joining Al alloys [104]. The technique is schematically shown in Fig. 13 [105].

This relatively novel solid-state joining technique has several advantages in joining Al alloys, particularly high-strength grades that are widely used in aerospace industry and suffer from solidification-cracking when fusion-welded and when the heat input is not sufficiently low. These advantages include the avoidance of solidification defects encountered in fusion-joining of these alloys, low distortion, and low residual stresses, all of which are due to the solid-state nature of the technique, and thus lower heat inputs compared to those in fusion welding. In addition to these advantages, FSW usually also offers the additional advantage of lower strength losses in the weld region than fusion-joining techniques, leading to improved joint strength (both static and fatigue), owing to the fact that fine equiaxed grains evolve in the stir zone (SZ) due to dynamic recrystallization. Moreover, it also offers joint weight reduction, which in turn allows fuel consumption reduction in transportation structures. Consequently, FSW is a useful alternative joining technique for joining Al alloys - particularly higher strength grades used in aerospace industry, such as 2xxx series (Al-Cu) series, 7xxx series (Al-Zn), Al-Cu-Li, Al-Mg-Sc, and Al-Cu-Ag alloys.

In order to keep the peak temperature reached during FSW as low as possible, various attempts were made in the FSW of these high-strength aerospace Al alloys. These measures to reduce the heat input include the use of a stationary shoulder tool in FSW (so-called stationary shoulder FSW or SSFSW) and employing external cooling during FSW (such as the use of a high conductivity base plate and an external cooling system). However, this joining technique also has some disadvantages that should be kept in mind - it requires special fixture systems, access to both sides of the workpieces is difficult, and joint geometries are limited (i.e. welding of T-corners is not possible with the conventional FSW process). Thus, the FSW technique is usually more advantageous in joining along a straight line but it is not as flexible as LBW.

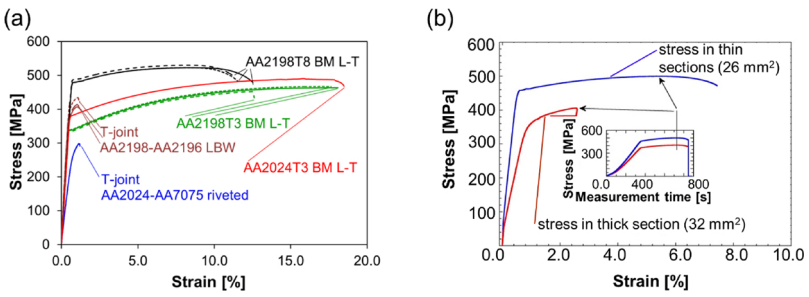

Fig. 12. (a) Tensile test results (with hoop-stress test); (b) Stress-strain curve of laser-beam-welded AA2198-AA2196 T-joint with milled socket [101].

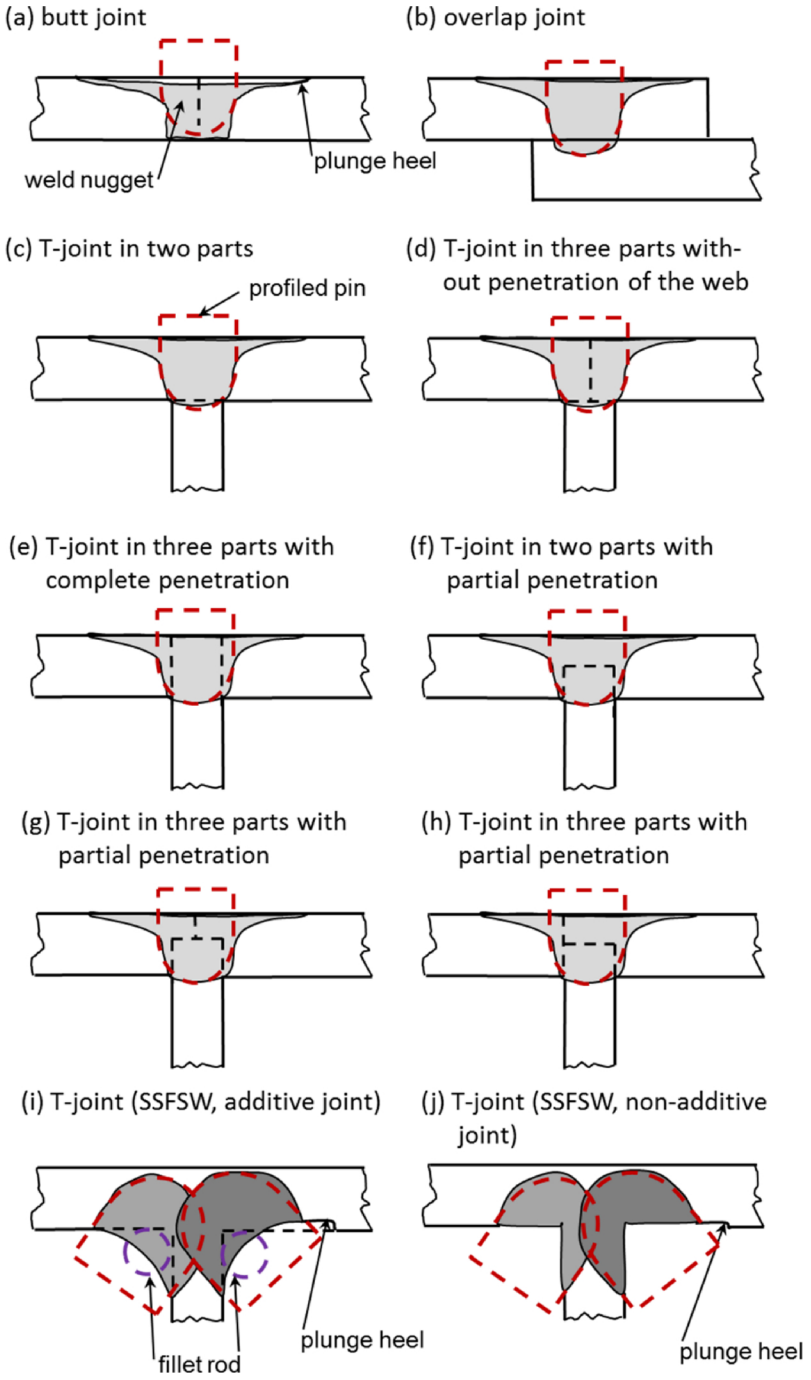

Fig. 14. (a)-(b) Typical joint configurations and (c)-(j)) design solutions to produce T-joints by FSW. Depicted and adopted according to Tavares and Li et al. [106,107].

4.1. The process and joint design

The basic concept of FSW process is quite simple: A non-consumable tool with a specially designed pin and shoulder rotating at a relatively high speed is inserted into the abutting edges of sheets or plates to be joined and subsequently traversed along the joint line. The FSW process is schematically shown in Fig. 13. Heating is generated both by friction between the workpiece and the rotating tool pin and shoulder and by the severe plastic deformation of the workpiece within the SZ and thermo-mechanically affected zone (TMAZ). This localized heating softens the material around the pin and - combined with the tool rotation and translation - leads to the movement of material from the front to the back of the pin, which is very similar to hot-forging. The tool shoulder restricts the metal flow from the joint region.

FSW can be applied to a variety of joint configurations. The most common joint configurations for structural applications, as mentioned earlier, are butt joint and T-joint, both of which can be made by FSW in addition to the lap joint. Fig. 14(a)-(b) shows the butt and overlap joints that can be produced by this joining technique, while Fig. 14(c)-(h) illustrates various design solutions for producing T-joints by the FSW process [106]. In addition, Li et al. recently conducted a study in which they used SSFSW process to produce additive and non-additive T-joints in 5 mm-thick AA6061-T4 alloy plates [107]. The authors clearly demonstrated that full penetration and defect-free T-joints can be readily produced by double-pass welding at the internal corners of T-joint, as shown in Fig. 14(i)-(j). However, the most widely studied friction-stir-

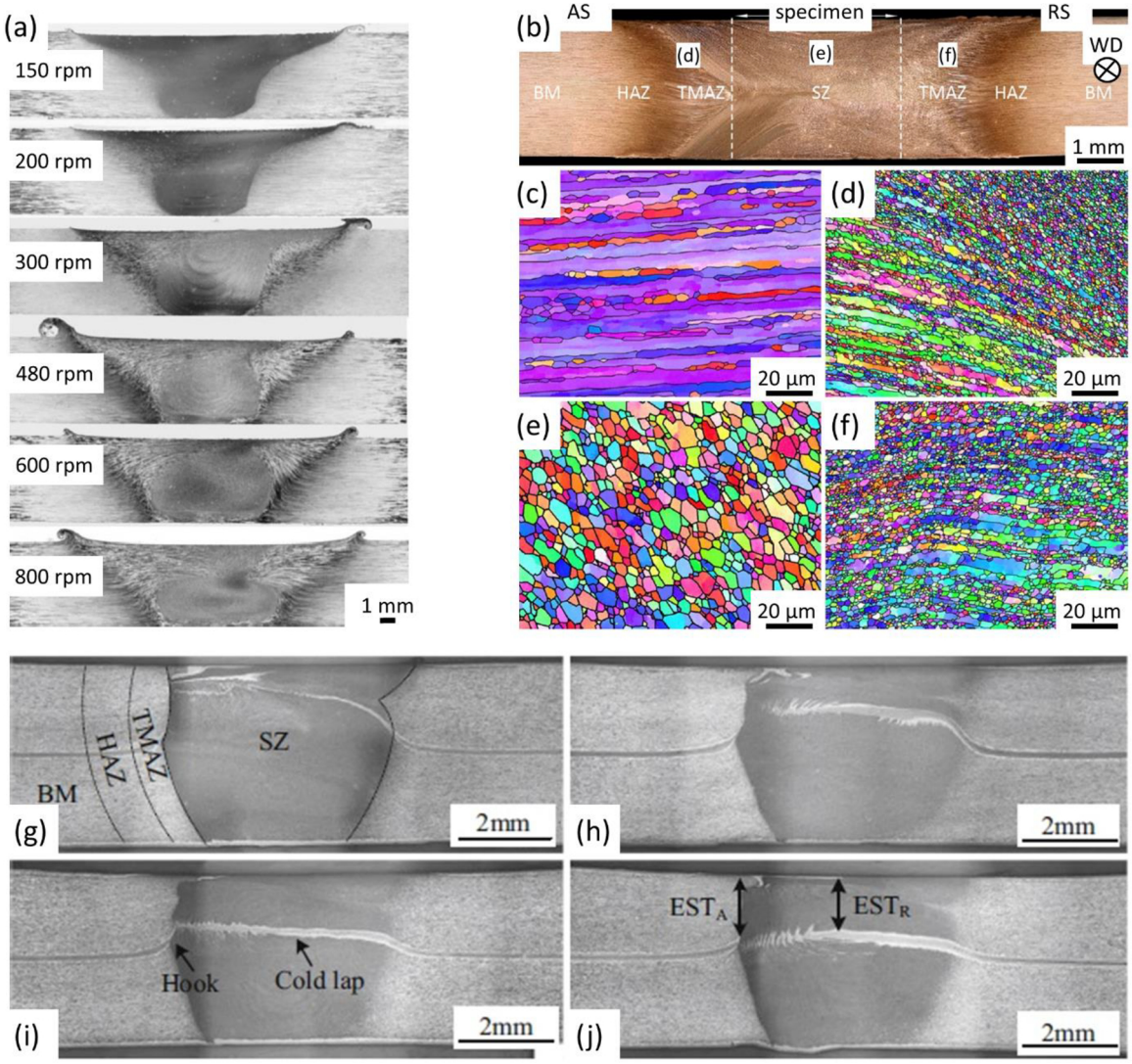

Fig. 15. (a) Macrosections of the welds produced by conventional FSW using various rotational speeds (rpm = rotation per minute) (at constant welding speed and vertical force) illustrating the shape of the weld nugget formed according to Yan et al. [108]. Reprinted with permission from Taylor & Francis.
(b) A macrograph showing a typical weld nugget (X-type) formed in a BT-FSW process; and EBSD micrographs illustrating the grain morphologies of (c) the BM, (d) the TMAZ on the advancing side (AS), (e) the SZ, and (f) the TMAZ on the retreating side (RS) according to Wang et al. [109]. Reprinted with permission from Elsevier.
Cross-section of the stationary-shoulder friction-stir-lap-welded joint using different welding speeds: (g) 40 mm/min, (h) 70 mm/min, (i) 100 mm/min, and (j) 130 mm/min according to Xu et al. [114]. Reprinted with permission from Springer Nature.

welded (FS-welded) joint configuration is the butt joint, since the process is most suited for joining two sheets or plates along a straight joint line.

Most of the research on FSW of high-strength aerospace Al alloys were conducted on butt joints. Fig. 15(a) and (b) show FS-welded butt joints produced by conventional FSW and bobbin tool (BT) FSW processes in AA2524-T351 (Fig. 15(a)) and AA2198 (Fig. 15(b)-(f)) alloys [108,109]. The weld nugget produced by conventional FSW is much wider at the top region due to the shoulder effect, whereas BT-FSW generates an X-type weld nugget, as shown in Fig. 15(a) and (b), respectively. Fig. 16(c) also shows a typical weld nugget produced by conventional FSW. Although most FSW studies have been conducted on butt joint, there are also various reports on the production of T-joints by FSW. For instance, Cui et al. conducted a study to produce T-joint in AA6061-T4 alloy plates by FSW [110]. However, they report that it is hardly possible to produce full-penetration and defect-free joints by conventional FSW, which employs a rotational shoulder. Similar observations are also reported by Penalva et al., Cui et al., and Donati et al. [111–113]. There are also a few reports on FS-welded lap joints in the open literature. For instance, Xu et al. conducted a study aiming to produce lap joints in 2 mm-thick AA2024-T4 alloys by employing the SSFSW process and reported that lap joints without any shoulder marks and surface defects can be readily obtained [114]. Fig. 15(g)-(j) shows the lap joints produced by SSFSW employing various traverse speeds.

4.2. Challenges in FSW of high-strength aluminum alloys

As already mentioned, this relatively novel solid-state joining technique has several advantages in joining Al alloys, particularly high-strength grades widely used in the aerospace industry, such as avoidance of solidification defects and evolution of low-distortion and low-residual stresses. However, a strength loss in the weld region takes place when a high-strength Al-alloy is FS-welded, although improved mechanical performance is expected from FS-welded joints compared to those produced by fusion-joining processes like LBW. Thus, the most striking challenge in the FSW of these alloys is that the strength loss in

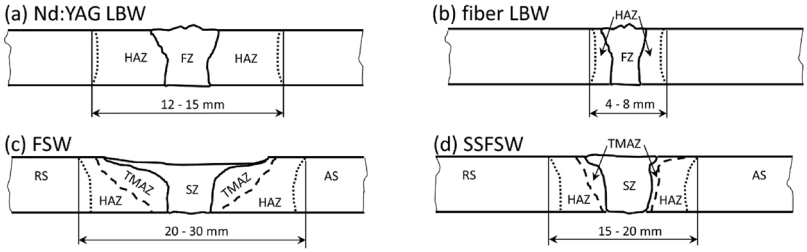

Fig. 16. Typical shapes of butt joints: (a) Nd:YAG LBW, (b) fiber LBW, (c) FSW, and (d) SSFSW.

the weld region should be overcome or kept at an acceptable level by taking appropriate measures, such as external cooling to keep the heat input - and thus the peak temperature - as low as possible during FSW. Another issue is that lower welding speeds are achieved by FSW compared to LBW. Therefore, traverse speeds in the FSW of these alloys should be selected as high as possible. It should, however, be kept mind that excessive welding speed may give rise to weld defects such as tunnel-like defects or cold-bonding in the root regions due to insufficient heat input. In addition to these shortcomings, FSW possesses another disadvantage - it is not as flexible as LBW since it involves very demanding clamping requirements. On the other hand, it is a very attractive alternative to fusion welding processes such as LBW in the joining of high-strength aerospace Al alloys where lower residual stresses and distortion as well as lower strength loss are of paramount importance, particularly in joining applications along a straight line.

4.2.1. Al-Cu-Mg alloys

As in the case of all the heat-treatable Al alloys, FSW leads to a grain refinement in the weld region of Al-Cu alloys, as shown in Fig. 15(c–f), the degree of which depends on the welding parameters and thus the heat input experienced during the FSW [108]. However, this grain refinement does not lead to a hardness increase in the weld region of the FS-welded joints of these alloys, since the most effective strengthening mechanism in these alloys is precipitation-hardening and FSW results in the dissolution and/or coarsening of the strengthening precipitates in the weld region. This in turn results in the softening of both SZ and HAZ.

For instance, as Niu et al. report, these alloys also experience softening in the SZ and HAZ due to the dissolution and/or coarsening of strengthening particles, namely Guinier-Preston-Bagaryatskii (GPB) zones, θ phases (Al_2Cu), and S phases (Al_2CuMg) [115]. As a result, it is usual for the hardness profiles of FS-welded Al-Cu alloys joints to exhibit a typical “W”-shape, as illustrated in Fig. 17 in case of AA6013 and AA7050 alloys. The lowest hardness value for the AA2024-T3 alloy is just above 110 HV. They also report that FS-welded 3.2 mm-thick AA2024-T3 alloy joints exhibited a joint performance of 87%, as seen in Table 3. Similar results are also reported by Dalle Donne et al. for the same alloy with thicknesses of 1.6 and 4.0 mm, yielding joint efficiencies of 89% and 83% respectively [116]. Moreover, Khodir et al. also demonstrated that 3.0 mm-thick AA2024-T3 alloy joints produced by FSW displayed a relatively high joint performance value of 87% [117]. It is also worth pointing out that plate thickness is another important factor affecting the joint performance. As the plate thickness increases, higher heat input is usually applied to workpieces; thus, joint performance decreases. For instance, Zhang et al. report a joint performance of 75% for 6.0 mm-thick BT-FS-welded joints at a rotational rate of 400 rpm at various welding speeds [118].

The hardness loss in the weld region is more significant when the base alloy is the higher-strength Al-Cu alloy, although a grain refinement in the weld region is achieved. For instance, Li and Liu report a significant hardness loss in FS-welded AA2218 joint [119]. Similarly, a hardness loss of 75 HV is also reported by Liu et al. for FS-welded 5 mm-thick AA2219-T6 joints produced at a rotation rate of 800 rpm at various traverse speeds ranging from 50 to 300 mm/min [120]. They also report a relatively low joint performance value of 69%. Similarly, significant hardness loss and thus a relatively low joint performance value (72%) are also reported by Bala Srinivasan et al. for the same alloy, namely AA2219 in T87 condition FS-welded at a rotational speed of 400 rpm and welding speed of 180 mm/min [121]. They also clearly demonstrated that the reason for the hardness loss in the SZ is the dissolution and/or coarsening of strengthening particles. Furthermore, Sree Sabari et al. also FS-welded AA2519-T87 plates at a rotational rate of 1300 rpm using various welding speeds ranging from 20 to 40 mm/min and observed a significant hardness decrease in the weld region [122]. They conducted TEM studies to demonstrate the reason for this softening.

Similarly, a significant hardness decrease in the weld region is also reported by Xu et al. for 6 mm-thick AA2219-T6 alloy joints FS-welded using various rotational rates ranging from 900 to 1200 rpm at a constant welding speed of 140 mm/min [123]. They also report that the highest joint performance (80%) was exhibited by the joint produced using a rotational rate of 1100 rpm and a welding speed of 140 mm/min. Similar results are also reported by Yang et al. for AA2024 and AA2524 alloys [124]. Furthermore, Liu et al. conducted underwater FSW of 7.5 mm-thick AA2219-T6 alloy plates using a rotational rate of 800 rpm [125]. They also employed various welding speeds ranging from 50 to 200 mm/min to investigate the effect of heat input on the precipitates and thus the hardness and strength of the produced joints. They report that the width of the softened zone and the degree of the hardness loss decrease with the increasing weld speed (decreasing heat input). They also report that the welding speed plays an important role in the dissolution of strengthening precipitates and clearly show that a

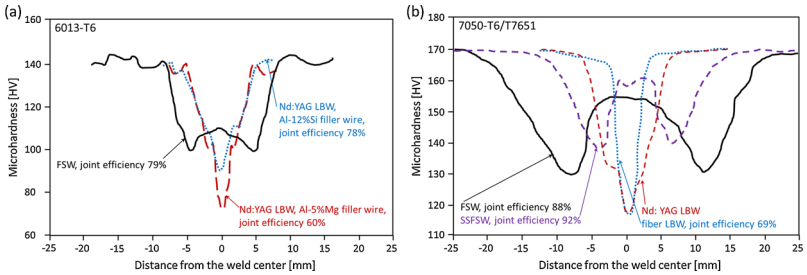

Fig. 17. Microhardness profiles of laser-beam-welded and FS-welded butt joints of (a) AA6013 and (b) AA7050 alloys. Depicted and adopted according to Braun et al. [166], Wu et al. [175], Enz et al. [39], and Enz et al. [40].

Table 3
Joint efficiency values of FS-welds of high-strength aerospace Al alloys.

Material	Thickness, mm	R_m of BM, MPa	R_m of FSW, MPa	Joint Efficiency, %	Reference
Al-Cu-Mg Alloys					
AA2024-T3	1.6	417	369	88	Dalle Donne et al. [116]
AA2024-T3	3.0	457	402	88	Khodir et al. [117]
AA2024-T3	3.2	543	470	87	Niu et al. [115]
AA2024-T3	4.0	497	413	83	Dalle Donne et al. [116]
AA2A14-T6	6.0	460	345	75	Zhang et al. [118]
AA2219-T87	5.0	–	–	72	Bala Srinivasan et al. [121]
AA2219-T6	5.0	445	307	69	Liu et al. [120]
AA2219-T6	6.0	416	329	80	Xu et al. [123]
AA2219-T6	7.5	432	347	80	Liu et al. [125]
Al-Cu-Mg-Ag Alloys					
AA2139-T8	3.2	451	412	91	Campanile et al. [129]
AA2139-T3	3.2	415	397	88	Velotti et al. [130]
AA2139-T8	3.2	451	404	89	Velotti et al. [130]
Al-Cu-Mg-Ag Alloy (T8)	5.0	455	400	89	Nikulin et al. [132]
Al-Cu-Li Alloys					
AA2195-T8	1.0	614	432	app. 70	Shukla and Baeslack [134]
AA2198-T8	1.8	518	386	75	Gao et al. [139]
AA2198-T8	2.0	479 (430[a])	348 (326)	72 (76)	Li et al. [132]; Ma et al. [133]
AA2198-T851	3.0	510	417	82	Goebel et al. [141]
AA2198-T851	3.1	530 (515[a])	413	78 (80)	Le Jolu et al. [137,138]
AA2198-T851	3.2	475	379	80	Wang et al. [109]
AA2198-T8	3.2	–	418	app. 80	Rao et al. [140]
AA2050-T3	20.0	390	292	75	Sidhar et al. [142]
AA2060-T8	2.0	532	435	82	Cai et al. [144]
Al-Mg-Li Alloys					
01420 Al-Li	2.0	481	414	86	Wei et al. [145]
Al-Mg-Sc Alloys					
AA5024-H116 Al-3.9Mg-0.4Sc	3.3	392	326	83	Besel et al. [149]
Al-4.5Mg-0.26Sc (H116)	4.0	app. 374	app. 305	app. 82	Cabello Munoz et al. [148]
Al-4.5Mg-0.45Sc + Zr (H116)	4.0	410	339	83	Lapasset et al. [147]
Al-5.4Mg-0.35Sc + Zr (H323)	2.4	404	382	95	Malopheyev et al. [151]
Al-5.4Mg-0.35Sc + Zr (H18)	2.4	519	385	74	Malopheyev et al. [151]
Al-5.4Mg-0.35Sc + Zr (Hot-rolled)	2.0	440	405	92	Malopheyev et al. [152]
Al-5.4Mg-0.35Sc + Zr (Cold-rolled)	2.4	590	395	67	Malopheyev et al. [152]
Al-5.8Mg-0.25Sc (Cold-rolled)	2.0	423	391	92	Peng et al. [153]
Al-5.8Mg-0.25Sc (Hot-rolled)	6.0	411	380	93	Peng et al. [153]
Al-6.0Mg-0.45Sc + Zr (Hot-rolled)	10	555	520	94	Zhemchuzhnikova et al. [154]
Al-6.0Mg-0.20Sc (Hot-rolled)	10.0	450	410	91	Zhemchuzhnikova et al. [155]
Al-6.0Mg-0.4Sc + Zr (Cold-rolled)	2.0	430	394	94	Zhao et al. [156]
Al-Mg-Si Alloys					
AA6013-T4	1.6	346	252	73	Dalle Donne et al. [116]
AA6013-T4	1.6	397	331	83	Braun et al. [166]
AA6013-T4	4.0	320	249	78	Dalle Donne et al. [116]
AA6013-T4	4.0	320	300	94	Heinz and Strotzki [167]
AA6013-T6	4.0	394	295	75	Heinz and Strotzki [167]
AA6016-T4	1.0	226	185	82	Leitao et al. [168]
AA6061-T6	3.0	342	232	68	Moreira et al. [157]
AA6061-T6	3.17	335	249	74	İpekoğlu et al. [159,160]
AA6061-T6	3.0	350	310	89	Malopheyev et al. [164]
AA6061-T6	4.0	284	196	69	Liu et al. [120]
AA6061-T651	4.0	311	243	78	Lim et al. [161]
AA6061-T6	5.0	300	224	75	Zhou et al. [174]
AA6061-T6	6.0	283	226	80	Chandu et al. [162]
AA6061-T6	6.0	–	–	83	Kumar et al. [163]
AA6061-T6	6.35	310	209	69	Trueba Jr. et al. [158]
Al-Zn-Mg-Cu Alloys					
AA7050-T7451	6.35	555	429	77	Jata et al. [170]
AA7050-T7451	6.35	558	427	77	Pao et al. [171]
AA7050-T7451	5.0	513	app. 415	app. 81	Zhou et al. [174]
AA7050-T7651	6.3	552	486 (505)[b]	88 (91)[b]	Wu et al. [175]
AA7075-T6	3.17	580	474	82	İpekoğlu et al. [178,179]
AA7075-T6	3.0	490	412	app. 84	Fratini et al. [182]
AA7075-T6	3.0	520	450	87	Lotfi and Nourouzi [183]
AA7075-T6	4.0	583	496	85	Lim et al. [161]
AA7075-T651	5.0	583	app. 410	app. 70	Li et al. [185]

(*continued on next page*)

Table 3 (*continued*)

Material	Thickness, mm	R_m of BM, MPa	R_m of FSW, MPa	Joint Efficiency, %	Reference
AA7075-T6	5.0	485	373	77	Rajakumar et al. [177]
AA7075-T6	5.0	559	460	82	Bayazid et al. [181]
AA7075-T6	5.0	567	518	91	Azimzadegan et al. [187]
Al-Zn-Mg-Cu	6.0	656	484	74	Zhang et al. [176]
AA7075-T651	10.0	609	424	app. 70	Srinivasa Rao et al. [188]
AA7075-T651	16.0	610	330	app. 55	Srinivasa Rao et al. [188]

[a] R_m in traverse direction (TD).
[b] value obtained from the stationary shoulder FS-welded joint.

lower welding speed (thus higher heat input) results in a more significant dissolution of precipitates, and thus decreased hardness in the weld region.

It can be concluded that the joint performances of these alloys are determined by heat input during FSW and the initial strength and thickness of the plate prior to FSW. The strength loss is higher when the initial strength of the alloy is higher. Moreover, lower joint efficiencies are usually obtained in FS-welded thicker plates, since higher heat inputs are required to FS-weld them. Joint performance values can be optimized up to a certain value by keeping the heat input as low as possible.

4.2.2. Al-Cu-Mg-Ag alloys

As in the case of all Al alloys, the evolution of recrystallized grains also takes place in the weld nugget of FS-welded Al-Cu-Ag alloys; their grain size gets finer as the heat input experienced during FSW becomes lower. However, usually a hardness decrease in the weld region of these alloys also takes place, although grain refinement occurs, as is usual for all heat-treatable Al alloys. For instance, Hornbuckle et al. conducted FSW of approx. 25.4 mm-thick AA2139-T8 plates using a rotational rate of 250 rpm and a travel speed of 50.8 mm/min. They report that a grain refinement took place in the weld nugget [126]. They also report that the recrystallized grains in the upper-weld nugget are coarser than those in the lower-weld nugget zone due to the higher heat input in the upper-weld nugget during FSW, resulting from the shoulder. In addition, they also observed that the strengthening precipitates did not dissolve in the lower-weld nugget zone, while a near-complete dissolution of the strengthening precipitates took place in the higher heat-input upper-weld nugget. Furthermore, they observed that the main strengthening phase (Ω precipitates) did not coarsen or dissolve in the HAZ while they coarsened and reduced in number density in the TMAZ. This indicates that Ω precipitates are also relatively stable and they do not dissolve or coarsen except at sufficiently high temperature. Similar results are also reported by Grujicic et al. for FS-welded 25.4 mm-thick AA2139-T8 alloy joints produced using a rotational rate of 250 rpm and a traverse speed of 50.8 mm/min [127,128]. They observed a “U”-type hardness profile for these joints and a significant hardness loss within the weld nugget.

On the other hand, Campanile et al. also investigated FS-weldability of relatively thin AA2139-T8 alloy plates (plate thickness 3.2 mm) [129]. They employed a rotational rate ranging from 800 to 2000 rpm and a welding speed ranging from 50 to 300 mm/min. They reportedly achieved a joint efficiency value as high as 91% using a rotational rate of 1400 rpm and a welding speed of 300 mm/min.

Similarly, Velotti et al. also studied the FSW of 3.2 mm-thick AA2139 alloy plates in both T3 and T8 conditions [130]. They employed a rotational rate ranging from 500 to 900 rpm for T3-tempered plates, whereas a rotational rate ranging from 800 to 2000 rpm was used for T8-tempered plates; a welding speed ranging from 50 to 300 mm/min was used. The authors report that a maximum joint efficiency value of 88% was achieved for the joint produced in T3-tempered condition at a rotational rate of 900 rpm and a welding speed of 225 mm/min while a slightly lower joint efficiency (89%) was obtained for the joint produced in T8-tempered condition using a rotational rate of 2000 rpm and a welding speed of 300 mm/min, indicating that high joint efficiencies can be obtained after FSW of AA2139 alloy plates with different initial tempering conditions, provided a suitable welding parameters are used (Table 3). Similarly, Nikulin et al. also conducted FSW on 4 mm-thick Al-Cu-Mg-Ag-Zr alloy plates employing a rotational rate of about 1000 rpm and a traveling speed of about 150 mm/min [131]. They report a relatively high joint efficiency (89%) for the joint. Moreover, the authors also observed that a post-weld T8 heat treatment further improved the joint efficiency to a value of about 98%.

The heat input applied to the workpiece during FSW and the initial strength (temper condition) of the alloy prior to FSW are the main factors that determine the joint performances achieved in these alloys by FSW, as well as the plate thickness to be welded. The strength loss is usually higher when the initial strength of the alloy is higher. However, the strength loss during FSW is significantly lower in these alloys than that experienced in conventional high-strength heat-treatable aerospace Al alloys, i.e. Al-Cu alloys, when they are FS-welded using the same weld parameter (thus the same heat input). This is because the strengthening particles in these alloys (Ω precipitates) are somehow stable; they do not coarsen and/or dissolve, provided the heat input is kept sufficiently low. Thus, it is worth noting that the heat input experienced during FSW must be kept as low as possible for optimum joint efficiencies in these alloys.

4.2.3. Al-Cu-Li alloys

The evolution of fine recrystallized grains also takes place in the weld nugget of FS-welded Al-Cu-Li alloys, as is the case in all Al alloys. Moreover, a hardness decrease in the weld region of these alloys also usually takes place, although grain refinement occurs, which is usual for all heat-treatable Al alloys. For instance, Li et al. and Ma et al. conducted FSW of AA2198-T8 alloy plates employing a rotational rate of 600 rpm and a welding speed of 200 mm/min and observed a “U”-shaped hardness profile with significant softening in the weld nugget [132,133]. They also report a joint efficiency of about 72% for the joints, as seen in Table 3.

Similarly, Shukla and Baeslack studied the FSW of AA2195-T8 alloy plates and used various weld parameters in their study, namely rotational rates ranging from 1800 rpm to 2400 rpm and welding speeds ranging from 75 to 300 mm/min [134]. They observed significant softening in the weld nugget and a U-type hardness profile. They also report a joint performance value of about 70%, as seen in Table 3. They conducted a detailed TEM study in order to determine the reason for this softening and attributed it to the complete dissolution of T_1 and θ ‘precipitates in the weld nugget. In another work, Steuwer et al. also observed an “U”-type hardness profile for FS-welded 5 mm-thick AA2199-T8E74 alloy plates using a rotational rate of 800 rpm and a welding speed of 400 mm/min, as opposed to a more common W-type hardness profile with little hardness recovery in the weld nugget [135]. They also demonstrated by TEM investigations that T_1 precipitates—the main strengthening phase in this alloy—completely dissolved in the weld nugget. In contrast, Tavares et al. observed a “W”-type hardness profile for FS-welded AA2198-T851 alloy joint produced using a rotational rate of 600 rpm and a welding speed of 5 mm/s, which is probably due to a higher heat input experienced during FSW, leading to

some degree of over-aging in the HAZ on both sides [136].

In another work, Le Jolu et al. FS-welded 3.1 mm-thick AA2198-T8 alloy plates using a rotational rate of 1200 rpm and a welding speed of 480 mm/min. They report a slightly higher joint efficiency value of 78% [137,138]. Similarly, Gao et al. have more recently reported a hardness decrease in the weld nugget of the FS-welded 1.8 mm-thick AA2198-T8 alloy plates produced at a rotational rate of 800 rpm and a welding speed of 300 mm/min, the joint efficiency being 75% [139]. They have also conducted detailed TEM studies, which indicate that the dissolution of T_1 precipitates is the reason for the strength loss taking place in the weld nugget. In another recent work, Wang et al. carried out a study on BT-FSW of 3.2 mm-thick AA2198-T851 alloy plates and produced several joints by employing various rotational rates ranging from 400 to 1000 rpm at a constant welding speed of 42 mm/min in order to determine the effect of rotation rate on the joint properties [109]. They observed that a grain refinement took place in the SZ of all the produced joints. They also clearly demonstrated that the finest grain structure in the weld nugget was obtained with the lowest rotational rate of 400 rpm, due to the lowest heat input involved. However, they report that the maximum joint efficiency value of 80% was demonstrated by the joint produced using a rotational rate of 800 rpm (Table 3). Similar joint efficiency values of about 80% are also reported by Rao et al. for FS-welded 3.2 mm-thick AA2198-T8 alloy joint produced using a rotational rate of 1200 rpm and a welding speed of 1000 mm/min [140]. In a very recent work, Goebel et al. have conducted both BT-FSW and semi-stationary shoulder with a static upper shoulder (SSU) BT-FSW of 3 mm-thick AA2198-T851 alloy plates using a rotational rate of 400 rpm and a traverse speed of 500 mm/min; they report that SSUBT-FS-welded joints display a “W”-type hardness profile and a better joint efficiency of about 82% [141].

In another very recent work, Sidhar et al. have studied the FS-weldability of 20 mm-thick AA2050-T3 Al-Cu-Li alloy plates and conducted FSW at various rotational rates ranging from 200 to 420 rpm using various welding speeds [142]. They observed “W”-type hardness profiles for the joints produced and detailed TEM investigations indicate that dissolution and/or coarsening of the strengthening particles took place in the weld region (both in HAZ and SZ), leading to softening. They report a joint efficiency of about 75%. This significant loss of strength is usual in FS-welded thick plates, since higher heat inputs are generally required for the joining of these thicker plates. Similarly, Pouget and Reynolds also report that significant loss of hardness took place in the weld nugget of FS-welded 15 mm-thick AA2050-T851 alloy joints produced at a rotational rate of 290 rpm and a welding speed of 200 mm/min [143]. On the other hand, Cai et al. carried out FSW of thin (2 mm-thick) AA2060-T8 alloy plates using a rotational rate of 2400 rpm and a translational speed of 100 mm/min. They report a much higher joint efficiency value of 82% [144]. They also observed a “W”-type hardness profile. They conducted detailed TEM investigations to explain the reason for the softening in the weld region and observed that although T_1 precipitates are retained in the HAZ, they completely dissolve in the weld nugget, which is the reason for the strength loss in this region.

Al-Cu-Li alloys exhibit a behavior similar to Al-Cu alloys when they are subjected to FSW. Thus, the heat input applied during FSW and the initial strength and thickness of the plate prior to FSW are the main factors determining the joint performances of these alloys. The strength loss is higher when the initial strength of the alloy is higher. In addition, FSW results in lower joint efficiencies in thicker plates due to higher heat inputs required. Again, as in the case of all Al alloys, joint performance can be optimized up to a certain value by keeping the heat input as low as possible.

4.2.4. Al-Mg-Li alloys

Al-Mg-Li alloys (such as alloy AA1420) possess low density but display low ductility. Thus, they are susceptible to cracking in fusion welding, even in low-heat-input LBW. As a solid-state joining technique, FSW offers a potential for the defect-free joining of these alloys, which are susceptible to cracking. Some of these alloys, such as 01424 Al-Li alloy, are considered to be thermally stable. Thus, low-heat-input joining techniques can be successfully be used to join these alloys. FSW offers a good potential in this respect due to the fact that the heat input is low during FSW, since it is a solid-state joining process. However, information on the FSW of precipitation-strengthened Al-Mg-Li alloys is very scarce. There are only two studies on FSW of these alloys reported in the open literature. In one of them, Wei et al. investigated the FS-weldability of 2 mm-thick 01420 Al-Li alloy by employing various weld parameters, namely rotational rates ranging from 480 rpm to 1960 rpm and welding speeds ranging from 23.5 mm/min to 85.7 mm/min [145]. They clearly demonstrated that defect-free joints can be readily be produced in this alloy using a wide range of weld parameters. They studied the effect of FSW parameters on the mechanical properties of the FS-welded joints produced using different weld parameters and observed that the weld parameters do not play an important role in the joint strength. They also report that a joint efficiency value as high as 86% can be achieved. However, the precipitation behavior of the alloy is not addressed.

In the other work, which is very recent, Sidhar et al. have conducted FSW of 01424 Al-Li alloy, the joining of which is of special interest, using a rotational rate of 800 rpm and a welding speed of 305 mm/min [146]. They obtained a joint efficiency of 76% in the as-welded condition and also reported that the joint efficiency value was increased to 92% by employing a PWHT. They conducted TEM investigations which indicate that a softening takes place in the weld nugget due to dissolution of strengthening precipitates in the as-welded condition. They also clearly demonstrated that by employing a PWHT fine strengthening particles precipitate and thus, the strength is recovered up to the level of that of the base alloy.

As already mentioned, the number of works on FSW of this group of Al alloys is very low. However, it can be concluded that although a material softening takes place in the weld region of these alloys, it is not as significant as in more conventional Al alloys such as Al-Cu (2xxx series) and Al-Mg-Si (6xxx series) alloys. The heat input should be kept as low as possible during FSW, as in the case of all Al alloys, for obtaining better joint properties.

4.2.5. Al-Mg-Sc alloys

Fine grains also evolve in the weld nugget of FS-welded Al-Mg-Sc alloys, as in the case of all Al alloys. Moreover, usually a hardness decrease in the weld region of these alloys also takes place, although grain refinement occurs, as is the usual case in all heat-treatable Al alloys. For instance, Lapasset et al. report a hardness decrease in the weld region of FS-welded 4 mm-thick Al-Mg-Sc (C557) alloy in H116 temper condition [147]. They do not give any details about the weld parameters they used, but they report a joint performance value of about 87% (Table 3). As seen in Table 3, similar joint performance values of 82% and 83% are also reported by Cabello Muñoz et al. and Besel et al. respectively for FS-welded Al-Mg-Sc alloy in H116 temper condition [148,149]. Furthermore, Cabello Muñoz et al. also demonstrated that the hardness decrease in the weld region was lower than those experienced in other types of high-strength heat-treatable Al alloys, such as Al-Cu alloys [148]. Similarly, Sauvage et al. studied the FSW of Al-Mg-Si alloy (AA6061-T6) and Al-Mg-Sc alloy (T6) and demonstrated that a lower hardness decrease takes place in Al-Mg-Sc alloy due to the stable strengthening particles in this alloy, i.e. Al_3Sc ($L1_2$ phase), which is stable to dissolution and/or coarsening during FSW [150]. They have also conducted detailed TEM studies in order to determine the reason for different hardness alterations in these two alloys after FSW; it was demonstrated that no dissolution of strengthening particles took place within the weld nugget of Al-Mg-Sc alloys. The authors also report that the recrystallized grain size is much smaller in the weld nugget of FS-welded Al-Mg-Sc alloy because of the pinning effect of nanoscale Al_3Sc particles in this alloy.

Recently, Malopheyev et al. studied the FSW of Al-Mg-Sc-Zr alloy plates in annealed (O), quarter-hardened (H323), and fully hardened (H18) conditions [151]. They conducted FSW using a rotational rate of 500 rpm and a welding speed of 75 mm/min. They report that the joint produced in fully hardened state displayed the lowest joint efficiency of 74% (Table 3), whereas the joints produced in the quarter-hardened and annealed conditions exhibited 95% and about 100% joint efficiency, respectively. Similarly, Malopheyev et al. conducted FSW trials for joining hot- and cold-rolled Al-Mg-Sc-Zr alloys. They report that the joint efficiency of the joint produced in hot-rolled condition was higher (92%) than that of the cold-rolled plate, which was relatively low (67%) (Table 3) [152]. In contrast, Peng et al. report that a relatively high joint performance value can be achieved for Al-Mg-Sc-Zr alloys in both hot- and cold-rolled conditions - 93% and 92% respectively - as seen in Table 3 [153]. They do not, however, give any details about the welding parameters they used. They point out that the strengthening particles in this alloy - namely $Al_3(Sc,Zr)$ phase - have a high thermal stability; thus, they do not coarsen and/or dissolve at temperatures up to 550 °C. They observed that the strengthening particles only partly dissolved in the weld nugget. A strength loss of about 8% was experienced in the weld nugget of the FS-welded joints even in the cold-rolled state, which is much lower than that of conventional high-strength aerospace Al alloys. Similarly, relatively high joint efficiency values of 94% and 91% were reported for FS-welded 10 mm-thick hot-rolled Al-Mg-Sc-Zr alloy joints produced with a rotational rate of 500 rpm and a welding speed of 150 mm/min by Zhemchuzhnikova et al. [154,155]. They also demonstrated that the strengthening particles, i.e. $Al_3(Sc,Zr)$ phase, were preserved in the weld nugget of the FS-welded joint. They claim that the subtle softening in the SZ was due to the elimination of the initial work-hardening resulting from the recrystallization taking place during FSW [154]. Moreover, Zhao et al. even report quite a high joint performance value of 94%, for FS-welded 2 mm-thick cold-rolled Al-Mg-Sc-Zr alloy joints [156]. However, they do not give any detail about the weld parameters they used. They propose that the reason for such high joint efficiency was due to the excellent thermal stability of the strengthening particles, i.e. $Al_3(Sc,Zr)$ phase.

As in the case of Al-Cu alloys, the heat input applied to the workpiece during FSW and the initial strength (temper condition) of the alloy prior to FSW are the main factors that greatly determine the joint performances achieved in these alloys by FSW. The strength loss is usually higher when the initial strength of the alloy is higher. However, the strength loss occurring during FSW is significantly lower in these alloys than that experienced in conventional high-strength heat-treatable aerospace Al alloys, i.e. Al-Cu alloys, when they are FS-welded using the same weld parameter (and thus the same heat input). The reason for this is that the strengthening particles in these alloys, i.e. $Al_3(Sc,Zr)$ precipitates, are much more stable; thus, they do not coarsen and/or dissolve even at relatively high temperatures of up to 650 °C. On the other hand, the plate thickness does not play an important role in FSW of Al-Mg-Sc alloys, in contrast to Al-Cu alloys. For instance, a joint efficiency as high as 94% can be achieved in 10 mm-thick FS-welded joints provided the heat input is kept sufficiently low. Thus, it is worth noting that the heat input achieved during FSW must be kept as low as possible for optimum joint efficiency.

4.2.6. Al-Mg-Si alloys

FSW leads to a grain refinement in the weld nugget of these alloys, as in the case of all Al alloys. However, it also results in a significant softening in the weld region, due to the dissolution and/or coarsening of strengthening precipitates. For instance, Sauvage et al. studied the FS-weldability of AA6061-T6 alloy plates and conducted welding using a rotational rate of 400 rpm and a weld speed of 2 mm/s [150]. They also conducted detailed TEM investigations, which demonstrate that the dissolution of the strengthening precipitates took place in the weld nugget, leading to a sharp hardness drop in the weld region. Similarly, Moreira et al. also observed a significant decrease in the strength in the weld nugget of FS-welded 3 mm-thick AA6061-T6 alloy joints produced using a rotational rate of 1120 rpm and a weld speed of 224 mm/min [157]. They report a weld efficiency of about 68%. Moreover, Liu et al. conducted FSW of 4 mm-thick AA6061-T6 alloy plates at a constant rotational rate of 600 rpm using various traverse speeds ranging from 50 to 200 mm/min [120]. They also report a significant strength loss in the weld nugget, the maximum joint efficiency value being 69% obtained from the joint produced at the highest traverse speed of 200 mm/min. Their TEM observations also indicate that the dissolution of the strengthening particles was the reason for the strength loss in the weld nugget. A slightly lower joint efficiency value for FS-welded thicker AA6061-T6 alloy joints (plate thickness 6.35 mm) produced using a rotational rate of 1200 rpm and a travel speed of 810 mm/min is reported by Trueba Jr. et al. [158].

İpekoğlu et al. also studied the effect of weld parameters on the joint quality of AA6061-T6 alloy plates by varying the rotational rate from 750 to 1500 rpm and the weld speed from 150 to 400 mm/min [159]. They report that the highest joint efficiency (74%) was exhibited by the joint produced at a rotational rate of 1500 rpm using a traverse speed of 400 mm/min. İpekoğlu et al. also demonstrated that by applying PWHT, the joint efficiency value can further be increased up to 90% [160]. Similarly, Lim et al. also report a joint efficiency of about 78% for the FS-welded 4 mm-thick AA6061-T651 alloy joints produced using a rotational rate of 2000 rpm and a weld speed of 400 mm/min (Table 3) [161]. In another work, Chandu et al. also studied the weldability of 6 mm-thick AA6061-T6 alloy plates; they varied the rotational rate from 800 to 1600 rpm and kept the weld speed constant at 28 mm/min [162]. They report that the highest joint efficiency value of 80%, was displayed by the joint produced with a rotational rate of 1200 rpm. A slightly higher efficiency value of 83% is also reported by Kumar et al. for the FS-welded 6 mm-thick AA6061-T6 alloy joints produced using a rotational rate of 355 rpm and a welding speed of 400 mm/min [163]. Recently, Malopheyev et al. have conducted FSW of 3 mm-thick AA6061-T6 alloy plates using a constant rotational rate of 1100 rpm and three different travel speeds of 125, 380 and 760 mm/min; they report that the increasing welding speed increased the joint efficiency value, the maximum joint efficiency being 89%, obtained for the joint produced at a travel speed of 620 mm/min [164]. They conducted detailed TEM investigations and observed that the reason for the high joint efficiency was the prevention of the coarsening of the strengthening precipitates when FSW was conducted at higher welding speeds, which decrease the heat input. On the other hand, Zhou et al. report much lower joint efficiency values for the 3 mm-thick self-reacted (SR) FS-welded AA6061-T6 alloy joints, produced at a constant travel speed of 350 mm/min using rotational rates varying from 300 to 600 rpm (the best result of 75% was displayed by the joint produced at a rotational rate of 400 rpm) [165]. The results indicate that the welding parameters (thus heat input during FSW) and the initial plate thickness play an important role in the joint properties produced by FSW.

In another work, Dalle Donne et al. investigated FSW of 1.6 and 4 mm-thick Al-Mg-Si-Cu alloy (i.e. AA6013-T4) plates and reported joint efficiencies of 73% and 78% respectively (Table 3) [116]. They proposed that the dissolution of the strengthening precipitates in the weld nugget was the reason for the loss of strength. In a more recent work, Braun et al. also conducted FSW of 4 mm-thick AA6013-T4 alloy plates using a rotational rate of 2500 rpm and a travel speed of 800 mm/min; they report slightly higher joint efficiency value of 83% [166]. They also observed that the dissolution of the strengthening precipitates took place in the weld nugget. Similarly, Heinz and Strotzki also studied FSW of 4.0 mm-thick AA6013 alloy in both T4 and T6 conditions; they produced FS-welded joints using a rotational rate of 1400 rpm and a travel speed of 400 mm/min [167]. They reported a much higher joint efficiency for the joint produced in T3 condition (94%) compared to Braun et al., but a relatively lower joint performance value of 75% for the joints produced in T6 condition [166]. Their detailed TEM

investigations demonstrate that the dissolution of the strengthening precipitates took place in the weld nugget, leading to strength loss. In another work, Leitao et al. also conducted FSW of 1 mm-thick AA6016-T4 alloy plates using a rotational rate of 1120 rpm and a traverse speed of 320 mm/min. They also report a quite high joint efficiency value of 82% [168].

In a recent work, Zhao et al. demonstrated that FSW can be successfully used to produce AA6013-T6 alloy T-joints in two configurations for skin and stringer applications, namely T-lap and T-butt-lap joints [169]. They produced defect-free FS-welded T-lap and T-butt-lap joints by employing a rotational rate of 1000 rpm and welding speeds of 100 mm/min and 200 mm/min respectively. They also report that the T-lap joints welded with die radii of 3 mm exhibited higher strength than those with die radii of 2 mm.

As in the case of Al-Cu alloys, the heat input applied to the workpiece during FSW and the initial strength (temper condition) of the alloy prior to FSW are the main factors that greatly determine the joint performances achieved in these alloys by FSW. The strength loss is usually higher when the initial strength of the alloy is higher. The strength loss occurring during FSW is similar to those experienced in Al-Cu alloys. The reason for this is the dissolution and/or coarsening of strengthening precipitates within the weld region. Moreover, the plate thickness also plays an important role in FSW of Al-Mg-Si as in the case of Al-Cu alloys. As seen from Table 3, as the plate thickness increases, the joint efficiency value somewhat decreases. Finally, it is worth noting that the heat input achieved during FSW must be kept as low as possible for optimum joint efficiency.

4.2.7. Al-Zn-Mg-Cu alloys

As previously pointed out, 7xxx series Al alloys are widely used in aerospace applications. These alloys exhibit weldability similar to 2xxx series Al alloys and they are difficult to fusion-weld—particularly AA7075 alloy. Thus, even FSW as a solid-state welding technique causes a significant strength loss in the weld nugget due to the dissolution and/or coarsening of strengthening precipitates. There are several publications in the open literature reporting a strength loss taking place in the weld nugget of FS-welded 7xxx series alloy joints, although fine grains are recrystallized. For instance, Jata et al. studied FS-weldability of 6.35 mm-thick AA7050-T7451 alloy plates by employing a rotational rate of 400 rpm and a travel speed of 120 mm/min and reported that fine recrystallized grains (i.e. 1–10 microns) evolved in the weld nugget after FSW [170]. They also reported a joint efficiency of 77%. Similarly, Pao et al. also conducted FSW of the same alloy (the thickness being the same) by employing similar weld parameters (rotational rate = 400 rpm and weld speed = 100 mm/min). They also report the same joint efficiency value of 77% [171]. In another work, Su et al. conducted detailed TEM investigations to understand the material softening in the weld region of the FS-welded 6.35 mm-thick AA7050-T651 alloy joints produced using a rotational rate of 350 rpm and a travel speed of 15 mm/min and observed that the strengthening precipitates actually redissolve in both TMAZ and dynamically-recrystallized zone (DXZ) regions, leading to the loss of strength [172]. Similarly, Reynolds et al. also studied the FS-weldability of 6.4 mm-thick AA7050-T7451 alloy plates using various rotational rates and travel speeds; they also observed a significant hardness decrease in the weld mugget and a W-type hardness profile [173]. In a more recent work, Zhou et al. produced FS-welds of 5 mm-thick AA7050-T7451 alloy plates using a rotational rate of 600 rpm and a weld speed of 100 mm/min; they report that defect-free joints were obtained which exhibited quite high joint efficiency of about 81% [174]. Similarly, Wu et al. also conducted both conventional FSW and SSFSW for joining 6.3 mm-thick AA7050-T7651 alloy plates by employing a constant weld speed of 400 mm/min at a rotational rate of 700 rpm and 1500 rpm respectively [175]. They point out that the joints exhibit U-shaped hardness profile when hardness measurements are done right after the welding and a W-type hardness profile if a sufficient time is allowed to pass, since natural aging in these alloys (7xxx series alloy) significantly recovers the hardness in the weld nugget. They also report relatively high joint efficiency values of 88% and 91% for both conventional FS-welded and SSFS-welded joints respectively.

The FSW process leads to similar joint properties in other 7xxx series alloys such as very difficult-to-fusion-join AA7075 alloy - i.e. significant material softening in the weld region - unless the heat input is not kept sufficiently low due to the redissolution and/or coarsening of strengthening precipitates. For instance, Zhang et al. report a relatively low joint efficiency value of 74% for the FS-welded 6 mm-thick Al-*Zn*-Mg-Cu alloy (in aged condition) joints produced using a rotational rate of 350 rpm and a welding speed of 100 mm/min [176]. Similarly, Rajakumar et al. conducted FSW of 5 mm-thick AA7075-T6 alloy plates using a rotational rate of 1400 rpm and a welding speed of 60 mm/min; they report that a significant strength loss (about 23%) took place, leading to a joint efficiency of about 77%, as seen in Table 3 [177]. On the other hand, İpekoğlu et al. also studied the effect of welding parameters on the joint quality of AA6061-T6 alloy plates using a rotational rate ranging from 750 to 1500 rpm and a weld speed ranging from 100 to 300 mm/min; they report that the highest joint efficiency (82%), which is quite high per se, was exhibited by the joint produced at a rotational rate of 1000 rpm using a traverse speed of 150 mm/min [178]. İpekoğlu et al. also report that a PWHT could further improve the tensile strength of the joint, taking it to the level of that of the base alloy [179]. İpekoğlu et al. also report a relatively high joint performance value of 77% for FS-welded AA6061/AA7075 (both in T6 condition) dissimilar joint produced at a rotational rate of 1500 rpm using a traverse speed of 400 mm/min; they also further report that it was improved up to 88% by a PWHT [180]. A similar joint efficiency value of 85% was also reported by Lim et al. for the FS-welded 4 mm-thick AA7075-T6 alloy joints produced using a rotational rate of 1400 rpm and a weld speed of 400 mm/min (Table 3) [161].

A similar joint efficiency value of 82% was also reported very recently by Bayazid et al. for the FS-welded 5 mm-thick AA7075-T6 alloy joints produced using a rotational rate and a welding speed of 1250 rpm and 31.5 mm/min, respectively (Table 3) [181]. They also report that the strength of the joints could be increased to the level of that of the base material by applying a PWHT. Similarly, Fratini et al. also investigated the FSW of 3 mm-thick AA7075-T6 alloy plates with and without external water cooling during FSW [182]. They obtained a quite high joint efficiency value of 84% for the joint they produced at a rotational rate of 715 rpm and a welding speed of 214 mm/min (Table 3). They also clearly demonstrated that external water-cooling during FSW further increased the joint efficiency value to 88% and thus reduced the material softening by decreasing the heat input. A similar joint efficiency of 87%, was also reported by Lotfi and Nourouzi for the FS-welded 3 mm-thick AA7075-T6 alloy joint produced using a rotational rate of 1050 rpm and a welding speed of 100 mm/min (Table 3) [183]. Fuller et al. also observed a more significant softening in the weld regions of the FS-welded AA7075-T651 and AA7050-T7651 alloys joints [184]. They also investigated the effect of natural aging after FSW and observed that a strength recovery up to the level of the strength of the base material was achieved after natural aging following FSW. Similarly, Li et al. also conducted SSFSW of 5 mm-thick AA7075-T651 alloy plates using a rotational rate of 1500 rpm and a travel speed of 50 mm/min and observed a significant material softening in the weld region, the maximum joint efficiency being about 70% (Table 3) [185].

On the other hand, FSW and SSFSW were carried out by Barbini et al. for the butt joining of dissimilar AA2024-T3 and AA7050-T7651 aluminum alloys with thicknesses of 2 mm; very high joint efficiency values were observed, particularly for the SSFSW joints [186]. The highest tensile strength achieved with the FSW process was 421 MPa, which corresponds to 86.4% of the base material. In comparison, the highest tensile strength for the SSFSW specimens reached 460 MPa with a joint efficiency of 94%. Similarly, Azimzadegan and Serajzadeh also

studied FSW of 5 mm-thick AA7075-T6 alloy plates and conducted several FS-welds of this alloy using a rotational rate ranging from 1000 to 1300 rpm and a welding speed ranging from 40 to 80 mm/min [187]. They also report very high joint efficiency values for the joints, the best joint efficiency being as high as 91%, as was exhibited by the joint produced at a rotational rate of 1300 rpm and a welding speed of 40 mm/min.

In contrast, Srinivasa Rao et al. conducted FSW of thicker (10 and 16 mm-thick) AA7075-T651 alloy plates and report that the best joint efficiencies, namely about 70% and 55%, were obtained from the 10 and 16 mm-thick joints produced using welding parameters of 700 rpm/120 mm/min and 500 rpm/25 mm/min, respectively [188]. These results clearly demonstrate that higher heat inputs are involved in the FSW of thicker plates and thus more significant material softening takes place within the weld nugget, indicating that the plate thickness is an important factor affecting the performance of FS-welded joints of this alloy.

4.3. Microstructure and mechanical properties of welded joints

FSW usually results in the formation of fine equiaxed grains in the SZ of all Al alloys, including high-strength aerospace grades due to dynamic recrystallization resulting from the combined effect of excessive plastic deformation and temperature. Fine grains also evolve in TMAZ. There are several studies in the literature reporting grain refinement in FSW of high-strength heat-treatable Al alloys. For instance, İpekoğlu et al. report that grain refinement occurs in FS-welded AA6061-T6 alloy joints [159,160]. Similarly, İpekoğlu et al. also report that finer grains evolved in the weld region of FS-welded AA7075-T6 alloys joints [178,179]. Grain refinement is also reported in dissimilar FS-welded AA6061-T6 and 7075-T6 joints by İpekoğlu and Çam and dissimilar FS-lap-welded AA5754-H22/AA2024-T3 joints by Bozkurt et al. [180,189]. Çam et al. also observed the evolution of fine grains in the weld region of FS-welded AA6061 alloy joints using a higher strength interlayer [190].

Similarly, grain refinement also takes place in aerospace Al alloys unless the initial grain structure is not extremely fine. For instance, Yang et al. and Yan et al. report that fine grains are formed in the weld nugget of high toughness aerospace Al-Cu alloy, namely AA2524-T351, plates [108,124]. Fig. 15(b–f) shows grain refinement in the weld nugget of FS-welded AA2524-T351 alloy joints. Lower heat inputs during FSW lead to the evolution of finer grains in the weld zone.

Similarly, Cabello Munoz et al. and Peng et al. both report that fine equiaxed grains (a few microns in size) formed in weld nugget of FS-welded Al-Mg-Sc alloy, which is a new-generation aerospace alloy [148,153]. Similar results are also reported by several researchers for Al-Li aerospace alloys, namely AA2050-T34 and AA2198, claiming that fine grains evolved in the weld nugget of the FS-welded joints [109,132,191]. Moreover, Campanile et al. and Hornbuckle et al. also report that grain refinement takes place in the weld nugget of FS-welded Al-Cu-Ag alloys (i.e. AA2139-T8) [126,129].

It may be thought that high mechanical properties are obtained in the weld area of FS-welded high-strength aerospace Al alloys joints as a result of grain refinement. This is true for non-heat-treatable Al alloys which are not heavily cold-worked prior to FSW; in the weld region of these alloys, mechanical properties are even higher than those of the respective base alloys are achieved owing to grain refinement [16]. Moreover, FSW results in some softening of the weld region of these non-heat-treatable alloys when they are cold-worked to a sufficient degree prior to FSW, due to the annealing effect [192]. On the other hand, the strength of high-strength heat-treatable Al alloys arise mainly from the fine strengthening precipitates homogeneously distributed in the matrix alpha phase. FSW results in the dissolution of these precipitates in the SZ and the coarsening and/or dissolution of these strengthening particles in the HAZ regions [16]. Thus, a significant strength loss takes place in the weld region (particularly in the HAZ) of high-strength age-hardened Al alloys after FSW. Table 3 summarizes the mechanical properties of FS-welded high-strength heat-treatable Al alloys. This strength loss may be partly overcome by controlling the welding parameters, so that the heat input is sufficiently low. However, even then, a strength loss is encountered.

New-generation high-strength aerospace alloys, on the other hand, do not exhibit significant strength loss in the weld region after FSW. This is because the strengthening particles in these new-generation high-strength Al alloys resist coarsening and/or dissolution. For instance, the strengthening phase in Al-Mg-Sc and Al-Mg-Sc-Zr alloys is Al_3Sc and $Al_3(Sc,Zr)$, respectively [150,152,155,156]. These precipitates are stable against coarsening for temperatures up to 350 °C; the decomposition temperature can sometimes reach as high as 650 °C. Thus, FSW does not give rise to strength loss in the weld region, since the precipitates resist dissolution and/or coarsening in the SZ and HAZ regions. Similarly, precipitates of the Ω phase forming in new-generation 2xxx series Al-Cu alloys, namely Al-Cu-Ag alloys such as AA2139, instead of θ' (Al_2Cu) phase, exhibit good thermal stability. Hence, the strength loss in the weld region of these alloys after FSW is not as significant as those encountered in conventional high-strength 2xxx series aerospace Al alloys [128,129].

5. Comparison of the two welding processes

Both LBW and FSW can be successfully applied for the joining of high-strength aircraft aluminum alloys. In the case of optimized processes, high joint efficiencies can be achieved for a wide range of structural aluminum alloys (Tables 2 and 3). The differences lie in the microstructure of the joints; as the FSW process is conducted at temperatures under the melting points of the respective materials, higher hardness and strength can be achieved in the SZ (FSW process) in comparison to the hardness and strength in the FZ (LBW process). However, due to the higher heat input, the larger TMAZ + HAZ is present (Fig. 16(c)) in comparison to the HAZ obtained in the case of the laser welding process (Fig. 16(a)). Even in the case of the SSFSW process (Fig. 16(d)), the HAZ width is higher than that of Nd:YAG LBW (Fig. 16(a)) and is much higher than that of the fiber LBW (Fig. 16(b)), with a very narrow beam diameter and a high Rayleigh length. The differences between LBW and FSW are clearly seen in hardness profiles of AA6013 (Fig. 17(a)) and AA7050 (Fig. 17(b)) alloys.

In the case of the structural applications, the low strength in the weld zone (FZ + HAZ in the case of the LBW and HAZ + TMAZ + SZ in the case of the FSW) has to be normally compensated through geometrical reinforcements. As the HAZ + TMAZ + SZ is normally larger than the HAZ + FZ, the width of the reinforcement required for FSW is higher than that for LBW. This can be attributed to the better lightweight potential of LBW in comparison to the FSW, if the joining process is applied in airframe.

The fatigue behavior of typical FS-welded and laser-beam-welded butt joints and T-joints is compared in Fig. 18 [17,62,101,136,193–195]. Welded joints show a level of fatigue strength similar to that of the state-of-the-art riveting. Franchim et al. investigated the fatigue behavior of FS-welded AA2024-T3 butt joints and compared it to the base material specimens notched with a stress concentration $K_t = 2$, which is the case of riveted joint (Fig. 18(a)) [193]. They reported that the fatigue strength of the FS-welded joints is comparable to those of the riveted joints. Due to the reduced fatigue strength, the riveted joints between fuselage structures, typically with three rivet lines, always shows thickness increase in the overlapped regions to compensate the fatigue strength reduction. FS-welded fuselage structures in butt joint show a reduced weight, where at similar reinforcement thickness, the weight reduction can be achieved through the absence of overlapped material and rivets. By using materials with higher specific strength, e.g. Al-Cu-Li alloys AA2198 and AA2196, the fatigue strength of laser-beam-welded AA2198-AA2196 T-joint can even be higher than that of the state-of-the-art riveted AA2024-AA7075

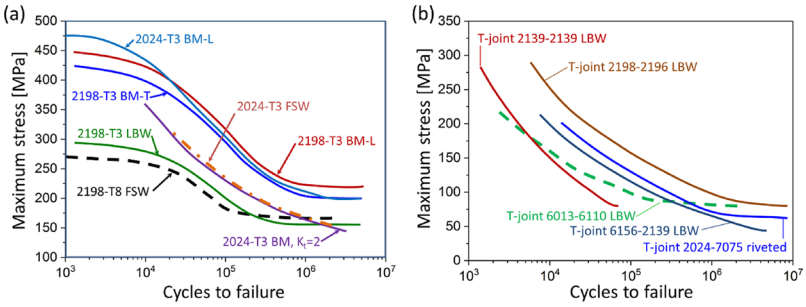

Fig. 18. Fatigue properties of laser-beam-welded and FS-welded (a) butt joints and (b) T-joints (hoop-stress). The data were collected from different sources: Groth et al. (AA2024-T3 BM-L), Franchim et al. (AA2024-T3 FSW and AA2024-T3 BM, fatigue test of notched specimens with a stress concentration K_t = 2), Kashaev et al. (AA2198-T3 BM-L, AA2198-T3 BM-T, AA2198-T3 BM-L), Tavares et al. (AA2198-T8 FSW), Kashaev et al. (T-joint AA2198-T8-AA2196-T8 LBW, T-joint AA2024-AA7075 riveted), Prisco et al. (T-joint AA2139-AA2139 LBW, T-joint AA6156-AA2139 LBW), and Schmidt and Schmidt-Brandecker (T-joint AA6013-AA6110 LBW). Tests were performed at load ratio of 0.1 [194,193,62,136,101,195,17].

(Fig. 18(b)).

The reduced strength of laser-beam-welded and FS-welded joints requires the introduction of reinforcement to compensate the strength decrease in the joint area. As the heat input in the case of the FS-welded joints is even higher than that the laser-beam-welded joints (Fig. 16 and 17), the width of the socketing should be larger for the FSW process. As the reinforcement width results in additional weight, the lightweight potential of the LBW process could be a little higher in comparison to the FSW process.

It is clearly seen from Fig. 18(b) that the fatigue strength of laser-beam-welded AA2198/AA2196 T-joint is determined to be 80 MPa - i.e. 23% higher than the strength of riveted AA2024/AA7075, which is 65 MPa. The laser-beam-welded joints suffer from relatively sharp inconsistencies in the weld zone, where cracks can initiate more easily compared to the riveted joints with relatively large smooth holes. Theoretically, with fatigue loading (R = 0.1) transverse to stringer, AA2198-T8 skin must be 1.625 mm thick to bear the same load as a 2.0 mm AA2024-T3 skin. For 1 m^2, the weight-saving would be 25% without taking the stringers into consideration and calculating with the following densities: AA2198 = 2.619 g/cm^3 and AA2024 = 2.79 g/cm^3 [101].

Two welding processes - LBW and FSW - have been considered to replace extensive riveting used in aircraft structures [7]. Sound joints with high mechanical performance can be achieved through both LBW and FSW. Both technologies are very promising for the joining of aircraft aluminum alloys for structural applications. The FSW process is a promising joining technology for long-distance butt-joints or overlapped joints of aircraft structures [136]. In particular, long-distance butt-joint of high surface quality can be achieved by using the semi-stationary shoulder BT-FSW [141]. However, it is quite challenging to apply the conventional FSW process with the rotating shoulder for the joining of T-joints at the internal corners so as to not damage the outer skin surface, which normally consists of a clad layer for protection against corrosion. SSFSW, which is a novel variant of conventional FSW, employs a stationary shoulder and therefore provides accessibility from the inner corners that can be used for the welding of defect-free T-joints [107]. Notwithstanding the good microstructural and mechanical performance of FS-welded T-joints that can be welded at relatively lower welding speeds (1 m/min, as reported by Li et al.), the FSW process is often uncommon or even not applicable for high-capacity industrial productions because of the difficulties posed by it in welding complex structures and in controlling tolerances [14,107,196]. In contrast, a gap-bridging ability in the case of LBW of thin aluminum sheets was successfully demonstrated by Schultz et al. [197]. Hence, LBW has a clear advantage for T-joints because the joining can be performed from the stringer side, thus leaving the skin surface undamaged.

6. Damage-tolerance behavior of welded integral structures

The qualification of LBW and FSW technologies requires comprehensive tests to meet the required fatigue and damage-tolerance regulations. Therefore, independent of the joining technology, fatigue and residual strength tests have to be performed with coupons, components, and panels during the development of the joining technologies [198,199]. Full-scale tests have to be performed for the final verification and type certification [17].

An example of the development tests performed for laser-beam-welded and FS-welded AA6013-T6 panels is the residual strength test. Vaidya et al. investigated the deformation and fracture behavior of laser-beam-welded and FS-welded AA6013-T6 panels [198]. The deformation in the vicinity of crack under static load was obtained by image evolution techniques (Fig. 19). In both panels - laser-beam-welded and FS-welded - and at all load levels, the plastic deformation remained confined entirely to the lower yield strength weld zone. As a result, the confined plasticity within a narrow weld seam detrimentally affected the load capacity of the panel and reduced the deformation capacity while increasing the crack tip constraint. Therefore, in high-stressed airframe applications, local joint design solutions like the introduction of local thickness increase in the form of so-called “sockets are applied.” The local increase of plate thickness in the weld by providing a “socket” would reduce the stress, thus improving the strength performance of the joints. Depending on other structural requirements, the geometry of the socket (width and height) needs to be optimized so that the growing crack can deviate out of the weld (skin-skin and skin-stringer) and grow further into the skin [198].

How the socketing can improve the residual strength of an integral panel with laser-beam-welded stringers is illustrated in Fig. 20. In

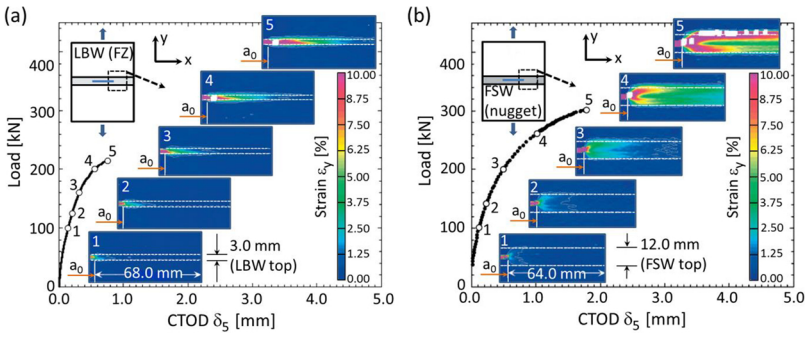

Fig. 19. Evolution of the plastic zone ahead of the crack tip in the center-cracked middle-tension panel with the crack in the weld center (butt-joint). (a) Laser-beam-welded 760 mm wide AA6013-T6 panel and (b) FS-welded AA6013-T6 750 mm wide panel. The value a_0/W = 0.33. According to Vaidya et al. [198]. Reprinted with permission from Wiley.

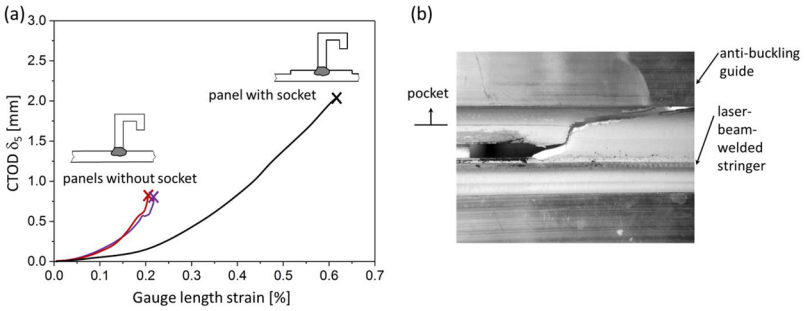

Fig. 20. (a) Effect of local thickness increase (socket) on the crack-driving force curves of the laser-beam-welded skin-stringer panels of AA6013-T6 alloy. The higher deformation capacity in terms of the gauge length strain of the panel with socket, which provides higher damage tolerance in terms of the CTOD due to the fracture path deviation into the skin (pocket). (b) Fracture path deviation from the thicker (socket), lower strength laser-beam-welded T-joint area into the higher strength base material due to the decrease in the local thickness (pocket) during the residual strength test of 400 mm wide AA6013-T6 center-cracked panel under static tensile loading. Depicted and adopted according to Vaidya et al. [198].

regard to the deformation behavior and residual strength, the performance of the panel with socket is significantly higher than that of panels without sockets (Fig. 20(a)). This is seen as an increase of the applied gauge length strain for a given crack-tip opening displacement (CTOD). In the case of the panel with the socket, the crack deviates from the weld into the skin (Fig. 20(b)). The improvement can be achieved if the socket dimensions are properly selected [198].

While the fatigue and fracture mechanical properties of laser-beam-welded 6xxx series aluminum alloys were extensively studied by the end of 20th/beginning of 21st century, recent interest is growing toward the direction of lightweight and high-strength aluminum-lithium or aluminum-magnesium-scandium alloys. In the last few years, some developments have been accomplished for the optimization of the Al-Cu-Li alloy AA2198 in order to achieve higher static strength and better damage-tolerance properties compared to AA2524 (Al-Cu-Mg-alloy developed toward the end of the last century to replace the widely used standard AA2024), such that the resistance to fatigue-crack growth and to fracture in terms of R-curve has significantly improved [7]. Studies pertaining to damage tolerance of welded integral structures of Al-Cu-Li alloys are, however, scarce. Whereas some data are available on FS-welded Al-Cu-Li joints, data on laser-beam-welded stiffened panels are lacking [200–204]. Comprehensive research regarding the damage tolerance behavior of the laser-beam-welded Al-Cu-Li structures is required to fill the gap in structural integrity investigations.

The assessment of residual strength of aircraft structures has been in focus since the launch of NASA's Airframe Structural Integrity Program (ASIP), and several studies have been carried out on mechanical properties of AA2198 base materials (BMs) in regard to fatigue, fatigue-crack propagation, and resistance against crack extension (R-curve) [62,136,200,204–209]. Kashaev et al. investigated the fracture mechanical behavior of AA2198 laser-beam-welded joints as well as laser-beam-welded integral structures [63]. Special emphasis was placed on the characterization of the mechanical properties of the AA2198 for providing an understanding of the fracture mechanisms involved in such material, together with an analysis of the weld and base material interaction. The authors performed a systematic analysis to clarify the deformation and fracture behavior of the laser-beam-welded AA2198 butt joints in different temper conditions. The question raised in their study pertains to how the unavoidable decrease in mechanical properties in the welding zone determines the deformation behavior of the butt joints. The R-curves of the investigated materials are represented in Fig. 21. It was shown that the AA2198, as a third-generation Al-Li alloy, offers better resistance against fracture than the well-known AA2024 alloy, even though AA2198 is known as a material with a relatively lower ductile fracture behavior. It was shown that it is possible to weld AA2198 with good results and that the welds also exhibit a slightly higher fracture resistance than AA2024 base material.

From the structural integrity point of view, cracks initiated and propagated along the stringer in the airframe structure are less critical than cracks that can propagate into a direction transverse to the stringer. If the crack growth is transverse to the stringer, the stringer can fail, which in turn can cause serious structural problem. Therefore, the investigation of residual strength behavior of welded panels with

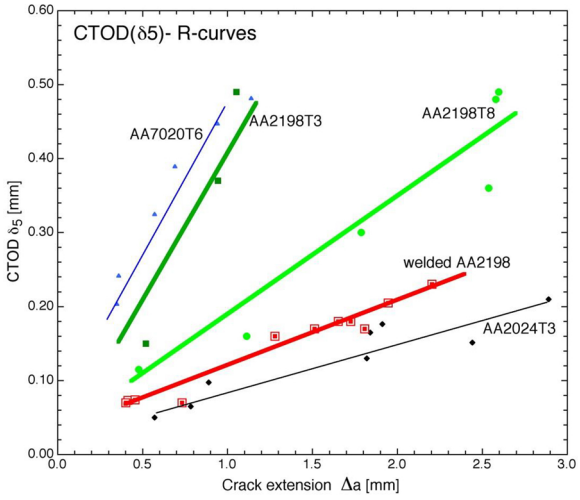

Fig. 21. δ_5-R curves of AA2198-T3 base material, AA2198-T8 base material, laser-beam-welded AA2198-T8, AA2024-T3 base material and AA7020-T6 base material. Reprinted with permission from Emerald [63].

initial cracks in transverse direction to the stringers is of high importance.

The work of Seib aimed to improve the understanding of the failure behavior of FS-welded and laser-beam-welded AA6013-T6 integral structures [94]. The author proposes a verified approach to predict the residual strength of the welded aircraft structure based on the European structural integrity procedure (SINTAP) [210]. As mentioned, the FS-welded and laser-beam-welded joints have yielded strength undermatched welds. Therefore, the accurate prediction methodologies are of high importance for identifying the design under the structural integrity requirements. The investigated methodology in the work of Seib show a strong agreement with experiment results [94].

Moreover, Kashaev et al. investigated the fracture mechanical behavior of laser-beam-welded AA2198 integral structures in order to understand the mechanisms that can influence the crack-driving force [63]. It was demonstrated that the laser-beam-welded four-stringer panels exhibit a residual strength behavior superior to that of the flat base material panel. The results indicate that it should be possible to achieve the required residual strength performance of the laser-beam-welded AA2198 structure by optimizing the structural design. It was experimentally observed that crack-tip blunting and crack branching are two mechanisms that decrease the crack-driving forces. Therefore, the positive effects of crack-tip blunting and crack branching can be taken into account while designing future laser-beam-welded Al-Cu-Li-alloy structures.

Several studies have also investigated the fatigue-crack growth behavior of FS-welded and laser-beam-welded butt joints and integral structures [62,71,136,198,199,211–215]. However, it should be noted that the fatigue-crack propagation behavior is also influenced by the presence of residual stresses as a result of the applied joining process. Geometry of specimens welded, specimens used for investigating the

fatigue-crack propagation behavior, and the applied welding process all have a significant influence on the distribution and amount of residual stresses. Therefore, in the case of fatigue-crack propagation tests of specimens with welded joints, it is difficult to differentiate the effect of residual stresses from the effect of microstructure on the fatigue-crack propagation behavior. Therefore, a conclusion cannot be really drawn about the improved fatigue behavior of an FS-welded specimen in comparison to a laser-beam-welded specimen based on the fatigue-crack propagation test of a small coupon specimen. A test of larger specimens with welded stringers is required because the residual stress state in the real component can be completely different from the residual stress state in a small coupon specimen. A possible relaxation of residual stresses due to cyclic loading also has to be taken into account.

As the aircraft skin panels are subjected to the complex loads acting in orthogonal directions, Richter-Trummer et al. investigated the fatigue-crack growth behavior of FS-welded AA2198 panels subjected to biaxial loads [215]. The authors investigated specimens where the fatigue crack was initiated in the TMAZ of the weld and propagated parallel to the weld joint line. The important result of the study is that the rolling direction of the AA2198 alloy strongly affects the crack growth path. The specimens welded orthogonally to the rolling direction exhibit a shorter fatigue-crack growth life in comparison to the specimens welded parallel to the rolling direction.

Nesterenko reported that the durations of fatigue growth up to the loss of structural integrity (the so-called durations of fatigue damage) in integrally stiffened panels, produced through extrusion process, and riveted panels are practically identical when the initial damage is a skin crack between stringers, provided that the skins of integral and riveted panels are made of the same material [216]. Therefore, for the first estimation of the quality assessment of fatigue-crack propagation behavior of welded integral structures, the behavior of welded structures can be evaluated according to the fatigue-crack propagation in the reference base material specimen. This has been done for the laser-beam-welded AA2198 integral laser-beam-welded four-stringer panels, for example [71]. In the work of Kashaev et al., the fatigue-crack growth behavior of the welded four-stringer panels was found to be comparable to that of the base material [71]. The weld achieved better mechanical properties than commonly expected. This indicates that high-quality LBW of AA2198 can be produced using the developed LBW process, which is suitable for the production of future aircraft structures.

Lanciotti et al. collected test data regarding the fatigue-crack propagation in integrally stiffened two-stringer panels (Fig. 22(a)) produced by the use of high-speed machining, LBW (double-sided successive and single-sided), and FSW (from the skin surface). The results of fatigue-crack propagation test are represented in Fig. 22(b). In this kind of test, with the initial crack placed between the two stringers, the fatigue-crack growth rate decreases when the fatigue crack approaches the stringer and increases rapidly after the stringer is broken [199]. Therefore, the metallurgical conditions in the weld should have less influence on the test results. The difference in the number of cycles required for propagating the crack until the stringer is broken can be explained by the presence of residual stresses, which have a significant retardation effect on the fatigue-crack propagation. The authors measured the residual stresses using the electric strain gauge measurement technique [217]. It is a destructive residual stress measurement, whereby strain gauges are bonded in the area of interest and then the structure is sectioned to allow the relaxation of the residual stress. The residual stresses are obtained by measuring the difference between the final relaxed state and the initial deformed configuration. The results are presented in Fig. 23.

Both welding processes resulted in the generation of residual stresses in the integral welded structures: longitudinal tensile residual stresses in the weld zone (stringer positions in Fig. 23), which are compensated by the presence of compressive residual stresses outside the welded stringers. The longitudinal compressive residual stresses have a significant retardation effect on the fatigue crack propagating in transverse direction. As the high-speed machining should not generate noticeable residual stresses in the integral two-stringer-panel, the fatigue life of the two-stringer panel produced by high-speed machining is lower than those of FS-welded and laser-beam-welded two-stringer panels, where the longitudinal compressive residual stresses retard the fatigue-crack propagation between the welded stringers. The difference in the fatigue-crack propagation behavior between the FS-welded and laser-beam-welded panels can be attributed to the different values of compressive residual stresses in the longitudinal direction in the areas between the stringers, which suppress the fatigue crack propagating in the transverse direction (Fig. 23(a–b), longitudinal residual stresses in the distance between 150 mm and 300 mm). It can be expected that due to the lower heat input in the case of the LBW, the level of tensile residual stresses is lower in comparison to the FSW. Thus, in the case of the LBW, lower compressive residual stresses are present and therefore the retardation effect on the fatigue-crack propagation in the case of the laser-beam-welded two-stringer panel is lower than that of the two-stringer panel produced by FSW.

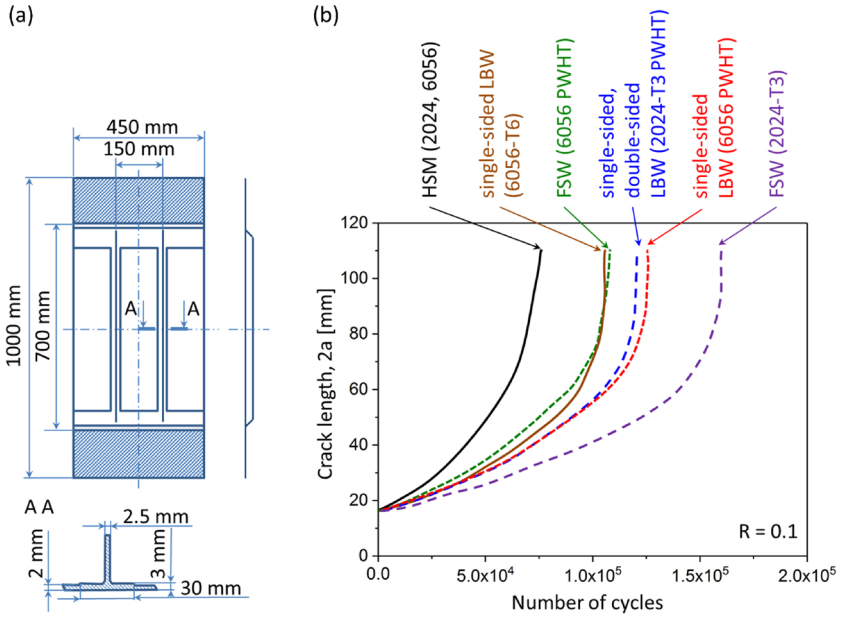

Fig. 22. (a) Geometry of the integral panels with two stringers and (b) the results of fatigue-crack growth test of two-stringer panels fabricated by using high-speed machining (HSM), LBW and FSW. Initial crack was placed in the middle of specimen. Mean curves from various panels tested with the same condition. Depicted and adopted according to Lanciotti et al. [199].

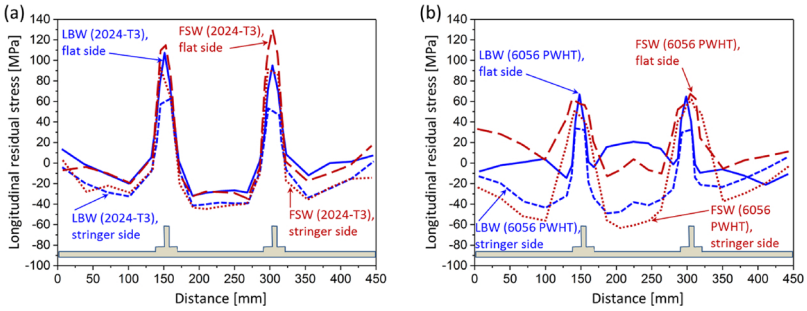

Fig. 23. Longitudinal residual stresses in integral-stiffened two-stringer panels measured using the electric strain gauge measurement technique. Depicted and adopted according to Lanciotti et al. [199].

However, the high-tensile residual stresses in combination with possible welding defect can have a negative effect, such that the crack is initiated in the stringers. Therefore, PWHT after the welding process can be recommended as the level of the tensile residual stresses can be reduced. This is why laser-beam-welded skin-stringer structures of Airbus airplanes are post-weld heat-treated. In the case of welded AA6013 alloy, the LBW is performed in T4 and then laser-beam-welded structure post-weld heat-treated into T6 condition. Similarly, the laser-beam-welded AA6056 in T4 is aged to T76 condition [17].

The fatigue-crack propagation and residual strength behavior of welded panels and riveted or bonded panels are different. In the case of crack growth, the integral structure behaves like a monolithic material. If a crack grows in the skin toward a stringer in a riveted or bonded structure, it just grows in the skin without penetrating the stringer. The stringer stays intact and lowers the stress concentration at the crack tip by carrying a part of the applied load. If a crack grows in the skin toward a welded stringer of an integral structure, the crack branches and the second crack tip grows vertically into the stringer. When the stringer breaks, its stress-bridging effect is lost. This leads to a premature failure of the whole structure. The crack growth rate in the skin is significantly higher and the stringer fails at a lower load due to the active crack tip in the stringer (Fig. 24) [17].

The different crack scenarios and crack growth rates of integral structures compared to the differential structures lead to reduced allowable stress for crack growth and residual strength levels. According to Schmidt and Schmidt-Brandecker, the allowable stress level for residual strength is reduced by approximately 65%, which limits the application of welded structures. Therefore, welded structures have been used so far only in those aircraft parts for which damage tolerance is not the main design criterion, such as the lower fuselage panels, which are under compression in a longitudinal direction to the aircraft fuselage [17].

Before LBW or FSW is widely applied in more sensitive areas of the fuselage construction, it is necessary to achieve significant improvements in fatigue resistance and residual strength of the welded structure. In this context, residual stress-based methods, for example, can be applied to significantly improve the fatigue behavior of the metallic structures [218]. Numerous researchers have already proposed various local engineering techniques such as crenellation (introduction of systematic thickness variations) and laser heating or laser shock peening (introduction of beneficial residual stresses), to further improve the fatigue performance of airframe structures [219–222]. Compared to some other fatigue-crack retardation techniques like bonded crack retarders, which add up additional materials, the crenellation concept, which can be combined with the introduction of residual stresses by laser shock peening or laser heating, is considered to be more advantageous from the point of view of manufacturing and recycling [223,224]. The optimized engineering approaches and residual stress engineering can significantly improve the damage tolerance behavior of welded integral airframe structures [224]. The main challenge to be addressed in the future work will be to develop and optimize technologies in order to increase the residual strength of integral welded structures without increasing their weight.

7. Summary and outlook

Advanced joining techniques like LBW and FSW promise high joint efficiencies and can be used for the realization of aircraft fuselage structures of high-strength aluminum alloys. LBW and FSW are suitable for efficiently joining both precipitation-hardened and naturally hardened aluminum alloys into integral structures with complex geometries. They have the potential to reduce the total weight of the structure. The FSW process is a promising joining technology for long-distance butt joints or overlapped joints of aircraft structures, whereas the high-speed and easily controllable LBW process allows the joining of complex geometrical forms. Therefore, in the long-term, these innovative

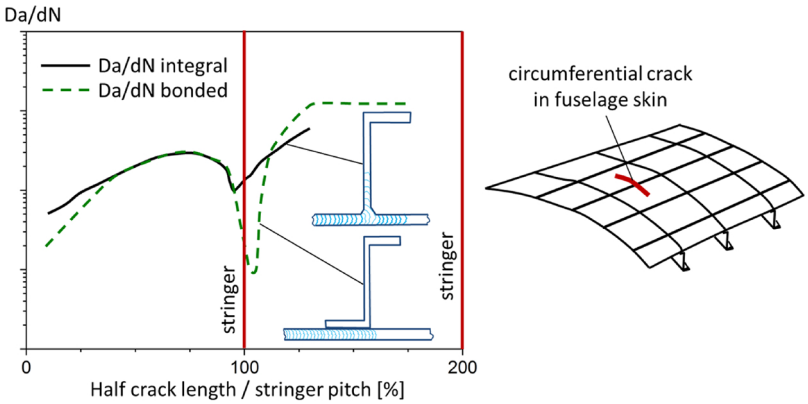

Fig. 24. Crack scenarios and crack growth rates in integral structures and built-up structures. Depicted and adopted according to Schmidt and Schmidt-Brandecker [17].

joining techniques can replace the state-of-the-art riveting design in the aircraft industry and reduce the weight and manufacturing costs of airframe structures. Laser-beam-welded and FS-welded aluminum alloy structures show high integrity in their behavior under mechanical load. It is not very simple to determine which of these joining technologies (LBW or FSW) is preferable for the joining of airframe structures of high-strength aluminum alloys. On the contrary, it is more accurate to say that these two joining techniques actually complement each other instead of competing against each other. They are expected to expand together toward a constructive freedom for the design and realization of lightweight load-bearing structures in near future.

The joining techniques LBW and FSW lead to a type of structure that is close to an integral structural design. This design offers benefits from the weight-reduction and manufacturing-cost points of view. However, there are some concerns regarding the damage tolerance behavior of integral structures in comparison to the differential state-of-the-art riveted design. This is a crucial point in the application of these new techniques and their application at present is limited because of it.

This situation can be radically changed if damage tolerance properties of welded integral structures are improved together with a better understanding of damage mechanisms and main design issues. Since the development and industrial implementation of CO_2 LBW for aluminum airframe fuselage components at Airbus by the end of last century [28], local engineering techniques were further developed, that can significantly improve the fatigue resistance of fuselage structures without introducing extra weight [219–222]. The local engineering techniques are based either on optimization of structural design or introduction of beneficial residual stresses.

The introduction of systematic thickness variations in fuselage skin (crenellation) e.g. through an extrusion process can be considered more advantageous from the point of view of manufacturing and recycling compared with some other fatigue crack retardation techniques, such as bonded crack retarders, which adds additional mass. By applying of systematic thickness variations with introduction of beneficial residual stresses, e.g. through laser heating, a fatigue life extension of 38–77 % in comparison to a reference welded structure can be achieved [224]. One of the promising technique for introducing deep compressive residual stresses in fatigue critical areas is the laser shock peening. In case of the laser shock peening process applied in the vicinity of a welded stringer, an increase of 200–400 % in fatigue lifetime can be achieved [225].

For an industrial implementation of the advanced welding and local modification technologies in fabrication of airframe structures, they have to undergo a certification process [28]. The certification process is preceded by multiple coupon tests (e.g. fatigue crack propagation and residual strength tests on center-crack tension specimens, C(T)-specimens, or middle-crack tension specimens, M(T)-specimens), sub-component tests (e.g. fatigue crack propagation tests, residual strength tests and compression tests (buckling behavior) on panels with several welded stringers) and full-scale structural tests (e.g. barrel test of fuselage section) to verify design failure loads and meet the actual fatigue and damage tolerance regulations and the corresponding advisory circular AC 25.571-1D [226]. After validation of the technologies through the certification process, recommendations can be formulated for the industrial implementation.

Acknowledgements

The authors especially thank their colleagues Dr.-Ing. Josephin Enz and Mr. Dipl.-Ing. Stefan Riekehr from the Helmholtz-Zentrum Geesthacht, Assoc. Prof. Dr. Güven İpekoğlu from the Iskenderun Technical University, and Prof. Dr. Ali Naci Çelik from Abant İzzet Baysal University for their valuable comments and discussions.

References

[1] Chady T. Airbus versus boeing – composite materials: the sky's the limit… Le mauricien magazine. 2013 [accessed 23 October 2017]. http://www.lemauricien.com/article/airbus-versus-boeing-composite-materials-sky-s-limit.
[2] Murphy A, McCune W, Quinn D, Price M. The characterization of friction stir welding process effects on stiffened panel structures. Thin Wall Struct 2007;45(3):339–51.
[3] Starke Jr. EA, Staley JT. Application of modern aluminum alloys to aircraft. Prog Aerosp Sci 1996;32:131–72.
[4] Wilson R, Murphy A, Price MA, Glazebrook C. A preliminary structural design procedure for laser beam welded airframe stiffened panels. Thin Wall Struct 2012;55:37–50.
[5] Alexopoulos ND, Gialos AA, Zeimpekis V, Velonaki Z, Kashaev N, Riekehr S, et al. Laser beam welded structures for a regional aircraft: weight, cost and carbon footprint savings. J Manuf Syst 2016;39:38–52.
[6] Gialos AA, Zeimpekis V, Alexopoulos ND, Kashaev N, Riekehr S, Karanika A. Investigating the impact of sustainability in the production of aeronautical sub-scale components. J Clean Prod 2018;176:785–99.
[7] Pacchione M, Telgkamp J. Proc. 25th International Congress of the Aeronautical Sciences. 2006.
[8] Cao X, Wallace W, Poon C, Immarigeon JP. Research and progress in laser welding of wrought aluminum alloys. I. Laser welding processes. Mater Manuf Proc 2003;18(1):1–22.
[9] Cao X, Wallace W, Poon C, Immarigeon JP, Poon C. Research and progress in laser welding of wrought aluminum alloys. II. Metallurgical microstructures, defects, and mechanical properties. Mater Manuf Proc 2003;18(1):23–49.
[10] Ion JC. Laser beam welding of wrought aluminium alloys. Sci Technol Weld Join 2000;5(5):265–76.
[11] Sánchez Amaya JM, Amaya-Vázquez MR, Botana FJ. Laser welding of light metal alloys: aluminium and titanium alloys. In: Katayama S, editor. Handbook of laser welding technologies. Cambridge: Woodhead Publishing; 2013. p. 215–54.
[12] Oladimeji OO, Taban E. Trend and innovations in laser beam welding of wrought aluminum alloys. Weld World 2016;60(3):415–57.
[13] Hong KM, Shin YC. Prospects of laser welding technology in the automotive industry: a review. J Mater Proc Technol 2017;245:46–69.
[14] Threadgill PL, Leonard AJ, Shercliff HR, Withers PJ. Friction stir welding of aluminium alloys. Int Mater Rev 2009;54(2):49–93.
[15] Çam G, Mıstıkoğlu S. Recent developments in friction stir welding of Al-alloys. J Mater Eng Perform 2014;23(6):1936–53.
[16] Çam G, İpekoğlu G. Recent developments in joining of aluminum alloys. Int J Adv Manuf Technol 2017;91(5-8):1851–66.
[17] Schmidt HJ, Schmidt-Brandecker B. Proc. 18th European Conference on Fracture, Fracture of Materials and Structures from Micro to Macro Scale. 2010.
[18] Eberl F, Gardiner S, Campanile G, Surdon S, Venmans M, Prangnell P. Proc. Aeronautics days 2006, Aerodays 2006, Vienna. 2006.
[19] Prasad NE, Gokhale AA, Wanhill RJH. Merken S, Freeland J, editors. Aluminium-lithium alloys. Oxford: Elsevier Inc; 2014.
[20] Aleris International Inc. Aerospace aluminium AA5028 AlMgSc - the strong lightweight. 2015 [accessed 18 October 2017]. https://www.aleris.com/wp-content/uploads/2016/02/AL-2342_012-Aktualisierung-BR-AlMgSc-2015-06-03-WEB.pdf.
[21] Schubert E, Klassen M, Zerner I, Walz C, Sepold G. Light weight structures produced by laser beam joining for future applications in automobile and aerospace industry. J Mater Process Technol 2001;115:2–8.
[22] Rath W. CO_2 laser-workhorse for industrial manufacturing. Laser Technol J 2009;6(3):32–8.
[23] Behler K, Berkmanns J, Ehrhardt A, Frohn W. Laser beam welding of low weight materials and structures. Mater Des 1997;18(4-6):261–7.
[24] Quintino L, Miranda R, Dilthey U, Iordachescu D, Banasik M, Stano S. Laser welding of structural aluminium. In: Moreira PMGP, da Silva LFM, de Castro PMST, editors. Advanced structured materials, vol. 5: structural connections for lightweight metallic structures. Berlin, Heidelberg: Springer-Verlag; 2012. p. 33–57.
[25] Verhaeghe G. Laser welding automotive steel and aluminium. Make it with lasers™ workshop. 2000 Great Abington, UK http://www.twi-global.com/technical-knowledge/published-papers/laser-welding-automotive-steel-and-aluminium-july-2000/ [accessed 18 October 2017].
[26] Katayama S. Katayama S, editor. Handbook of laser welding technologies. Cambridge: Woodhead Publishing Ltd, UK; 2013.
[27] Badini C, Pavese M, Fino P, Biamino S. Laser beam welding of dissimilar aluminium alloys of 2000 and 7000 series: effect of post-welding thermal treatments on T joint strength. Sci Technol Weld Join 2009;14(6):484–92.
[28] Schmidt HJ, Schmidt-Brandecker B, Ohrloff N, Fleischer T. Rudd JL, Bader RM, editors. Proc. of the 20th symposium of the International committee on aeronautical fatigue, ICAF 1999 - structural integrity for the next millennium, Vol. 1. Bellevue: Electronic Print Imaging Corp; 1999. p. 537–52.
[29] Curcio F, Daurelio G, Memola Capece Minutolo F, Caiazzo F. On the welding of different materials by diode laser. J Mater Process Technol 2006;175(1-3):83–9.
[30] Giesen A, Hügel H, Voss A, Wittig K, Brauch U, Opower H. Scalable concept for diode-pumped high-power solid-state lasers. Appl Phys B 1994;58(5):365–72.
[31] Brockmann R, Havrilla D. Proc. of the SPIE 7193, Solid State Lasers XVII: Technology and Devices. 2009.
[32] Poprawe R. Lasertechnik für die Fertigung. Berlin, Heidelberg: Springer-Verlag; 2005.

[33] www.trumpf.com [accessed 23 October 2017].
[34] www.ipgphotonics.com [accessed 23 October 2017].
[35] Braun R. Nd: YAG laser butt welding of AA6013 using silicon and magnesium containing filler powders. Mater Sci Eng A 2006;A426:250–62.
[36] Han B, Tao W, Chen Y. New technique of skin embedded wire double-sided laser beam welding. Opt Laser Technol 2017;91:185–92.
[37] Dittrich D, Standfuss J, Liebscher J, Brenner B, Beyer E. Laser beam welding of hard to weld Al alloys for a regional aircraft fuselage design – first results. Phys Procedia 2011;12:113–22.
[38] Enz J, Khomenko V, Riekehr S, Ventzke V, Huber N, Kashaev N. Single-sided laser beam welding of a dissimilar AA2024-AA7050 T-joint. Mater Des 2015;76:110–6.
[39] Enz J, Riekehr S, Ventzke V, Huber N, Kashaev N. Laser weldability of high-strength Al-Zn alloys and its improvement by the use of an appropriate filler material. Metall Mater Trans A 2016;47A:2830–41.
[40] Enz J, Riekehr S, Ventzke V, Huber N, Kashaev N. Fibre laser welding of high alloyed Al–Zn–Mg–Cu alloys. J Mater Process Technol 2016;237:155–62.
[41] Enz J, Kumar M, Riekehr S, Ventzke V, Huber N, Kashaev N. Mechanical properties of laser beam welded similar and dissimilar aluminum alloys. J Manuf Process 2017;29:272–80.
[42] Ahn J, Chen L, He E, Davies CM, Dear JP. Effect of filler metal feed rate and composition on microstructure and mechanical properties of fibre laser welded AA 2024-T3. J Manuf Process 2017;25:26–36.
[43] Ahn J, He E, Chen L, Dear J, Davies C. The effect of Ar and He shielding gas on fibre laser weld shape and microstructure in AA 2024-T3. J Manuf Process 2017;29:62–73.
[44] Alfieri V, Caiazzo F, Sergi V. Autogenous laser welding of AA 2024 aluminium alloy: process issues and bead features. Procedia CIRP 2015;33:406–11.
[45] Wang L, Wei Y, Zhao W, Zhan X, She L. Effects of welding parameters on microstructures and mechanical properties of disk laser beam welded 2A14-T6 aluminum alloy joint. J Manuf Process 2018;31:240–6.
[46] Daneshpour S, Koçak M, Langlade S, Horstmann M. Effect of overload on fatigue crack retardation of aerospace Al-alloy laser welds using crack-tip plasticity analysis. Int J Fatigue 2009;31:1603–12.
[47] Carrarin C. Approach of autogenous fibre-laser beam welding of Al-Cu alloys. Master thesis. Rome, Italy: Sapienza University of Rome; 2015.
[48] Janasekaran S, Jamaludin MF, Muhamad MR, Yusof F, Shukor MHA. Autogenous double-sided T-joint welding on aluminum alloys using low power fiber laser. Int J Adv Manuf Technol 2017;90(9-12):3497–505.
[49] Kutsuna M, Suzuki J, Kimura S, Yamaoka H. CO2 laser welding of A2219, A5083 and A6063 aluminium alloys. Weld World 1993;31(2):126–35.
[50] Weston JP, Jones IA, Wallach ER. Proc. of the 6th International Conference on Welding and Melting by Electron and Laser Beams. 1998.
[51] Kimura S, Kubo T, Makino Y, Honda K, Sugiyama S. IIW document IV-565-91. Vienna, Austria: International Institute of Welding; 1991.
[52] Haynes MJ, Ganglof RP. Elevated temperature fracture toughness of Al-Cu-Mg-Ag sheet: characterization and modeling. Metall Mater Trans A 1997;28A:1815–29.
[53] Bakavos D, Prangnell PB, Bes B, Eberl F. The effect of silver on microstructural evolution in two 2XXX series Al-alloys with a high Cu:Mg ratio during aging to a T8 temper. Mater Sci Eng A 2008;A491:214–23.
[54] Kermanidis AT, Zervaki AD, Haidemenopoulos GN, Pantelakis SG. Effects of temper condition and corrosion on the fatigue performance of a laser-welded Al-Cu-Mg-Ag (2139). alloy. Mater Des 2010;31(1):42–9.
[55] Zervaki AD, Haidemenopoulos GN, Lambrakos SG. Trends in welding research 2012. Proc. of the 9th International Conference 2012:117–24.
[56] Viscusi A, Leitão C, Rodrigues DM, Scherillo F, Squillace A, Carrino L. Laser beam welded joints of dissimilar heat treatable aluminium alloys. J Mater Process Technol 2016;236:48–55.
[57] Kostrivas A, Lippold JC. Weldability of Li bearing aluminium alloys. Int Mater Rev 1999;44:217–37.
[58] Enz J, Riekehr S, Ventzke V, Kashaev N, Huber N. Process optimisation for the laser beam welding of high-strength aluminium-lithium alloys (in German). Schweißen und Schneiden 2012;64(8):482–5.
[59] Enz J, Riekehr S, Ventzke V, Kashaev N. Influence of the local chemical composition on the mechanical properties of laser beam welded Al-Li alloys. Phys. Procedia 2012;39:51–8.
[60] Lippold JC, Lin W. Weldability of commercial Al-Cu-Li alloys. Mater Sci Forum 1996;217-222:1685–90.
[61] Jan R, Howell PR, Martukanitz RP. Smartt HB, editor. Proc. of 4th International Conference on Trends in Welding Research. 1995. p. 329–34.
[62] Kashaev N, Chupakhin S, Enz J, Ventzke V, Groth A, Horstmann M, et al. Fatigue and fatigue crack propagation of laser beam-welded AA2198 joints and integral structures. Adv Mater Res 2014;891-892:1457–62.
[63] Kashaev N, Riekehr S, Erdmann K, Carvalho AA, Nurgaliev M, Alexopoulos N, et al. Fracture mechanical behaviour of laser beam-welded AA2198 butt joints and integral structures. Int J Struct Integr 2015;6(6):787–98.
[64] Zhang X, Huang T, Yang W, Xiao R, Liu Z, Li L. Microstructure and mechanical properties of laser beam-welded AA2060 Al-Li alloy. J Mater Process Technol 2016;237:301–8.
[65] Zhang X, Yang W, Xiao R. Microstructure and mechanical properties of laser beam welded Al–Li alloy 2060 with Al–Mg filler wire. Mater Des 2015;88:446–50.
[66] Tian Y, Robson JD, Riekehr S, Kashaev N, Wang L, Lowe T, et al. Process optimization of dual-laser beam welding of advanced Al-Li alloys through hot cracking susceptibility modeling. Metall Mater Trans A 2016;47A:3533–44.
[67] Han B, Tao W, Chen Y, Li H. Double-sided laser beam welded T-joints for aluminum-lithium alloy aircraft fuselage panels: effects of filler elements on microstructure and mechanical properties. Opt Laser Technol 2017;93:99–108.
[68] Enz J, Carrarin C, Riekehr S, Ventzke V, Kashaev N. Hot cracking behaviour of an autogenously laser welded Al-Cu-Li alloy. Int J Adv Manuf Technol 2018;95(1-4):299–310.
[69] Ning J, Zhang L-J, Bai Q-L, Yin X-Q, Niu J, Zhang J-X. Comparison of the microstructure and mechanical performance of 2A97 Al-Li alloy joints between autogenous and non-autogenous laser welding. Mater Des 2017;120:144–56.
[70] Fu B, Qin G, Meng X, Ji Y, Zou Y, Lei Z. Microstructure and mechanical properties of newly developed aluminum-lithium alloy 2A97 welded by fiber laser. Mater Sci Eng A 2014;A617:1–11.
[71] Kashaev N, Enz J, Horstmann M, Groth A, Ventzke V, Riekehr S, et al. Proc. of the 27th Symposium of the International Committee on Aeronautical Fatigue and Structural Integrity. 2013. p. 737–49.
[72] Tempus G. Materials day - Werkstoffe für Transport und Verkehr, Zurich, Switzerland. 1999 https://www.ethz.ch/content/dam/ethz/special-interest/matl/department/ news/materialsday/materialsday-2001-tempus.pdf, (accessed 30 October 2017).
[73] Fridlyander IN. Memoirs Generating Aerospace and Nuclear Energy Technologies from Aluminum Alloys, 2nd ed. (in Russian) Nauka, Moscow, Russia 2006.
[74] Melzer C. Eigenschaften und metallkundliche Untersuchungen von scandiumhaltigen Laserstrahl- und WIG-Schweißnähten an Aluminium-Lithium-Legierungen, Doctor thesis (in German). Clausthal, Germany: Clausthal University of Technology; 1997.
[75] Rendigs K-H. Aluminium structures used in aerospace - Status and prospects. Mater Sci Forum 1997;242:11–24.
[76] Ovsyannikov BV, Zamyatin VM, Smirnov VL, Myshnikov VS. Thermal and microstructural analysis of Al-Mg-Li alloys (in Russian). Alloys 2008;4:22–8.
[77] https://viam.ru/en; (Accessed 30 October 2017).
[78] Shi Y, Zhonga F, Li X, Gong S, Chen L. Effect of laser beam welding on tear toughness of a 1420 aluminum alloy thin sheet. Mater Sci Eng A 2007;A465:153–9.
[79] Zhuang L, Meng Q-S, Chen L. Laser welding of 1420 aluminium-lithium alloys under the keyhole regime. Laser Eng 2016;35(5-6):303–14.
[80] Yan J, Gao M, Li G, Zhang C, Zeng X, Jiang M. Microstructure and mechanical properties of laser-MIG hybrid welding of 1420 Al-Li alloy. Int J Adv Manuf Technol 2013;66(9-12):1467–73.
[81] Santos TG, Miranda RM, Vilaça P, Teixeira JP, dos Santos J. Microstructural mapping of friction stir welded AA 7075-T6 and AlMgSc alloys using electrical conductivity. Sci Technol Weld Join 2011;16(7):630–5.
[82] http://www.twi-global.com/industries/aerospace/joining-of-airframe-structures/laser-beam-welding-of-airframe-structures/; (Accessed 7 November 2017).
[83] Lenczowski B. Innovative aluminium lightweight technologies for aerospace applications. Aachen, Germany: AMAP Colloquium; 2016.
[84] Metallurgist, http://www.france-metallurgie.com/31923/; 2016 (Accessed 7 November 2017).
[85] Palm F, Leuschner R, Schubert T. Scalmalloy® - a unique high strength AlMgSc type material solution prepares the path towards eco-efficient aerospace applications Aeromat 2009, Dayton, USA 2009.
[86] Polmear IJ. Light alloys. 4th ed. Amsterdam, The Netherlands: Elsevier Ltd.; 2005.
[87] Lampman S. Lampman S, editor. Weld integrity and performance. Materials Park, USA: ASM International; 1997. p. 283–309.
[88] Fabrègue D, Deschamps A, Suéry M. Influence of the silicon content on the mechanical properties of AA6xxx laser welds. Mater Sci Eng A 2009;A506(1–2):157–64.
[89] Pakdil M, Çam G, Koçak M, Erim S. Microstructural and mechanical characterization of laser beam welded AA6056 Al-alloy. Mater Sci Eng A 2011;A528(24):7350–6.
[90] Ventzke V, Riekehr S, Horstmann M, Haack P, Kashaev N. One-sided Nd:YAG laser beam welding for the manufacture of T-joints made of aluminium alloys for aircraft construction. Weld Cut 2014;13(4):245–9.
[91] Wang XJ, Lu FG, Wang HP, Cui HC, Tang XH, Wu YX. Experimental and numerical analysis of solidification cracking behaviour in fibre laser welding of 6013 aluminium alloy. Sci Technol Weld Join 2015;20(1):58–67.
[92] Oliveira AC, Siqueira RHM, Riva R, Lima MSF. One-sided laser beam welding of autogenous T-joints for 6013-T4 aluminium alloy. Mater Des 2015;65:726–36.
[93] Zhang L, Li X, Nie Z, Huang H, Sun J. Microstructure and mechanical properties of a new Al–Zn–Mg–Cu alloy joints welded by laser beam. Mater Des 2015;83:451–8.
[94] Seib E. Residual strength analysis of laser beam and friction stir welded aluminium panels for aerospace applications, Doctor thesis. Hamburg, Germany: Hamburg University of Technology; 2006.
[95] Daneshpour S, Kocak M, Bayraktar FS, Riekehr S. Damage tolerance analyses of laser welded “Skin-Clip” joints for aerospace applications. Weld World 2009;53(3-4):R90–8.
[96] Kou S. Welding metallurgy and weldability of high strength aluminum alloys. New York, USA: Welding Research Council; 1986.
[97] Gutierrez A, Lippold JC. A proposed mechanism for equiaxed grain formation along the fusion boundary in aluminum-copper-lithium alloys. Weld Res Suppl 1998;77(3):123s–32s.
[98] Edwards GA, Stiller K, Dunlop GL, Couper MJ. The precipitation sequence in Al–Mg–Si alloys. Acta Mater 1998;46(11):3893–904.
[99] Esmaeili S, Wang X, Lloyd DJ, Poole WJ. On the precipitation-hardening behavior

of the Al-Mg-Si-Cu alloy AA6111. Metall Mater Trans A 2003;34A(3):751–63.
[100] Yang JG, Sung SH, Chen CS, Tan AH. Study of microstructural and mechanical properties of weld heat affected zones of 2024-T3 aluminium using gleeble simulation. Mater Sci Technol 2011;27(1):357–65.
[101] Kashaev N, Riekehr S, Falck R, Enz J, Tian Y, Robson JD, et al. Proc. of the 5th CEAS Air & Space Conference—Challenges in European Aerospace. 2015. Paper no. 015.
[102] Çam G. Friction stir welded structural materials: beyond Al-alloys. Int Mater Rev 2011;56(1):1–48.
[103] Thomas WM, Nicholas ED, Needham JC, Murch MG, Temple-Smith P, Dawes CJ. International patent application PCT/GB92/02203 and GB patent application 9125978.8. London, UK: UK Patent Office; 1991.
[104] Çam G, İpekoğlu G, Küçükömeroğlu T, Aktarer SM. Applicability of friction stir welding to steels. J Achiev Mater Manuf Eng 2017;80(2):65–85.
[105] Toumpis A, Galloway A, Cater S, McPherson N. Development of a process envelope for friction stir welding of DH36 steel - a step change. Mater Des 2014;62:64–75.
[106] Tavares SMO. Design and advanced manufacturing of aircraft structures using FSW, Doctor thesis. Porto, Portugal: University of Porto; 2011.
[107] Li D, Yang X, Cui L, He F, Zhang X. Fatigue property of stationary shoulder friction stir welded additive and non-additive T joints. Sci Technol Weld Join 2015;20(8):650–4.
[108] Yan J, Sutton MA, Reynolds AP. Process-structure-property relationships for nugget and heat affected zone regions of AA2524-T351 friction stir welds. Sci Technol Weld Join 2005;10(6):725–36.
[109] Wang FF, Li WY, Shen J, Hu SY, dos Santos JF. Effect of tool rotational speed on the microstructure and mechanical properties of bobbin tool friction stir welding of Al–Li alloy. Mater Des 2015;86:933–40.
[110] Cui L, Yang X, Zhou G, Xu X, Shen Z. Characteristics of defects and tensile behaviors on friction stir welded AA6061-T4 T-joints. Mater Sci Eng A 2012;A543:58–68.
[111] Penalva ML, Otaegi A, Pujana J, Rivero A. AIP Conf Proc 2009;118(1). https://doi.org/10.1063/1.3273630.
[112] Cui L, Yang X, Xie Y, Hou X, Song Y. Process parameter influence on defects and tensile properties of friction stir welded T-joints on AA6061-T4 sheets. Mater Des 2013;51:161–74.
[113] Donati L, Tomesani L, Morri A. Structural T-joint produced by means of friction stir welding (FSW) with filling material. Int J Mater Form 2009;2(1):295–8.
[114] Xu Z, Li Z, Lv Z, Zhang L. Effect of welding speed on joint features and lap shear properties of stationary shoulder FSLWed Alclad 2024 Al alloy. J Mater Eng Perform 2017;26(3):1358–64.
[115] Niu P, Li W, Zhang Z, Yang X. Global and local constitutive behaviors of friction stir welded AA2024 joints. J Mater Sci Technol 2017;33(9):987–90.
[116] Dalle Donne C, Braun R, Staniek G, Jung A, Kaysser WA. Mikrostrukturelle, mechanische und korrosive Eigenschaften reibrührgeschweißter Stumpfnähte in Aluminiumlegierungen (in German). Mat.-wiss u Werkstofftech 1998;29(10):609–17.
[117] Khodir SA, Shibayanagi T, Naka M. Microstructure and mechanical properties of friction stir welded AA2024-T3 aluminum alloy. Mater Trans 2006;47(1):185–93.
[118] Zhang H, Wang M, Zhang X, Yang G. Microstructural characteristics and mechanical properties of bobbin tool friction stir welded 2A14-T6 aluminum alloy. Mater Des 2015;65:559–66.
[119] Li JQ, Liu HJ. Effects of tool rotation speed on microstructures and mechanical properties of AA2219-T6 welded by the external non-rotational shoulder assisted friction stir welding. Mater Des 2013;43:299–306.
[120] Liu HJ, Li JQ, Duan WJ. Friction stir welding characteristics of 2219-T6 aluminum alloy assisted by external non-rotational shoulder. Int J Adv Manuf Technol 2013;64:1685–94.
[121] Bala Srinivasan P, Arora KS, Dietzel W, Pandey S, Schaper MK. Characterisation of microstructure, mechanical properties and corrosion behaviour of an AA2219 friction stir weldment. J Alloy Compd 2010;492(1-2):631–7.
[122] Sree Sabari S, Malarvizhi S, Balasubramanian V. Influences of tool traverse speed on tensile properties of air cooled and water cooled friction stir welded AA2519-T87 aluminium alloy joints. J Mater Process Technol 2016;237:286–300.
[123] Xu W, Liu J, Luan G, Dong C. Microstructure and mechanical properties of friction stir welded joints in 2219-T6 aluminum alloy. Mater Des 2009;30(9):3460–7.
[124] Yang B, Yan J, Sutton MA, Reynolds AP. Banded microstructure in AA2024-T351 and AA2524-T351 aluminum friction stir welds: part I. Metallurgical studies. Mater Sci Eng A 2004;A364(1-2):55–65.
[125] Liu HJ, Zhang HJ, Yu L. Effect of welding speed on microstructures and mechanical properties of underwater friction stir welded 2219 aluminum alloy. Mater Des 2011;32(3):1548–53.
[126] Hornbuckle BC, Murdoch HA, Roberts AJ, Kecskes LJ, Tschopp MA, Doherty KJ, et al. Property mapping of friction stir welded Al-2139 T8 plate using site specific shear punch testing. Mater Sci Eng A 2017;A682:192–201.
[127] Grujicic M, Arakere G, Yen CF, Cheeseman BA. Computational investigation of hardness evolution during friction-stir welding of AA5083 and AA2139 aluminum alloys. J Mater Eng Perform 2011;20(7):1097–108.
[128] Grujicic M, Snipes J, Ramaswami S, Yen CF. Experimental characterization and numerical analysis of the weld-region material in friction stir welded thick AA2139-T8 plates. Int J Struct Integr 2016;7(3):429–54.
[129] Campanile G, Prisco A, Squillace A, Bitondo C, Dionoro G, Buonadonna P, et al. FSW of AA2139-T8 butt joints for aeronautical applications. Proc Ins Mech Eng L-J Mater Des Appl 2011;225(2):87–101.
[130] Velotti C, Astarita A, Buonadonna P, Dionoro G, Langella A, Paradiso V, et al. FSW of AA 2139 plates: influence of the temper state on the mechanical properties. Key Eng Mater 2013;554-557:1065–74.
[131] Nikulin I, Malopheyev S, Kipelova A, Kaibyshev R. Effect of SPD and friction stir welding on microstructure and mechanical properties of Al-Cu-Mg-Ag sheets. Mater Lett 2012;66(1):311–3.
[132] Li W, Jiang R, Zhang Z, Ma Y. Effect of rotation speed to welding speed ratio on microstructure and mechanical behavior of friction stir welded aluminum-lithium alloy joints. Adv Eng Mater 2013;15(11):1051–8.
[133] Ma YE, Xia ZC, Jiang RR, Li WY. Effect of welding parameters on mechanical and fatigue properties of friction stir welded 2198 T8 aluminum–lithium alloy joints. Eng Fract Mech 2013;114:1–11.
[134] Shukla AK, Baeslack WA. Study of process/structure/property relationships in friction stir welded thin sheet Al-Cu-Li alloy. Sci Technol Weld Join 2009;14(4):376–87.
[135] Steuwer A, Dumont M, Altenkirch J, Birosca S, Deschamps A, Prangnell PB, et al. A combined approach to microstructure mapping of an Al-Li AA2199 friction stir weld. Acta Mater 2011;59(8):3002–11.
[136] Tavares SMO, dos Santos JF, de Castro PMST. Friction stir welded joints of Al-Li alloys for aeronautical applications: butt-joints and tailor welded blanks. Teor Apl Fract Mech 2013;65:8–13.
[137] Le Jolu T, Morgeneyer TF, Gourgues-Lorenzon AF. Effect of joint line remnant on fatigue lifetime of friction stir welded Al-Cu-Li alloy. Sci Technol Weld Join 2010;15(8):694–8.
[138] Le Jolu T, Morgeneyer TF, Denquin A, Sennour M, Laurent A, Besson J, et al. Microstructural characterization of internal welding defects and their effect on the tensile behavior of FSW joints of AA2198 Al-Cu-Li alloy. Metall Mater Trans A 2014;45A(12):5531–44.
[139] Gao C, Zhu Z, Han J, Li H. Correlation of microstructure and mechanical properties in friction stir welded 2198-T8 Al–Li alloy. Mater Sci Eng A 2015;A639:489–99.
[140] Rao J, Payton EJ, Somsen C, Neuking K, Eggeler G, Kostka A, et al. Where does the lithium go? A study of the precipitates in the stir zone of a friction stir weld in a Li-containing 2xxx series Al alloy. Adv Eng Mater 2010;12(4):298–303.
[141] Goebel J, Reimann M, Norman A, dos Santos JF. Semi-stationary shoulder bobbin tool friction stir welding of AA2198-T851. J Mater Process Technol 2017;245:37–45.
[142] Sidhar H, Mishra RS, Reynolds AP, Baumann JA. Impact of thermal management on post weld heat treatment efficacy in friction stir welded 2050-T3 alloy. J Alloy Compd 2017;722:330–8.
[143] Pouget G, Reynolds AP. Residual stress and microstructure effects on fatigue crack growth in AA2050 friction stir welds. Int J Fatigue 2008;30(3):463–72.
[144] Cai B, Zheng ZQ, He DQ, Li SC, Li HP. Friction stir weld of 2060 Al-Cu-Li alloy: microstructure and mechanical properties. J Alloy Compd 2015;649:19–27.
[145] Wei S, Hao C, Chen J. Study of friction stir welding of 01420 aluminum-lithium alloy. Mater Sci Eng A 2007;452-453:170–7.
[146] Sidhar H, Martinez NY, Mishra RS, Silvanus J. Friction stir welding of Al-Mg-Li 1424 alloy. Mater Des 2016;106:146–52.
[147] Lapasset G, Girard Y, Campagnac MH, Boivin D. Investigation of the microstructure and properties of a friction stir welded Al-Mg-Sc alloy. Mater Sci Forum 2003;426-432:2987–92.
[148] Cabello Muñoz A, Rückert G, Huneau B, Sauvage X, Marya S. Comparison of TIG welded and friction stir welded Al-4.5Mg-0.26Sc alloy. J Mater Process Technol 2008;197(1-3):337–43.
[149] Besel Y, Besel M, Mercado UA, Kakiuchi T, Hirata T. Influence of local fatigue damage evolution on crack initiation behavior in a friction stir welded Al-Mg-Sc alloy. Int J Fatigue 2017;99:151–62.
[150] Sauvage X, Dédé A, Cabello Muñoz A, Huneau B. Precipitate stability and recrystallisation in the weld nuggets of friction stir welded Al-Mg-Si and Al-Mg-Sc alloys. Mater Sci Eng A 2008;A491(1-2):364–71.
[151] Malopheyev S, Kulitskiy V, Mironov S, Zhemchuzhnikova D, Kaibyshev R. Friction-stir welding of an Al-Mg-Sc-Zr alloy in as-fabricated and work-hardened conditions. Mater Sci Eng A 2014;A600:159–70.
[152] Malopheyev S, Mironov S, Kulitskiy V, Kaibyshev R. Friction-stir welding of ultra-fine grained sheets of Al-Mg-Sc-Zr alloy. Mater Sci Eng A 2015;A624:132–9.
[153] Peng Y, Yin Z, Lei X, Pan Q, He Z. Microstructure and properties of friction stir welded joints of Al-Mg-Sc alloy plates. Rare Metal Mater Eng 2011;40(2):201–5.
[154] Zhemchuzhnikova D, Malopheyev S, Mironov S, Kaibyshev R. Cryogenic properties of Al-Mg-Sc-Zr friction-stir welds. Mater Sci Eng A 2014;A598:387–95.
[155] Zhemchuzhnikova D, Mironov S, Kaibyshev R. Fatigue performance of friction-stir-welded Al-Mg-Sc alloy. Metall Mater Trans A 2017;A48(1):150–8.
[156] Zhao J, Jiang F, Jian H, Wen K, Jiang L, Chen X. Comparative investigation of tungsten inert gas and friction stir welding characteristics of Al-Mg-Sc alloy plates. Mater Des 2010;31(1):306–11.
[157] Moreira PMGP, Santos T, Tavares SMO, Richter-Trummer V, Vilaça P, de Castro PMST. Mechanical and metallurgical characterization of friction stir welding joints of AA6061-T6 with AA6082-T6. Mater Des 2009;30(1):180–7.
[158] Trueba Jr L, Heredia G, Rybicki D, Johannes LB. Effect of tool shoulder features on defects and tensile properties of friction stir welded aluminum 6061-T6. J Mater Process Technol 2015;219:271–7.
[159] İpekoğlu G, Erim S, Gören Kiral B, Çam G. Investigation into the effect of temper condition on friction stir weldability of AA6061 Al-alloy plates. Kovove Mater 2013;51(3):155–63.

[160] İpekoğlu G, Erim S, Çam G. Investigation into the influence of post-weld heat treatment on the friction stir welded AA6061 Al-alloy plates with different temper conditions. Metall Mater Trans A 2014;45A(2):864–77.
[161] Lim S, Kim S, Lee C-G, Kim SJ. Mechanical properties of friction stir welded Al alloys with different hardening mechanisms. Metal Mater Int 2005;11(2):113–20.
[162] Chandu KVPP, Venkateswara Rao E, Srinivasa Rao A, Subrahmanyam BV. The strength of friction stir welded aluminium alloy 6061. Int J Res Mech Eng Technol 2013;4(1):119–22.
[163] Kumar R, Singh RKR, Bajpai AK. Mechanical properties of friction stir welded 6061 aluminium alloy. Int J Eng Res Technol 2013;2(8):74–80.
[164] Malopheyev S, Vysotskiy I, Kulitskiy V, Mironov S, Kaibyshev R. Optimization of processing-microstructure-properties relationship in friction-stir welded 6061-T6 aluminum alloy. Mater Sci Eng A 2016;A662:136–43.
[165] Zhou Z, Yue Y, Ji S, Li Z, Zhang L. Effect of rotating speed on joint morphology and lap shear properties of stationary shoulder friction stir lap welded 6061-T6 aluminum alloy. Int J Adv Manuf Technol 2017;88(5-8):2135–41.
[166] Braun R, Dalle Donne C, Staniek G. Laser beam welding and friction stir welding of 6013-T6 aluminium alloy sheet. Mat-wiss u Werkstofftech 2000;31(12):1017–26.
[167] Heinz B, Skrotzki B. Characterization of a friction-stir-welded aluminum alloy 6013. Metall Mater Trans B 2002;B33(3):489–98.
[168] Leitao C, Leal RM, Rodrigues DM, Loureiro A, Vilaça P. Mechanical behaviour of similar and dissimilar AA5182-H111 and AA6016-T4 thin friction stir welds. Mater Des 2009;30(1):101–8.
[169] Zhao Y, Zhou L, Wang Q, Yan K, Zou J. Defects and tensile properties of 6013 aluminum alloy T-joints by friction stir welding. Mater Des 2014;57:146–55.
[170] Jata KV, Sankaran KK, Ruschau JJ. Friction-stir welding effects on microstructure and fatigue of aluminum alloy 7050-T7451. Metall Mater Trans A 2000;A31(9):2181–92.
[171] Pao PS, Gill SJ, Feng CR, Sankaran KK. Corrosion-fatigue crack growth in friction stir welded Al 7050. Scr Mater 2001;45(5):605–12.
[172] Su JQ, Nelson TW, Mishra R, Mahoney M. Microstructural investigation of friction stir welded 7050-T651 aluminium. Acta Mater 2003;51(3):713–29.
[173] Reynolds AP, Tang W, Khandkar Z, Khan JA, Lindner K. Relationships between weld parameters, hardness distribution and temperature history in alloy 7050 friction stir welds. Sci Technol Weld Join 2005;10(2):190–9.
[174] Zhou L, Wang T, Zhou WL, Li ZY, Huang YX, Feng JC. Microstructural characteristics and mechanical properties of 7050-T7451 aluminum alloy friction stir-welded joints. J Mater Eng Perform 2016;25(6):2542–50.
[175] Wu H, Chen Y-C, Strong D, Prangnell P. Stationary shoulder FSW for joining high strength aluminum alloys. J Mater Process Technol 2015;221:187–96.
[176] Zhang F, Su X, Chen Z, Nie Z. Effect of welding parameters on microstructure and mechanical properties of friction stir welded joints of a super high strength Al-Zn-Mg-Cu aluminum alloy. Mater Des 2015;67:483–91.
[177] Rajakumar S, Muralidharan C, Balasubramanian V. Influence of friction stir welding process and tool parameters on strength properties of AA7075-T6 aluminium alloy joints. Mater Des 2011;32(2):535–49.
[178] Ipekoğlu G, Kiral BG, Erim S, Çam G. Investigation of the effect of temper condition on friction stir weldability of AA7075 Al-alloy plates. Mater Technol 2012;46(6):627–32.
[179] Ipekoğlu G, Erim S, Çam G. Effects of temper condition and post weld heat treatment on the microstructure and mechanical properties of friction stir butt-welded AA7075 Al alloy plates. Int J Adv Manuf Technol 2014;70(1–4):201–13.
[180] İpekoğlu G, Çam G. Effects of initial temper condition and postweld heat treatment on the properties of dissimilar friction-stir-welded joints between AA7075 and AA6061 aluminum alloys. Metall Mater Trans A 2014;45A(7):3074–87.
[181] Bayazid SM, Farhangi H, Asgharzadeh H, Radan L, Ghahramani A, Mirhaji A. Effect of cyclic solution treatment on microstructure and mechanical properties of friction stir welded 7075 Al alloy. Mater Sci Eng A 2016;A649:293–300.
[182] Fratini L, Buffa G, Shivpuri R. Mechanical and metallurgical effects of in process cooling during friction stir welding of AA7075-T6 butt joints. Acta Mater 2010;58(6):2056–67.
[183] Lotfi AH, Nourouzi S. Effect of welding parameters on microstructure, thermal, and mechanical properties of friction-stir welded joints of AA7075-T6 aluminum alloy. Metall Mater Trans A 2014;45A(6):2792–807.
[184] Fuller CB, Mahoney MW, Calabrese M, Micona L. Evolution of microstructure and mechanical properties in naturally aged 7050 and 7075 Al friction stir welds. Mater Sci Eng A 2010;A527(9):2233–40.
[185] Li D, Yang X, Cui L, He F, Zhang X. Investigation of stationary shoulder friction stir welding of aluminum alloy 7075-T651. J Mater Process Technol 2015;222:391–8.
[186] Barbini A, Carstensen J, dos Santos JF. Influence of a non-rotating shoulder on heat generation, microstructure and mechanical properties of dissimilar AA2024/AA7050 FSW joints. J Mater Sci Technol 2018;34(1):119–27.
[187] Azimzadegan T, Serajzadeh S. An investigation into microstructures and mechanical properties of AA7075-T6 during friction stir welding at relatively high rotational speeds. J Mater Eng Perform 2010;19(9):1256–63.
[188] Srinivasa Rao T, Madhusudhan Reddy G, Koteswara Rao SR. Microstructure and mechanical properties of friction stir welded AA7075-T651 aluminum alloy thick plates. Trans Nonferrous Met Soc China 2015;25(6):1770–8.
[189] Bozkurt Y, Salman S, Çam G. Effect of welding parameters on lap shear tensile properties of dissimilar friction stir spot welded AA 5754-H22/2024-T3 joints. Sci Technol Weld Join 2013;18(4):337–45.
[190] Çam G, İpekoğlu G, Serindağ HT. Effects of use of higher strength interlayer and external cooling on properties of friction stir welded AA6061-T6 joints. Sci Technol Weld Join 2014;19(8):715–20.
[191] Mallard B, de Geuser F, Deschamps A. Microstructure distribution in an AA2050 T34 friction stir weld and its evolution during post-welding heat treatment. Acta Mater 2015;101:90–100.
[192] Çam G, Güçlüer S, Çakan A, Serindağ HT. Mechanical properties of friction stir butt-welded Al-5086 H32 plate. Mat-wiss u Werkstofftech 2009;40(8):638–42.
[193] Franchim AS, Fernandez FF, Travessa DN. Microstructural aspects and mechanical properties of friction stir welded AA2024-T3 aluminium alloy sheet. Mater Des 2011;32(10):4684–8.
[194] Groth A, Horstmann M, Kashaev N, Huber N. Proc. of the 34th Conference and the 28th Symposium of the International Committee on Aeronautical Fatigue and Structural Integrity. 2015. p. 477–82.
[195] Prisco A, Acerra F, Squillace A, Giorleo G, Pirozzi C, Prisco U, et al. LBW of similar and dissimilar skin-stringer joints part I: process optimization and mechanical characterization. Adv Mater Res 2008;38:306–19.
[196] Smith CB, Crusan W, Hootman JR, Hinrichs JF, Heideman RJ, Noruk HJS. Proc. of the 130th Annual Meeting and Exhibition TMS 2001. 2001. p. 175–85.
[197] Schultz V, Seefeld T, Vollertsen F. Gap bridging ability in laser beam welding of thin aluminum sheets. Phys Proc 2014;56:545–53.
[198] Vaidya WV, Horstmann M, Seib E, Toksoy K, Koçak M. Assessment of fracture and fatigue crack propagation of laser beam and friction stir welded aluminium and magnesium alloys. Adv Eng Mater 2006;8(5):399–406.
[199] Lanciotti A, Lazzeri L, Polese C, Rodopoulos C, Moreira P, Brot A, et al. Fatigue crack growth in stiffened panels, integrally machined or welded (LBW or FSW): the DaToN project common testing program. SDHM Struct Durab Hlth Monit 2011;7(3):211–29.
[200] Murray C. Hampshire, UKCost Effective Integral Metallic Structure (COINS), Final Report, European Commission, Cordis, Projects & Results Service2010. Cost Effective Integral Metallic Structure (COINS), Final Report, European Commission, Cordis, Projects & Results Service 2010.
[201] Irving P, Ma YE, Zhang X, Servetti G, Williams S, Moore G, et al. Proc. of the 25th ICAF Symposium of the International Committee on Aeronautical Fatigue. 2009. p. 387–405.
[202] Ma YE, Irving P. Residual stress effects and fatigue behavior of friction-stir-welded 2198-T8 Al-Li alloy joints. J Aircraft 2011;48(4):1238–44.
[203] Ma YE, Liu BQ, Zhao ZQ. Damage tolerance properties of 2198-T8 integral fuselage panel between double friction stir weld joints. Appl Mech Mater 2011;138-139:651–6.
[204] Cavaliere P, de Santis A. Effect of anisotropy on fatigue properties of AA2198 Al-Li plates joined by friction stir welding. Metall Sci Technol 2008;26(2):21–30.
[205] Harris CE. Atluri SN, Sampath SG, Tong P, editors. Structural integrity of aging airplanes. Berlin, Heidelberg, Germany: Springer-Verlag; 1991. p. 141–52.
[206] Alexopoulos ND, Migklis E, Stylianos A, Myriounis P. Fatigue behavior of the aeronautical Al–Li (2198) aluminum alloy under constant amplitude loading. Int J Fatigue 2013;56:95–105.
[207] Le Jolu T, Morgeneyer TF, Denquin A, Gourgues-Lorenzon AF. Fatigue lifetime and tearing resistance of AA2198 Al-Cu-Li alloy friction stir welds: effect of defects. Int J Fatigue 2015;70:463–72.
[208] Steglich D, Wafai H, Besson J. Interaction between anisotropic plastic deformation and damage evolution in Al 2198 sheet metal. Eng Fract Mech 2010;77(17):3501–18.
[209] Chen J. Ductile tearing of AA2198 aluminium-lithium sheets for aeronautic application, Doctor thesis. Paris, France: Ecole Nationale Superieure des Mines de Paris; 2011.
[210] Webster S, Bannister A. Structural integrity assessment procedure for Europe – of the SINTAP programme overview. Eng Fract Mech 2000;67(6):481–514.
[211] Vaidya WV, Staron P, Horstmann M. Fatigue crack propagation into the residual stress field along and perpendicular to laser beam butt-weld in aluminium alloy AA6056. Fatigue Fract Eng Mater Struct 2012;35(5):399–411.
[212] Liu H, Shang D-G, Guo ZK, Zhao YG, Liu JZ. Fatigue crack growth property of laser beam welded 6156 aluminium alloy. Fatigue Fract Eng Mater Struct 2014;37(8):937–44.
[213] de Siqueira RHM, Riva R, da Silva Costa DH, de Oliveira Gonçalves V, de Lima MSF. A crack propagation study on T-joints of AA6013-T4 aluminum alloy welded by an Yb:fiber laser. Int J Adv Manuf Technol 2017;92(5-8):2831–41.
[214] Akhtar N, Wu SJ. Macromechanics study of stable fatigue crack growth in Al-Cu-Li-Mg-Ag alloy. Fatigue Fract Eng Mater Struct 2017;40(2):233–44.
[215] Richter-Trummer V, Zhang X, Irving PE, Pacchione M, Beltrão M, dos Santos JF. Fatigue crack growth behaviour in friction stir welded aluminium-lithium alloy subjected to biaxial loads. Exp Techniques 2016;40(3):921–35.
[216] Nesterenko GI. Proc. of the 22nd Congress of International Council of the Aeronautical Sciences. 2000. p. 441.1–444.10.
[217] Ivetic G, Lanciotti A, Polese C. Electric strain gauge measurement of residual stress in welded panels. J Strain Anal Eng Des 2008;44:117–26.
[218] Sticchi M, Schnubel D, Kashaev N, Huber N. Review of residual stress modification techniques for extending the fatigue life of metallic aircraft components. Appl Mech Rev 2014;67(1):010801.
[219] Uz M-V, Koçak M, Lemaitre F, Ehrström J-C, Kempa S, Bron F. Improvement of damage tolerance of laser beam welded stiffened panels for airframes via local engineering. Int J Fatigue 2009;31(5):916–26.
[220] Schnubel D, Horstmann M, Ventzke V, Riekehr S, Staron P, Fischer T, et al. Retardation of fatigue crack growth in aircraft aluminium alloys via laser heating - experimental proof of concept. Mater Sci Eng A 2012;A546:8–14.

[221] Groth A, Horstmann M, Kashaev N, Huber N. Design of local heat treatment for crack retardation in aluminium alloys. Proc Eng 2015;114:271–6.
[222] Kashaev N, Ventzke V, Horstmann M, Chupakhin S, Riekehr S, Falck R, et al. Effects of laser shock peening on the microstructure and fatigue crack propagation behaviour of thin AA2024 specimens. Int J Fatigue 2017;98:223–33.
[223] Zhang X, Boscolo M, Figueroa-Gordon D, Allegri G, Irving PE. Fail-safe design of integral metallic aircraft structures reinforced by bonded crack retarders. Eng Fract Mech 2009;76(1):114–33.
[224] Lu J, Huber N, Kashaev N. Improving the fatigue performance of airframe structures by combining geometrical modifications and laser heating. Fatigue Fract Eng Mater Struct 2018;41(5):1183–95.
[225] Kashaev N, Chupakhin S, Ventzke V, Horstmann M, Riekehr S, Barbini A, et al. Fatigue life extension of AA2024 specimens and integral structures by laser shock peening. MATEC Web Conf 2018;165:18001.
[226] AC 25.571-1D - damage tolerance and fatigue evaluation of structure. Washington: United States Department of Transportation. Federal Aviation Administration; 2011.